CO Selectivity and Stability in Bicarbonate Electrolysis

Masters thesis in Chemical Engineering

Jón Kjartan Jónasson

Delft University of Technology

TU Delft

MSc Thesis project in Chemical Engineering

CO Selectivity and Stability in Bicarbonate Electrolysis

by

Jón Kjartan Jónasson

to obtain the degree of Master of Science
at Delft University of Technology

To be defended publicly on Wednesday, May 22, 2024 at 11:00 AM

This thesis was carried out in the Large Scale Energy Storage research group at the Process and Energy department, Faculty of Mechanical Engineering, TU Delft

J.K. Jónasson
Student number: 5844282
Project duration: September 11, 2023 – May 22, 2024
Thesis committee:

Ir. I.A.E Burgers,	TU Delft, Daily Supervisor
Prof.dr.ir. E.L.V. Goetheer	TU Delft, Supervisor
Prof.dr. R. Kortlever	TU Delft, Supervisor
Prof.dr. A. Urakawa	TU Delft, Committee member
Prof.dr. D. Vermaas	TU Delft, Committee member

An electronic version of this thesis is available at http://repository.tudelft.nl/.

TU Delft

Acknowledgements

Jón Kjartan Jónasson
Delft, May 2024

First of all I would like to thank my supervisors for their assistance and cooperation during the duration of this project. I.A.E (Iris) Burgers, my daily supervisor was always at hand to answer questions and clear up any doubts. We had many productive talks where we arrived at interesting points, during the experimental phase especially, which proved important in getting the results we did. My profound gratitude goes out to my supervisors, Prof.dr.ir. E.L.V. (Earl) Goetheer and Prof.dr. R. (Ruud) Kortlever, whose knowledge and expertise in the field proved invaluable during the course of this thesis. Their insight and advice was key in reaching the interesting findings. I also extend my gratitude to Prof.dr. A. Urakawa and Prof.dr. D. Vermaas for their valuable role as committee members.

I would like to thank all the members of the Large-Scale Energy Storage research group for great cooperation during the time of this project. Their helpful advice during our scientific discussions in the lab and elsewhere proved essential to the quality of the work. In particular the assistance of Asvin Kumar and Shilong Fu with the setup and equipment in the lab was crucial in carrying out the experiments. I extend my gratitude to Siddhartha Subramanian for taking the time to prepare electrodes for me for a set of experiments.

My most sincere gratitude goes out to my family and friends for their continuing support. For being good examples, for making precious memories and for all the good times together, this would not have been possible without you. To my sister and my father, thank you for always supporting and believing in me. Special thanks go to my mother who has always been a key influence on me with her endless support, both in my academic life and elsewhere.

Lastly I am grateful to TU Delft and the department of Chemical Engineering for these past 2 years, during which I have learned a lot. Further thanks go out to the department of Process and Energy at the Mechanical Engineering department, where this thesis project was carried out. To anyone else who has helped me in one way or another during the course of this project, I thank you.

Abstract

As global warming proceeds with increasing consequences, new and improved solutions that can mitigate the increasing CO_2 emissions are becoming ever more important. Renewable energy technologies are advancing and along with carbon capture technologies, they promise to lower global emissions and help combat climate change. Renewable energy sources can be used to form value-added chemicals from captured CO_2 through a method known as CO_2 electrolysis. A novel approach to CO_2 electrolysis is bicarbonate electrolysis, which uses carbon capture solutions directly to make products. By integrating the capture and conversion process this way, effectively bypassing the energy intensive steps of CO_2 recovery required for conventional gas fed operation, CO_2 conversion to products can become even more sustainable.

The objective of this thesis is to explore ways to improve the selectivity of carbon monoxide (CO) in a bicarbonate electrolyser. In this experimental study, focus is also placed on the stability of the process, characterising the selectivity over time. Causes of selectivity decline are examined as well as methods of improvement. Furthermore, the effect of pH on CO selectivity and stability is given special consideration. Literature in the field of (bi)carbonate electrolysis was reviewed to gather understanding on the process, to clarify recent advances made and to find areas for improvement. Based on the findings from the literature review the experimental study was designed.

Experiments were conducted in a membrane electrode assembly (MEA) flow-cell in constant current fashion, applying a current of 100 mA/cm^2. The membrane chosen was a bipolar membrane (BPM) as it offers the possibility of operating with distinct electrolyte environments, separating the 3M bicarbonate catholyte from the 1M potassium hydroxide anolyte. Gas diffusion electrodes (GDE) were prepared by spray-coating silver nanoparticles on the surface, using Nafion ionomer as binding material. An interdigitated catholyte flow plate was used which ensured the bicarbonate would pass through the GDE due to its discontinuous channels forcing the flow through.

By introducing a catalyst-membrane gap through inserting a hydrophilic porous spacer between the GDE and the BPM, CO selectivity was improved from 50% to 78% in peak production, recording 55% averaged over 3 hour operation. This enhancement in selectivity can be explained by the defined pH gradient resulting from the gap, permitting a low pH at the BPM for protons to react with the bicarbonate, liberating i-CO_2; and a higher pH at the catalyst for CO_2 conversion to CO while suppressing the hydrogen evolution reaction (HER). An optimum gap was found to be 135 - 270 μm. These results compare with the previously highest reported CO selectivity values from the literature at ambient conditions and 100 mA/cm^2. While improving the selectivity, the stability of CO was not improved by the catalyst-membrane gap. The pH was found to affect both the selectivity and stability of CO, with higher bicarbonate pH leading to reduced selectivity but improved stability. This behaviour is explained by the reduced i-CO_2 liberation and increased carbonation reactions taking place at higher pH levels. Moreover, it was shown that constant bicarbonate pH does not lead to improved CO stability. This drop in stability at a constant pH along with the observed rising CO_2 availability led to the hypothesis that a likely cause of reduced CO stability is unwanted changes taking place in the electrode during electrolysis.

By investigation into the optimum catalyst-membrane gap along with in operando pH measurements in the gap microenvironment, it is anticipated that CO selectivity can be improved further and valuable insight acquired into CO stability. Research into electrode modifications during operation can likely advance understanding of the stability of the process even more, bringing the sustainable process of integrated carbon capture and bicarbonate electrolysis closer to industrial application.

Contents

List of Figures

List of Tables

Nomenclature

Abbreviations

Abbreviation	Definition
GHG	Greenhouse Gas
IEA	International Energy Agency
CC	Carbon Capture
CCUS	Carbon Capture Utilization and Storage
DAC	Direct Air Capture
CCS	Carbon Capture and Storage
CCU	Carbon Capture and Utilization
BECCS	Bio-Energy with Carbon Capture and Storage
CO_2RR	Carbon Dioxide Reduction Reaction
Redox	Reduction-Oxidation
OER	Oxygen Evolution Reaction
WE	Working Electrode
CE	Counter Electrode
RE	Reference Electrode
M	Molar/Molarity
HER	Hydrogen Evolution Reaction
i-CO_2	In-situ CO_2
BPM	Bipolar Membrane
MEA	Membrane Electrode Assembly
GDE	Gas Diffusion Electrode
USD	United States Dollar
PTFE	Polytetrafluoroethylene
CL	Catalyst Layer
STP	Standard Temperature and Pressure
Sus	Sustanion
Naf	Nafion
FE	Faradaic Efficiency
RHE	Reversible Hydrogen Electrode
CD	Current Density
CEM	Cation Exchange Membrane
CEL	Cation Exchange Layer
AEM	Anion Exchange Membrane
AEL	Anion Exchange Layer
PVD	Physical Vapor Deposition
NP	Nanoparticles
RDS	Rate Determining Step
EDS/EDX	Energy Dispersive X-Ray Spectroscopy
SEM	Scanning Electron Microscopy
TEM	Transmission Electron Microscopy
MPL	Microporous Layer
CNT	Carbon Nanotubes
IL	Interface Layer
DoE	Design of Experiments
DIW	Deionized Water
IPA	Isopropyl Alcohol

Abbreviation	Definition
MCE	Mixed Cellulose Ester
GC	Gas Chromatography
MFM/MFC	Mass Flow Meter/Mass Flow Controller
HPLC	High-Performance Liquid Chromatography
ICP-OES	Inductively Coupled Plasma Optical Emission Spectroscopy
EPDM	Ethylene Propylene Diene Monomer
OCP	Open Cell Potential
FLIM	Fluorescence Lifetime Imaging Microscopy

Chemical Symbols

Chemical Symbol	Chemical Full Name
CO_2	Carbon Dioxide
CH_4	Methane
NO_2	Nitrous Oxide
CO	Carbon Monoxide
CH_3OH	Methanol
C_2H_4	Ethylene
C_2H_5OH	Ethanol
HCOOH	Formic Acid
$KHCO_3$	Potassium Bicarbonate
HCO_3^-	Bicarbonate
H^+	Hydrogen ion / proton
H_2O	Water
OH^-	Hydroxide
Ni	Nickel
Ag	Silver
KOH	Potassium Hydroxide
H_2	Hydrogen
C_{2+}	Multicarbon compound
Cu	Copper
C_1	Carbon compound with one carbon atom
Sn	Tin
Pb	Led
Au	Gold
Cs	Cesium
Li	Lithium
C	Carbon
O	Oxygen
C_3H_7OH	1-Propanol
Co	Cobalt
K	Potassium
K_2CO_3	Potassium Carbonate
CO_3^{2-}	Carbonate
NaCl	Sodium Chloride
Ar	Argon
N_2	Nitrogen
Ti	Titanium
NiO_2	Nickel Oxide

1 Introduction

1.1. Climate Change

Climate change can be defined as long-term changes in weather patterns and temperatures [1]. These changes can occur naturally, usually over long time periods, however the rapid changes we are experiencing in modern times are driven by anthropogenic activities [2]. Since the industrial revolution began in the 1800s, humanity has been releasing large amounts of greenhouse gases (GHG) into the environment through the combustion of fossil fuels. GHGs are mainly carbon-dioxide (CO_2), methane (CH_4), nitrous-oxide (NO_2) and fluorinated gases. These gases cause global warming by trapping the sun's heat in the atmosphere, causing temperatures to rise and resulting in more extreme weather patterns with adverse effects on ecosystems. Rising ocean acidity, extreme heat and diminishing fresh water supplies are just some of the problems associated. The Paris Agreement from 2015 states the goal to limit the global temperature rise to 2°C by 2100, while striving for no more than 1.5°C, when compared to preindustrial temperatures. However, for the year 2023 a temperature rise of 1.4°C has already been recorded, and the 1.5 mark is expected to be passed for at least one of the next 5 years, although it's hard to state when the limit has been surpassed officially as the agreement does not clearly state how that should be determined [3]. Despite the agreement, emissions are increasing and are expected to continue that trend in the near future [4], as current industries continue emitting and industrialization takes place in many developing countries. According to a study that analysed national contributions and policies resulting from the Paris Agreement, when comparing to emissions from the period 2005-2015 it is stated that a best-case scenario would be a roughly 20% increase in emissions by the year 2030, with a 3°C temperature rise, noting a 4°C rise if no measures are taken [5]. It is therefore clear that more is required to combat climate change.

Phasing out fossil fuels has already begun, with renewable energy sources like hydroelectric power, wind and solar energy comprising an ever larger part of energy production. Technological advancements along with government policies and research grants, pressured by public opinion, have helped to bring about this recent surge in clean energy. Although clean energy is one important way to protect the environment and combat climate change, it is not enough. A substantial part of the global power sector is fossil-fuel run, and the average age of power plants is quite young. A drastic reduction in their use would mean a dramatic financial loss. For example, according to a 2020 report by the IEA (International Energy Agency), about a third of the world's coal-fired plants is less than 10 years old [6]. With a normal lifespan of about 50 years, they will most likely operate for quite some time into the future. These power plants are also mainly based in developing countries, largely in Asia, which are less able or willing to prioritize environmental goals over economically driven energy production due to their developing status. In addition, there are still industries that rely on the combustion of fossil fuels, for example to reach sufficiently high temperatures for the desired reactions to take place. Natural CO_2 sinks also cannot keep up with emissions, or rather by doing so cause catastrophic effects on ecosystems, such as rising temperatures and ocean acidification [7]. In order to achieve net-zero emissions it is therefore also necessary to remove CO_2 from industrial waste streams as well as directly from the environment through a process know as Carbon Capture (CC). Negative emissions can even be

achieved via CC if industries remove more CO_2 from the environment than they emit, or purely function in CC.

1.2. Carbon Capture, Utilization and Storage

Carbon capture, utilization ad storage (CCUS) is an important tool in the combat against climate change. It is an integral part of meeting long-term climate goals, according to the IEA [6]. Carbon capture (CC) refers to the removal of CO_2 from either flue gas (exhaust gas from industrial hydrocarbon combustion) or the environment. The most developed and applied methods for removing CO_2 from flue gas is chemical absorption [8]. Carbon capture directly from atmospheric air is most commonly done via direct air capture (DAC). This method is already being applied worldwide, with 27 DAC plants currently in operation and 130 in various stages of development [9]. The main problem with DAC is the high energy consumption, owing to the fact that CO_2 is quite dilute in atmospheric air. Another promising approach is removing CO_2 from seawater. The oceans work as a CO_2 buffer as CO_2 can dissolve in water. The CO_2 reacts with water to form carbonic acid, which then dissociates to form (bi)carbonate and protons, causing ocean acidification and adversely affecting crustaceans [10]. Recently developed methods focus on reversing that reaction. They operate by acidifying seawater under applied voltage, causing bicarbonate in the water to convert to CO_2, which is then removed under vacuum and stored or transported [11]. CO_2 capture from seawater has not passed the pilot scale yet, but there are a number of companies currently working on it.

Captured CO_2 can either be stored or utilized. Storing CO_2 can be done by making use of emptied oil and gas fields, or by pumping it into basalt rock layers where it mineralizes into stable carbonates [12]. The most common method for storing carbon is however in saline aquifers [13]. Carbon capture and storage (CCS) can be used in industry to reduce emissions, such as the cement and steel industry, and in power plants [14]. Carbon capture and utilization (CCU) is another way of reducing carbon emissions and fighting climate change. Most of CO_2 use today is direct use where the CO_2 is bought and used as is, for example in fertilizer production, enhanced oil recovery and the food and beverage industry [15]. But CCU also brings the prospect of circularity as CO_2 can be chemically converted to useful compounds such as fuels, chemicals, polymers and building materials. Not only does chemical conversion of CO_2 offer up the prospect of a circular carbon life-cycle, but it can also create revenue where value-added chemicals and products are produced. However, in order for CO_2 utilization to fulfil its potential in supporting climate goals, detailed life-cycle assessments on the benefits and challenges of CO_2 applications must be carried out [15]. Importantly, CC from the environment combined with storage or utilization also brings the possibility of negative emissions, meaning that in theory more carbon can be removed from the environment than is released, which is an important step in mitigating climate change. One method of achieving net negative emissions is with a BECCS process (Bio-Energy with Carbon Capture and Storage) [13]. Sustainably grown biomass is then burned instead of fossil fuels for energy, applying CCS on the produced CO_2.

There are many methods of utilizing captured carbon such as carbon mineralization, producing carbonates for the construction industry; producing biofuel from microalgae which feed on CO_2; and chemical synthesis, whereby the captured carbon is used as feedstock for the production of other carbon containing compounds such as plastics or urea [16]. CO_2 can also be converted into other carbon compounds electrochemically. Electrochemical CO_2 reduction into value-added chemicals has been receiving much attention recently. It introduces a solution to intermittency problems with many renewable energy sources, such as solar and wind energy, as excess energy in times of high output and low demand can be utilized and stored as liquid fuels and various commodity chemicals. Common CO_2 reduction reaction CO_2 products include carbon monoxide (CO), formic acid (HCO_2H), methane (CH_4), methanol (CH_3OH), ethylene (C_2H_4) and ethanol (C_2H_5OH). Figure 1.1 shows an overview of these CO_2 reduction reaction CO_2RR products, and compares the current fossil-based methods used to manufacture each one [17]. Most of these currently applied processes require high temperatures and/or pressures, as well as fossil fuels. CO_2RR can be operated at ambient temperatures and pressures, which brings higher process simplicity and safety. Electrochemical reduction of CO_2 can in theory be a sustainable replacement for these current production methods when renewable electricity is used.

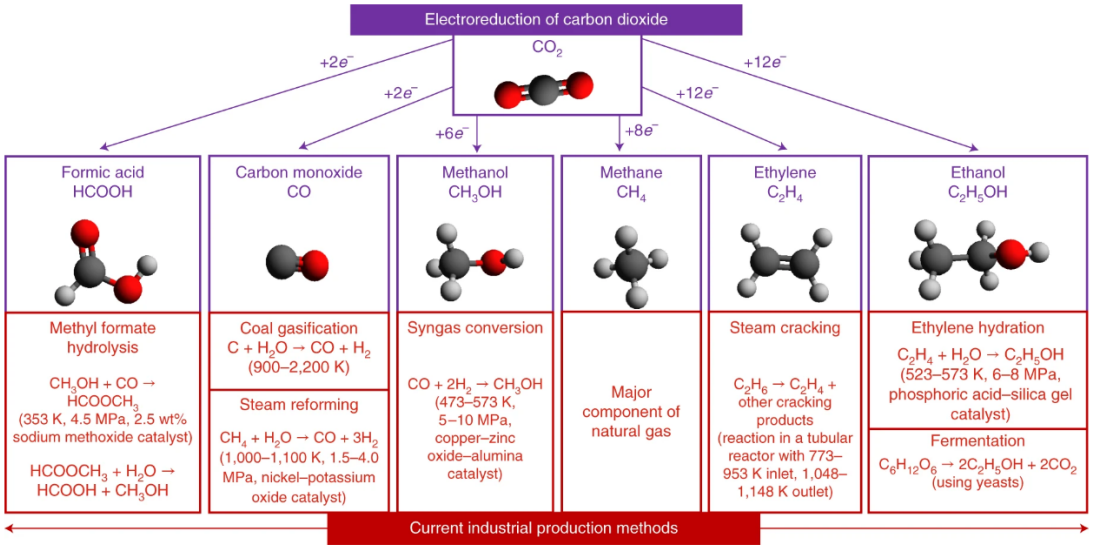

Figure 1.1: Comparison of commonly produced CO_2RR chemicals and their current production methods [17].

1.3. CO_2 Reduction Reaction

CO_2 can be electrolytically reduced to form various compounds. Electrolytic reduction (electrolysis) is a process wherein a current is applied over an electrolytic cell to drive a reaction. Such a reaction is a reduction-oxidation (redox) reaction, where electrons are freed during oxidation and subsequently used during reduction. Oxidation and reduction are so-called half-reactions, since they can be thought of as parts of one reaction, as one cannot take place without the other. In CO_2 electrolysis, the anodic reaction is usually the oxygen evolution reaction (OER). It uses water or hydroxide, depending on application, to form oxygen and release electrons, as per reaction 1.1. In CO production from CO_2, the corresponding reduction half-reaction is as per reaction 1.2. Together they make up the balanced redox reaction (reaction 1.3).

$$4OH^- \rightarrow O_2 + 4e^- \tag{1.1}$$

$$2H_2O + 2CO_2 + 4e^- \rightarrow 2CO + 4OH^- \tag{1.2}$$

$$2CO_2 \rightarrow 2CO + O_2 \tag{1.3}$$

A redox reaction requires at least two electrodes: a working electrode (WE) and a counter electrode (CE). A third electrode, a reference electrode (RE) can be used but often the CE is used as a reference. Whether or not a reference electrode is used depends on the focus of the experiment. The WE is where the reaction of interest takes place, which can be the anode or the cathode depending on the application. The reduction half-reaction takes place at the cathode, and the oxidation half-reaction at the anode. In CO_2 electrolysis a potential is applied across the cell, making the cathode negative and the anode positive. Electrons flow through an external circuit from the positively charged anode to the negatively charged cathode under an applied current (or voltage), which is controlled with respect to the cathode (the WE). The electrolytic cell is divided into two compartments by a separator, usually a membrane, and each half-reaction takes place in its perspective half-cell. The separator prevents the cell from short-circuiting and, as applicable, allows for controlled ion-crossover. The electrolyte's main purpose is to carry charges as well as transport reactants to and products from the electrodes.

1.4. Bicarbonate Electrolysis

The majority of CO_2 electrolysers studied have been based on gaseous CO_2 feedstock, either as saturated aqueous mediums or by directly feeding the CO_2 gas to the cathode without a liquid. Some impressive advancements have been made, however there are inherent limitations on electrolysers that depend on gaseous CO_2. Namely, the saturation concentration of CO_2 in an aqueous electrolyte is just 33mM at ambient temperature and pressure [18]. This results in CO_2 at the catalyst surface to quickly become depleted, leading to limitations on maximum achievable current densities caused by

mass-transfer related restrictions. The dissolved CO_2 also lowers the pH of the electrolyte, favoring the competing hydrogen evolution reaction (HER). The CO_2 utilization (the ratio of CO_2 converted to desired products to total CO_2 fed/released) of gas-fed electrolysers, especially those alkaline based, has also usually been quite low [19, 20]. In addition, the separation and compression steps required to produce purified CO_2 gas for utilization in gas-fed CO_2 electrolysers is energy intensive and expensive. Separation of unreacted CO_2 downstream also adds complexity and cost to the process [21].

CO_2RR through bicarbonate electrolysis is a method that has surfaced in recent years as an alternative to gas-fed CO_2 electrolysers. Bicarbonate electrolysis also has the potential to be integrated with CC (see section 1.6). In bicarbonate electrolysis, CO_2 and water are formed in the electrolyser when HCO_3^- reacts with protons (reaction 1.4). The protons can be supplied by a bipolar membrane (BPM), which splits water to protons and hydroxide ions (reaction 1.5).

$$HCO_3^- + H^+ \rightarrow CO_2 + H_2O \tag{1.4}$$

$$H_2O \leftrightarrow H^+ + OH^- \tag{1.5}$$

Bicarbonate electrolysis has the potential to overcome many of the difficulties of gas-fed electrolysers by bypassing the need for gaseous CO_2. Most importantly, by using liquid feed instead of gaseous, the energy intensive and expensive steps of desorption and compression during traditional CC can be avoided altogether. Bicarbonate electrolysers also have the possibility of reaching higher current densities than the often diffusion-limited gas-fed electrolysers. This is because the carbon donor is aqueous bicarbonate (HCO_3^-), which has a solubility limit of about 3.3M [18], 100 times higher than gaseous CO_2. In addition, CO_2 utilization via bicarbonate electrolysis has been shown to reach more than 40%, which is double that of commonly reported utilization from gas-fed CO_2 electrolysers, which is in the range of 1-20% [22, 23, 24].

When CO_2 reduction in alkaline electrolytes began to receive more attention, roughly 10 years ago, it was believed that the bicarbonate was directly reduced to carbon products [25, 26]. A few years later it was shown that the bicarbonate acts as carbon donor by converting to in-situ dissolved CO_2 ($i-CO_2$, locally released CO_2) [27], via an acid/base equilibrium reaction (reaction 1.4). The CO_2 is then the primary electrochemically active substrate that is reduced on the catalyst to form carbon products. There is general agreement in current literature regarding this reaction pathway, of HCO_3^- to CO_2 to carbon products, although the reaction mechanism is still not fully understood.

A problem faced in CO_2RR are the unwanted side reactions of CO_2 and OH^-, which lower the CO_2 utilization and electrolyser efficiency. Dissolved CO_2 can react with hydroxide and form bicarbonate, which can then further react with hydroxide again to form carbonate in so-called carbonation reactions (reactions 1.6, 1.7):

$$CO_2 + OH^- \leftrightarrow HCO_3^- \tag{1.6}$$

$$HCO_3^- + OH^- \leftrightarrow CO_3^{2-} + H_2O \tag{1.7}$$

At a high pH, carbonation will happen at a faster rate due to the higher concentration of OH^-. CO_2RR loss will therefore be a problem in processes that require a high pH, such as multicarbon production [13]. Controlling the pH of the electrolyser is therefore paramount for electrolyser efficiency, optimizing the local pH levels and $i-CO_2$ concentration. Indeed, this area of research is acknowledged as highly important in the literature. Another limiting factor is the competing HER, as previously mentioned. Due to its simple reaction pathway, low adsorption/desorption energy and ever-present hydrogen atoms, the HER proceeds favourably compared to CO_2RR. In acidic conditions, the HER follows one reaction pathway (reaction 1.8), while in neutral or alkaline conditions, it follows another (reaction 1.9.

$$2H^+ + 2e^- \rightarrow H_2 \tag{1.8}$$

$$4H_2O + 4e^- \rightarrow 2H_2 + 4OH^- \tag{1.9}$$

Minimizing the HER is therefore also a focus in improving the efficiency of $i-CO_2$ electrolysers. One method is to improve the hydrophobicity of the electrode, however the benefits of hydrophobicity is a contested topic in the literature on (bi)carbonate electrolysis.

1.5. Zero-gap Flow Electrolysers

For CO_2 electrolysis, the most commonly used reaction system is a flow-cell. The H-cell is a more basic electrochemical cell which consists of two compartments divided by a membrane. It is often used for initial experiments in screening suitable electrocatalysts [28] or for low current density experiments. Flow-cells are preferred over the simple H-cell mainly because of improved carbon selectivity [29, 30, 31, 32], higher partial current densities [33, 34], and less distance between the electrodes. The most frequent approach today to perform bicarbonate electrolysis is to use a zero-gap flow electrolyser, opting for a BPM for the membrane separator [35]. In a zero-gap design, the electrodes are separated only by the polymer membrane. Figure 1.2 shows the components of such a set-up, which was used in this study. The BPM lies between the anode and the cathode, delivering protons to the cathode and hydroxide ions to the anode by splitting water. The membrane and electrodes combined is often referred to as the membrane electrode assembly (MEA). The MEA is sandwiched between the flow plates. The flow plates deliver the electrolytes to the electrodes as well as collect the current, closing the electrical circuit. Next to the flow plates are gaskets which serve to provide electric insulation, preventing loss of charge. Thereafter come the cell housings, which provide structural integrity as well as deliver the electrolytes to the cell and remove the products.

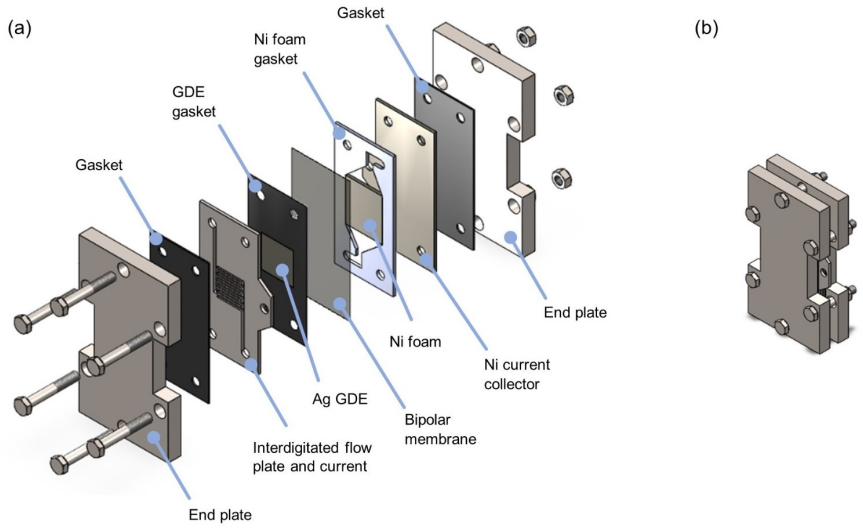

Figure 1.2: a) The components of a zero-gap flow-cell. b) An assembled (stacked) flow-cell.

1.6. Integrated Carbon Capture and Bicarbonate Electrolysis

Carbon capture and utilization (CCU) have typically been studied as seperate processes [35]. As previously mentioned, most CO_2 utilization requires purified CO_2 gas as feedstock. This involves the energy intensive steps of desorption and compression of the CO_2 during carbon capture (CC), as well as transportation, with associated costs and emissions. Desorption is an energy intensive and expensive process, requiring high temperatures and a large amount of steam [13]. Integrating carbon capture and utilization as a single process therefore has the potential to reduce the cost and improve the energy efficiency of the overall CCU process significantly.

CO_2 can be captured in KOH solution, forming bicarbonate, which then acts as the carbon donor forming CO_2 in-situ in the flow-cell for reduction. CO_2RR produce hydroxide ions as side products (reactions 1.2,**??**,**??**), which can then replenish the KOH used to capture CO_2. The alkaline offstream from the electrolyser can be passed to an absorption column, where CO_2 from DAC or flue gas is bubbled through, and bicarbonate thus produced for further reduction via the same reaction pathway in the backward direction of equilibrium (reaction 1.6). This way the carbonation reactions that reduce CO_2 electrolysis efficiency are in fact taken advantage of in the CC step in an integrated CC and bicarbonate electrolysis process. Bicarbonate feed for electrolysis and hydroxide ions for carbon capture

can then be circulated in the integrated system, forming a continous process. Figure 1.3 shows the steps involved in an integrated CCU process based on bicarbonate electrolysis, as well as the energy intensive steps that can be avoided. Here CO is the intended product. Importantly, in such a system the hydroxide solution does not need to be replenished as long as production of CO matches the rate of carbon capture [19]. In industrial applications, even when syngas (mixture of CO and H_2) is practically the only product [18, 23, 36], other products are also always formed to some degree. A separation step would therefore have to be added for the circulating KOH to the absorber, to remove liquid products such as alcohols and carboxylates (e.g. formate and acetate) and prevent buildup in the system.

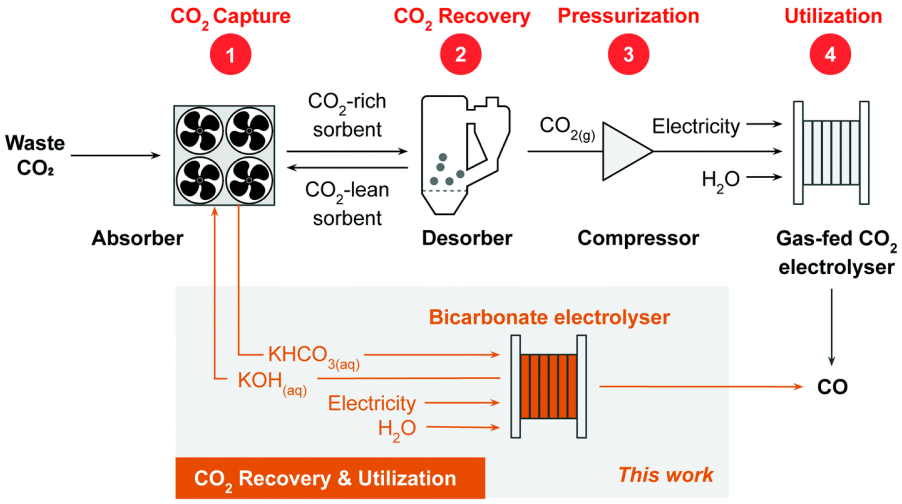

Figure 1.3: The diagram shows how the energy intensive steps of desorption (1) and compression (2) can be avoided by deploying a coupled CCU bicarbonate electrolysis system, circulating KOH and $KHCO_3$. The CO_2 feed to the absorber can be from flue gas or DAC. Figure taken from [37].

1.7. CO Production and Market Outlook

CO is an odorless, colorless and tasteless gas that is toxic to animals and humans. Typical manufacture of CO is based on syngas production, for instance through steam reforming, followed by purification of the syngas and finally extraction of the CO from the syngas [38]. Some advantages of producing CO electrolytically is being able to operate at much lower temperatures as well as more sustainably, with the possibility of using purely renewable energy and CO_2 sourced through CC as feedstock. Electrochemical product selectivity in CO_2RR depends primarily on the catalyst. CO is often produced using silver (Ag) [39], while copper (Cu) is used for C_{2+} production [40].

CO has many industrial uses. It is mainly used as a feedstock for the production of polymers such as polyurethane and polycarbonates, acids like formic acid and acetic acid, and phosgene gas which is used to produce plastics and pesticides. CO also has applications in the pharmaceutical industry, the automotive industry as well as the food and beverage industry as a preservative [41]. The CO market was valued at 5.6 billion USD in 2022 and is expected to grow in the coming years due to an increase in demand for organic and inorganic chemicals, projected to rise to 8.2 billion USD by 2032 [42]. CO production is among the most economically efficient CO_2RR products due to its high molecular weight to electrons transferred ratio [43].

Most CO_2RR research has focused on producing C_1 products, since these reaction pathways are kinetically more favourable than C_{2+} pathways, owing to the relative simplicity of the $2e^-$ transfer reactions [30, 44]. However, C_{2+} production is also receiving a lot of attention today, as C_{2+} products have some attractive qualities compared to C_1 products. These qualities along with C_{2+} production and market perspectives are examined in section C.5 in appendix C.

1.8. Research Topic

Bicarbonate electrolysis is a novel technology that presents a new method for CO_2 conversion, which when integrated with carbon capture has the potential to produce value-added compounds sustainably. This thesis focuses on the bicarbonate electrolysis aspect of the process. As CO_2 to CO is a relatively simple reaction pathway, and CO is a valuable feedstock in many chemical processes, CO was chosen as the intended product for the purpose of this study. (Bi)carbonate literature is reviewed along with selected gas-fed CO_2 electrolysis studies to gather information on cell and operation parameters' influence on product selectivity and stability (change in selectivity over time). By selecting, combining and modifying the most promising results from the literature, the objective of this thesis is to improve a bicarbonate electrolysis system with respect to CO selectivity and stability. Special consideration is given to the role of pH as it is considered a key factor in electrolyser efficiency.

The proposed main research question for this thesis is:

How can CO selectivity and stability be improved in bicarbonate electrolysis?

In order to assist in answering the main research question the following sub-research questions were posed:

1. **What are the parameters that influence CO selectivity in bicarbonate electrolysis?**
2. **What is the long-term stability of CO in bicarbonate electrolysis?**
3. **What is the effect of pH on CO selectivity and stability over time?**

The goal of this research is to further the understanding of how CO production efficiency can be improved in bicarbonate electrolysis. The hope is to provide insight that can also be used for different CO_2 product processes, for instance C_{2+} products, which present more complex reaction processes. Indeed, for future outlook references, this study includes an initial investigation into the effects of the CO production system improvements uncovered in this work on C_{2+} production using a bimetallic CuAg catalyst.

This thesis is part of a larger project which aims to integrate carbon capture (DAC or purified CO_2 from flue gas) with the production of value-added carbon products through bicarbonate reduction.

1.9. Chapter Overview

Following this first chapter, which provides context on the topic and states the research goals, comes chapter 2 in which an overview of the literature reviewed for this project is provided. The most important advances in the field of (bi)carbonate electrolysis are clarified and the results as well as their implications analysed. Chapter 3 explains the methodology of this work, outlining the experimental process including the equipment, setup, reactor and operational parameters. Also outlined in this section are the calculations associated with the project. In chapter 4 the results of the experimental work are presented alongside discussion. Finally, chapter 5 provides the conclusions of this work as well as recommendations for future research, based on the findings of this thesis.

2

Literature review

2.1. Preface

In this review, the most important recent developments in the field of bicarbonate electrolysis will be examined. Most of bicarbonate electrolysis literature is directed towards C_1 production, mainly CO, CH_4 and formate. Only one study was found that studies bicarbonate electrolysis to multicarbon products on Cu [45]. Carbonate electrolysis is much like bicarbonate electrolysis, both technologies have recently been developed to integrate a coupled CO_2 capture and conversion system [46]. In the literature, these systems are sometimes discussed as (bi)carbonate systems, due to their similarities. In this work, carbonate systems will also be examined, as they are quite similar to bicarbonate systems and because of a low number of publications in bicarbonate electrolysis, especially using Cu catalyst. Selected non-(bi)carbonate studies (gaseous-CO_2 electrolysers) are also included as their results might have an impact in a bicarbonate system.

Products and Selectivity

Product selectivity in CO_2RR has been shown to be highly dependent on the metal catalyst used as cathode [40, 47]. Tin (Sn) and led (Pb) are selective towards formate [47], whereas gold (Au) and Ag have been shown to be selective towards CO [39]. Back et al. have shown that Ag nanoparticles are superior to Au nanoparticles for CO_2/CO reduction, as they exhibit less HER as well as being inexpensive compared to Au [48]. Indeed, a vast majority of CO_2/CO research uses Ag as the chosen catalyst.Copper (Cu) is the only known metal to be selective towards multicarbon hydrogen compounds [40]. However, the selectivity of C_{2+} products varies significantly depending on the local environment as well as catalyst modifications such as oxidation and the inclusion of other metals or ionomers, among other factors. In order to tweak the selectivity of Cu various modifications have been studied. Among those is the addition of silver (Ag), for the intermediary production of CO, and so (bi)carbonate to CO reduction on Ag will also be discussed. The type of electrode is also important. The most frequently used is a gas diffusion electrode (GDE), an electrode designed for gaseous electrolysers but also utilized in purely liquid-fed operation. Other electrodes such as foams and meshes can also be used. Ionomers (ion containing polymers) have been shown to greatly affect carbon selectivity, particularly through HER reduction and influencing local CO_2:H_2O levels, and as such will be discussed. The effect of hydrophobicity on efficiency is an interesting topic, as it has the capacity to reduce HER thereby improving C_{2+} selectivity. Polytetrafluoroethylene (PTFE) is often used to this end, it can be added to the electrode or the catalyst material itself. The role of the electrolyte cation in carbon selectivity is a topic that has been receiving attention recently, with research suggesting methods to increase efficiency based on cation identity and concentration in the electric double-layer. Most bicarbonate electrolysers are based on a BPM MEA, and so the function and application of a BPM will be presented in this review. Furthermore, operating parameters show a strong correlation with product selectivity. Applied current density, temperature, pressure have been shown to impact efficiency and selectivity. In particular, a method known as pulsed electrolysis has been shown to be beneficial by allowing the catalyst microenvironment to revert to its original state, overcoming limitations caused by reactant deficiencies and changes in oxidation states. Finally, a critical parameter for electrolyser efficiency is the pH. Maintaining local pH levels,

namely low pH at the BPM and high pH at the catalyst, is paramount for CO_2 release and conversion efficiency. As such, the addition of an interposer material has shown great promise to help control local pH levels. An overview of the discussed factors on product selectivity in bicarbonate electrolysis on Cu can be seen in table 2.1.

Table 2.1: Important factors on CO_2RR selectivity and efficiency in bicarbonate electrolysis on Cu based on literature. The parameters are specific subcategories of the factors that have been studied.

Factor	Parameters
Catalyst	Composition, loading, coverage, surface structure, oxidation state
CuAg tandem systems	Catalyst ratio, positioning and layering, CO intermediate, lattice strain
Interposer	CL-BPM spacing, pH and species behavior
Electrode	Type (GDE, foam), thickness, porosity, stability
Ionomer	Type, loading, layering, effects on microenvironment
Hydrophobicity	Location (in GDL or CL), loading
Cation	Catholyte cation type, size, behavior in the Helmholtz double layer
pH	Local pH levels
BPM	Overpotential
Current density	Catalyst morphology changes, selectivity at higher current densities
Electrolyte	Type, concentration, flowrate
Temperature and Pressure	Reactant and intermediate kinetics, CO_2 solubility
Pulsed electrolysis	Catalyst surface reconstruction, catalyst oxidation, microenvironment

2.2. Catalysts

2.2.1. CO production on Ag catalyst

As previously mentioned, most of (bi)carbonate reduction research has been focused on C_1 production. CO has received quite some attention, mainly due to its simple reaction mechanism and its many uses. The Berlinguette group has been the most prolific in the field of bicarbonate electrolysis, publishing at least 13 papers over the past few years on the subject. Their main focus is on C_1 production, with bicarbonate reduction to CO being one of the group's main interests. In 2019, the group conducted experiments in a BPM-based bicarbonate electrolyser [18]. They achieved 81% CO FE at 25 mA/cm^2, dropping to 37% at 100 mA/cm^2 at STP (standard temperature and pressure). Their study provided a benchmark for bicarbonate electrolysis. In particular, they demonstrated that other carbon products than formate can be produced from bicarbonate, and that electrolytes with and without a saturation from a gas-CO_2 stream give comparable results. Lees et al. from the Berlinguette group improved upon these results in 2020, reaching CO FE of 82% at a total current density of 100mA/cm^2 at STP [23]. These formation rates - comparable to those of gas-fed CO_2 electrolysers - the group achieved by eliminating hydrophobic constituents from the GDE and by optimizing for catalyst coverage and loading. In the same study they tested the effect of pH on CO stability, finding that by reducing the pH periodically (adding H_2SO_4), and replenishing the electrolyte, they were able to improve CO selectivity which usually drops over time (see figure A.4 in appendix A). These two studies used GDEs coated with catalyst nanoparticles. In 2022, Zhang et al. from the Berlinguette group performed bicarbonate electrolysis using a free standing porous Ag electrode (Ag foam) instead of a GDE [37]. They attained 59% CO FE at 100mA/cm^2 using the Ag foam electrode, compared to 33% using a GDE control, which included hydrophobic microporous layer. When they raised the pressure from the previous STP conditions of 1 atm to 4 atm they saw 95% CO FE at 100mA/cm^2, associated with a higher CO_2 solubility at higher pressures. They also tested the effect of temperature, seeing the CO FE rise to 78% at 70°C inlet temperature of the HCO_3^- feed, which the group attributed to faster HCO_3^- to CO_2 kintetics and shifted equilibrium towards CO_2. At higher current densities, a drop in CO production was observed.

In all 3 of the studies discussed above by the Berlinguette group a 3M $KHCO_3$ catholyte and 1M KOH anolyte were used, and a BPM based flow-electrolyzer. The Berlinguette group has published papers in recent years on various topics related to bicarbonate electrolysis, such as cation identity implications on CO_2RR rate [36] and permeability and its trade-off relationship with catalyst active site density [49], among others.

The Sargent group is another research group that has been very active in recent years, publishing a number of papers on carbonate electrolysis as well as gaseous-fed CO_2 electrolysers. In 2019, Li et al. from the group produced syn-gas in a 3:1 ratio of H_2 to CO from carbonate electrolyte, using a BPM flow-cell and Ag GDE catalyst [50]. They achieved 28% CO FE at 100 mA/cm^2. Their study also set a benchmark in the field of (bi)carbonate electrolysis, demonstrating the possibility of producing CO without gaseous CO_2 feed, with benefits such as improved energy efficiency and high CO_2 conversion efficiency - something that many modern gas-fed CO_2 electrolysers struggle with. A main focus of the Sargent group's research is C_{2+} production on Cu catalysts as well as improving carbon and energy efficiency of CO_2 electrolysers, producing at least 9 papers in recent years. An overview of the main results of the discussed literature on (bi)carbonate reduction on Ag catalyst to CO can be seen in table 2.2.

Table 2.2: Main results of the literature discussed on Ag catalyst electroreduction to CO. B and S in the source column indicate the Berlinguette and Sargent research groups, respectively.

Source	FE_{CO}[%]	$J_{total}[mAcm^{-2}]$	Catholyte	Separator	Electrode	Ionomer	Other
[50] S	28	100	1M K_2CO_3	BPM	GDE	Nafion	PVD film before spray-coating, carbon black in ink
[18] B	81	25	3M $KHCO_3$	BPM	GDE	Nafion	
[18] B	37	100	3M $KHCO_3$	BPM	GDE	Nafion	
[23] B	62	200	3M $KHCO_3$	BPM	GDE	Nafion	PVD film before spray-coating
[23] B	82	100	3M $KHCO_3$	BPM	GDE	Nafion	PVD film before spray-coating
[37] B	59	100	3M $KHCO_3$	BPM	Foam	NA	
[37] B	95	100	3M $KHCO_3$	BPM	Foam	NA	Inlet electrolyte pressure of 4 atm
[37] B	78	100	3M $KHCO_3$	BPM	Foam	NA	Inlet electrolyte temperature of 70°C

2.2.2. Cu catalyst systems

Cu's ability as an electrocatalyst in the production of carbon products was discovered by Hori et al. about 40 years ago [51]. Ever since, advancements have been made in efficiency and selectivity. However, it is mainly in recent years that interest in Cu as an electrocatalyst has spiked along growing interest in sustainability. A main issue faced is that Cu is not selective in and of itself, but can produce a variety of carbon products. In the last few years, many have focused their efforts on steering the selectivity of Cu towards certain desired products. It is clear that the selectivity depends on numerous factors. Catalyst surface structure [52, 53], local pH levels and CO_2:H_2O ratio [54], cation concentration [55], metal compositions and hydrophobicity [56, 45] and ionomer coatings [54] are but to name a few. The underlying result is that by fine-tuning reactor and operational parameters, the product selectivity of Cu can be manipulated in many ways.

A benchmark for (bi)carbonate electrolysis into multicarbon products was set by Li et al. from the Sargent group in 2019, when in addition to studying syngas production on Ag catalyst they performed reduction on Cu GDE catalyst [50]. At 250mA/cm^2 they recorded the highest hydrocarbon partial current densities, producing about 14% multicarbon products (ethylene and ethanol).

Kim et al. performed multicarbon production in an electrochemical flow-cell using a Cu catalyst coated on a PTFE microporous GDL support, using an anion exchange membrane (AEM) and a CO_2 saturated $CsHCO_3$ feed [54]. They studied how the Cu catalyst selectivity and activity can be tuned by tailoring the catalyst layer microenvironment through ionomer layer addition. Ionomers, or ion-conducting polymers, are used as binder material for catalyst nanoparticles and for their ion selective conductive abilities. Particularly Nafion, a cation exchange ionomer and Sustanion, an anion exchange ionomer have been used to this effect (refer to 2.4 for a more detailed account on ionomers in CO_2RR). The group compared Nafion deposited layers with Sustanion and bare Cu catalyst. The Nafion layered

catalyst produced lower HER and higher C_{2+} FE, compared to bare Cu, while for the Sustanion layer the product distribution remained the same but total current density was higher. They also tested water concentration in the layers, and calculated the expected effect on local CO_2:H_2O ratio. As can be seen in figure 2.1, hydration in the layers reduces in the order of Cu > CuSus > CuNaf, which agrees with the product distribution results. Furthermore, the highest catalytic activity of the CuSus layer agrees with the highest expected CO_2:H_2O ratio. Sustanion's high CO_2 solubility can be explained by the presence of high CO_2 affinity imidazolium groups [57]. The effect of ionomers is discussed further in a separate section, see section 2.4. The group further improved Cu's C_{2+} selectivity and activity by incorporating pulsed electrolysis. Pulsed electrolysis is a technique that has surfaced as a means to improve electrolyser efficiency via resetting original catalyst microenvironment conditions such as high pH and high CO_2 concentration [58] (see section 2.7.4 on pulsed electrolysis). Along with pulsed electrolysis, they also tested the joint effect of Sustanion and Nafion layers on Cu. On a CuSusNaf catalyst coupled with pulsing, they achieved the best selectivity, reaching 90% C_{2+} FE and just 4% H_2, caused by the high CO_2:H_2O in the Sustanion layer, and high pH caused by OH^- trapping via the anionic Nafion being the outermost layer, as hypothesized. Kim et al. also studied the effect of electrolyte cation identity on product selectivity by comparing $LiHCO_3$ electrolyte with the $CsHCO_3$ electrolyte. The Li electrolyte produced lower total current density across all tested catalysts, but the authors state that the qualitative impact of the ionomers on Cu remains true regardless of electrolyte cation [54]. These observations are reviewed further in a seperate section on the effect of the electrolyte cation in section 2.5. In this study the researchers only ran experiments at low current densities (CD) of 10 and 20 mA/cm^2 (-0.8 to -1.15 V vs RHE (reversible hydrogen electrode)), citing mass transfer related difficulties that occur at higher CDs. These CDs are too low for any industrial implications, and it is known that in addition to mass-transfer effects CD impacts the morphology and surface structure of the catalysts, as well as the oxidation state, which all impact the selectivity. The authors do note that whether the ionomers limit electrolysis via ionic and/or mass transfer is an important issue, and mention only that it does not appear to do so at 10 mA/cm^2. It is important to understand to what extent the catalyst surface changes intrinsically during electrolysis at higher CDs, including the effect of ionomers. However, the study serves well in furthering understanding of the system, particularly different compositions and layering of ionomers on Cu catalyst and the effects on CO_2:H_2O ratio and local pH - key parameters in CO_2RR.

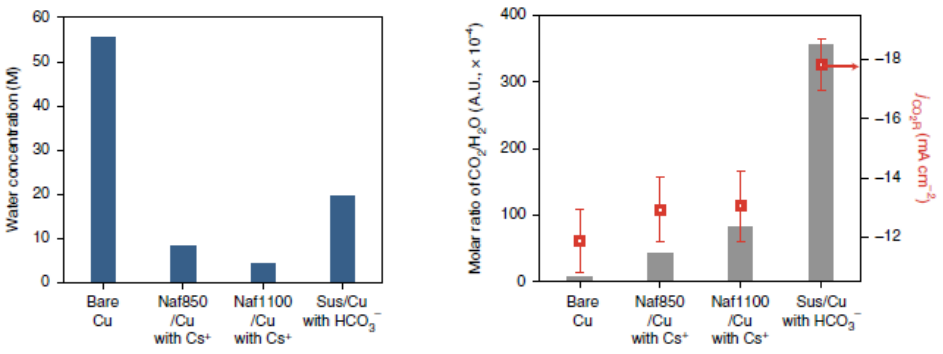

Figure 2.1: Water concentration (left) and CO_2:H_2O ratio (right) in different catalyst/ionomer/electrolyte configurations [54].

Lee et al. from the Sargent group performed a modeling and experimental study in 2023 [21], where they improved upon the benchmark Cu carbonate electrolysis study from 2019 [50]. They studied local pH and i-CO_2 concentration, achieving 47% C_{2+} FE at 300mA/cm^2, with roughly 30% C_2H_4 FE. Importantly, total C_1 compound concentration in the output gas stream was less than 1%, with no detectable CO_2 in the output, showing the minimal need for reactant separation and the resulting improved energy efficiency that can be achieved with (bi)carbonate electrolysis. Such high CO_2 utilization is rare in the field and raises some questions to the validity of the measurements. With that being said, as the pH of carbonate electrolyte is quite higher than that of bicarbonate, usually over 11 compared to around 8.5 for bicarbonate, it is possible that any unreacted CO_2 reverts back to carbonates at a fast rate due

to the high pH, which might explain the extremely low CO_2 in the output. The researchers conducted modeling of BPM-based carbonate electrolysis system, looking to explain the behaviour of chemical species in the reactor and to find reasons for low C_{2+} selectivity. The modeling results showed that local pH and species concentration is dependent on the spacing between the cation exchange layer (CEL) of the BPM and the catalyst layer (CL), with the concentration of i-CO_2 mainly affected by the distance of the spacing. According to the results, when the spacing is too small the pH at the CEL only goes as low as 10 and so protons are inhibited by carbonate and hydroxide ions, preventing CO_2 generation. When the spacing is too great, the long diffusion distances of the i-CO_2 increases chances of CO_2 reconverting to HCO_3^- via carbonation reactions as the CO_2 reacts with OH^-, lowering CO_2 conversion. The optimal spacing according to the modeling results is between 130 and 270 μm, where the concentration of i-CO_2 surpassed 4 vol% at the catalyst, an important marker to reach meaningful conversion rates at partial current densities of 100mA/cm^2 and above. In figure 2.2 the modeling results can be seen. The controlled local pH levels, low at the membrane and high at the catalyst can be seen in the frame marked H, representing a spacing of 135 μm. Across all tested applied current densities, at this spacing the local pH levels can be separated. Experimentally, they found that at a

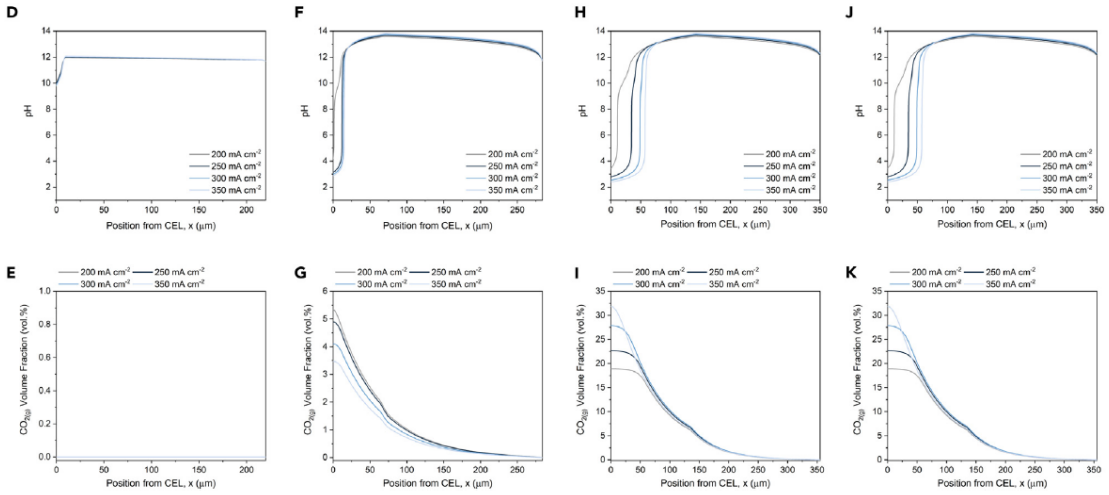

(D, F, H, and J) pH profile of 0, 64, 135, and 540 μm spacing, respectively, at the applied current densities from 200 to 350 mA cm^{-2} in 1.5 M of K_2CO_3 electrolyte.
(E, G, I, and K) *In situ* CO_2(g) volume fraction profile of 0, 64, 135, and 540 μm spacing, respectively, at the applied current densities from 200 to 350 mA cm^{-2} in 1.5 M K_2CO_3 electrolyte.

Figure 2.2: Modeling results of species behaviour in BPM based carbonate electrolyser [21]. The effect of CL-BPM spacing can clearly be seen, with the optimum spacing being 135 μm (frames H and I).

spacing of 60 μm, C_{2+} FE was just 14% at 250 mA/cm^2 [21]. At a spacing of 130-270 μm, they saw 40% C_{2+} FE. If the spacing was too small or too large, the C_{2+} selectivity was diminished as a result of lower concentration of i-CO_2 [21]. The spacing was constructed by inserting an interposer material, which was made of hydrophilic and porous mixed cellulose ester (MCE). The further improvement to 47% C_{2+} FE was achieved by adding a layer of cobalt phthalocyanines on carbon nanotubes (CoPCs-CNTs) on top of the Cu layer, in order to improve CO to CO_2 reaction kinetics. Furthermore, the group performed integrated direct air capture and electrolysis, maintaining stable C_{2+} FE of about 40% for over 20h. The group switched to a CEM from a BPM for their experiments, citing a reduced full cell voltage as the reason. The product distribution remained roughly equal for CDs ranging from 200-400 mA/cm^2 in the CEM and BPM systems without interposer and catalyst modifications, but it is uncertain what the effect would be in a BPM based system that included the modifications. However, the improvements in the system are impressive, and it is a promising avenue of research to see if a BPM based (bi)carbonate electrolyser would benefit similarly. Main results from the literature on Cu C_{2+} electroreduction discussed here can be found in table 2.3.

2.2.3. Catalyst loading and coverage on GDEs

Lees et al. also tested the effect of Ag nanoparticle catalyst loading on CO FE [23]. They varied the catalyst loading from 0.5 mg/cm^2 to 5.0 mg/cm^2 and ran experiments using 100 and 200 mA/cm^2

current densities. They reached a maximum CO FE of 82% with an optimum loading of 1.3 mg/cm^2 with the efficiency dropping at higher loadings. A possible explanation for this is that thinner catalyst layers (i.e. lower catalyst loadings) have higher concentrations of CO_2 at the catalyst due to shorter diffusion distances and thereby less interactions with the alkaline electrolyte, as was shown by Tan et al. [59]. That group however used gas-fed electrolysis in their study. It is unclear if thinner catalyst layers are also beneficial in bicarbonate electrolysis, where the CO_2 is only released from the aqueous bicarbonate upon reaction with protons supplied by the BPM. Therefore the electrolyte must pass through the GDE in order for CO_2 to be released. There have been limited studies done on the effect of catalyst loading and CL thickness on electrolyser efficiency in bicarbonate electrolysis.

It should be noted that before spray-coating the GDE, the Lees et al. group deposited a thin Ag film on the carbon substrate, by physical vapor deposition (PVD) [23]. The reason reported for doing so by the Lees et al. group is that the researchers observed they were to achieve complete coverage of the carbon paper with only spray-coating, citing a lack of hydrophobic microporous layer (MPL) on the carbon paper as the reason. They do not however mention how well they managed to cover the surface of a carbon paper that does include an MPL, which they did study as well. Catalyst coverage of GDL is a topic that has not received much attention, and the author of this work was unable to find other studies that examined it.

Other studies have also utilized this same method of first applying a thin catalyst film onto a carbon substrate and then spray-coating nanoparticles of the same catalyst on top [50]. However, they usually do not mention the reason for doing so. This presents an opportunity to examine if and to what extent catalyst surface coverage is limited without a catalyst PVD film, as it would be time and cost effective to skip that step if it is not necessary. Another variability is the application of catalyst layers via spray-coating. As it is usually a manual procedure, the catalyst coverage will be imperfect and nonuniform, and so difficult to replicate. Some researchers use a mechanical arm to perform the coating, but they do not share the settings or specific setup. Most studies do not mention how the spray-coating is performed. It is unclear to what extent the electrode preparation affects electrolyser efficiency. It would be recommendable for researchers however to clearly explain the steps taken in the preparation, for ease of replication.

2.2.4. Coupled CuAg catalyst systems

One of the reaction pathways of C_{2+} product formation is the dimerization of CO-CO on Cu active sites. An interesting approach in increasing C_{2+} product efficiency is then to selectively increase CO production in the system, which can then be further reduced to C_{2+} products. This is the idea behind bimetallic Cu catalyst systems, where Cu is combined with a second catalyst which exhibits good CO selectivity, such as Ag. For example, in a 2019 study, Du et al. more than doubled the ethylene (C_2H_4) FE by utilizing a CuAg catalyst, when compared with bare Cu catalyst [60]. CuAg tandem catalysts also have many desirable qualities over pure Cu. For example, CuAg is the most electrically conducive of all Cu-based alloys, it has higher mechanical hardness as well as oxidative resistance [61].

Chen et al. performed experiments in a gas-fed CO_2 flow-cell, comparing CO and C_{2+} production over Ag, Cu and tandem CuAg catalyst setups [56]. The electrolyte used was 1M KOH, paired with an AEM, and the catalysts were nanoparticles coated on carbon paper, with Nafion binder. The group found that CO production is the highest using pure Ag catalyst, but C_{2+} production is the highest when using a bimetallic CuAg catalyst system. Different Cu:Ag ratios were tested, with the optimum for C_{2+} selectivity being 2:1. At 400 mA/cm^2, they saw 40% C_{2+} FE, with about 20% C_2H_4 FE. They postulate that CO produced on the Ag is a key intermediate for subsequent C_{2+} production on Cu through C-C coupling. Importantly, the group found that the normalized intrinsic activity of the CuAg catalyst was higher than for pure Cu for both CO_2RR as well as CORR. Furthermore, they hypothesize that the active sites on each catalyst operate independently, i.e., the addition of Ag to Cu does not impact the Cu structure or function. The group also mentions that one of the main issues is the reaction of hydroxide with CO_2, i.e. carbonation reactions, which limits the CO_2RR. This obstacle can be at least partially mitigated by using bicarbonate electrolysis, as CO_2 is in much less contact with the alkaline electrolyte in such a system. HER suppression is typically also seen in Ag doped or alloyed Cu catalysts [62, 63], attributed to faster H_2 kinetics on Cu than Ag. Such was not the case in this study, which the authors

believe could be explained by the catalytic activity of Cu not being influenced by Ag atomic interactions.

Wang et al. performed CO_2 electrolysis in an H-cell using gaseous CO_2 feed and a Cu/CuO-Ag catalyst foam [64]. They compared the Cu/CuO-Ag foam with a copper foam without Ag addition (Cu/CuO) as well as with a copper foil electrode. At constant applied potentials, they saw increasingly higher total current density going from Cu foil to Cu/CuO foam and finally Cu/CuO-Ag foam, indicating higher catalytic activity of the silver doped copper foam. The C_{2+} FE increased by two thirds by the silver addition, with the C_2H_4 FE reaching about 40% and ethanol (C_2H_5OH) FE roughly 12%. They attribute this success to the lowering of C-C coupling activation energy on Cu due to the high surface coverage of *CO (adsorbed CO), as well as to the porous structure of the catalyst foam which induces temporary CO trapping and subsequent binding on Cu active sites. Importantly, the researchers saw improved C_{2+} selectivity with oxigenation derived Cu foam along with Ag when compared to Cu foam with Ag without oxygen, indicating synergistic effects of the Cu oxide and the Ag. Although the total current density was only about 20 mA/cm^2, as the experiments were performed in a small H-cell, they do give good insights into catalyst design for ethylene/ethanol selectivity. The silver doping was performed by submerging the copper-oxide foam into silver nitrate, prompting the Ag atoms to galvanically replace Cu^+ ions in the foam. The group also spray-coated the catalyst with Ag NP. It is not clear why they did so, but they do report that the longer the catalyst was submerged in acid during preparation, the larger the average size of the Ag NP. Despite the good results it is likely that the Cu oxide will reduce back to pure Cu during electrolysis at higher voltages, in which case the selectivity improvements should subside. The fact that the group did experiments at such low potentials means that it is unclear if these results would be beneficial for any industrially relevant cases, which require far greater current densities.

Lee et al. studied bicarbonate electroreduction on CuAg bimetallic catalyst systems [45]. Theirs is the only bicarbonate electrolysis study found in the literature that performs electrolysis on Cu towards C_{2+} products. They achieved about 42% C_{2+} FE at 100 mA/cm^2, with 20% C_2H_4 FE and 15% (C_2H_5OH) FE. The group experimented with different Cu:Ag ratios and found that the optimal catalyst ratio was 1:1. Lee et al. reached the same conclusion as Chen et al. and Wang et al., i.e. that the inclusion of Ag in the catalyst improved overall C+2 production through intermediate CO production on Ag sites which in turn reduced to C_{2+} on Cu sites. Figure 2.3 shows the setup of the flow-electrolyser, along with the overall i-CO_2 to C_{2+} product reactions. The group managed to improve the C_{2+} selectivity through step-wise modifications in the microenvironment around the catalyst layer, highlighting the importance of the local conditions of the catalyst environment for product selectivity. Namely, they optimized their system based on ionomers, local hydrophobicity and bilayer configurations. The best results were achieved when the two catalysts were in separate layers, with Ag nanoparticles (NP) spray-coated on top of a Cu NP layer, on a carbon paper substrate (GDE). The binder material was then Sustanion for the Cu (anion exchange layer, AEL), and Nafion for the Ag (cation exchange layer, CEL). Positively charged protons could then penetrate the AgNaf layer for conversion into i-CO_2 upon reaction with HCO_3^-, which was reduced to CO on the Ag. The CO could then further penetrate from the AgNaf to the CuSus layer to be reduced to C_{2+} products, via C-C coupling on Cu active sites. The beneficial high local pH in the CuSus layer caused by OH^- ion trapping in the AEL was also achieved via this configuration. A diagram of the layered catalyst/ionomer system with the intermediary CO formation can be seen in figure 2.4, along with the catalyst/ionomer layer configuration results. The inclusion of hydrophobic polytetrafluoroethylene (PTFE) in the AgNaf layer, as well as opting for hydrophobic carbon paper over hydrophilic, produced the best results. Ionomers and hydrophobicity will be discussed in more detail later in this work (see section 2.4). The work of Lee et al. reports the highest bicarbonate to C_{2+} conversion to date, as well as the highest bicarbonate to C_1 products. As such, it sets the benchmark for further research in the field. The study was mainly experimental, systematically improving C_{2+} selectivity through improvements. More thorough analysis of the reaction mechanisms at play would however be beneficial, the lack of which reflects the need in current literature for deeper understanding of the reaction pathways involved, as has been mentioned by many [56, 64]. As mentioned, the three studies on CuAg tandem catalysts discussed above agree on the role of adsorbed CO as a critical intermediary in the reduction of CO_2 to multicarbon products. Peterson et al. discussed the reaction mechanism of copper electroreduction catalysis to products such as CO and hydrocarbons [65]. The proposed reaction mechanism of CO_2 to CO involves two main steps. First, both an electron and a proton are transferred to a CO_2 molecule on the Cu surface, via reaction 2.1. Second, the CO_2

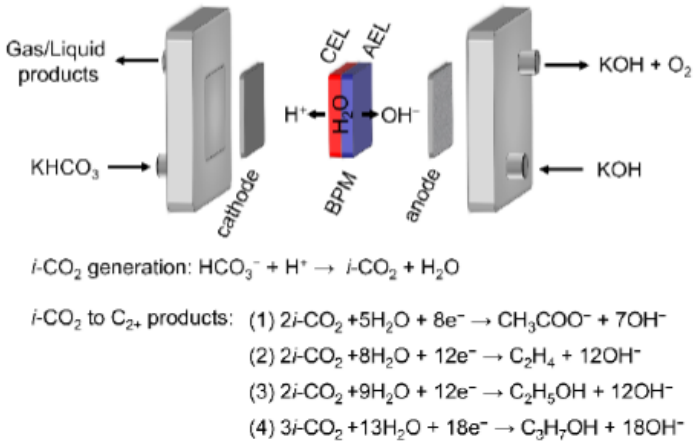

Figure 2.3: The BPM bicarbonate flow-electrolyser used in the Lee et al. study and the C_{2+} product reactions [45].

intermediate is reduced to *CO by reacting again with a proton and an electron, as per reaction 2.2. The * refers to an active binding site on the catalyst.

$$CO_2 + * + H^+ + e^- \rightarrow *COOH \tag{2.1}$$

$$*COOH + H^+ + e^- \rightarrow *CO + H_2O \tag{2.2}$$

CO binds more weakly to Ag than to Cu [66, 67, 68], so the desorption energy barrier is lower leading to higher CO production. In a CuAg system, the CO molecules can then either be transported through a bilayer or be temporarily trapped in a porous foam, leading to a high *CO surface coverage on the Cu. The further *CO reduction to a C_{2+} product, such as ethylene, then takes place through the aforementioned C-C dimerization on Cu, which is hypothesized to be the rate determining step (RDS) [69]. The presence of Ag catalyst in a Cu catalyst system has also been found to reduce the competing HER, which has been attributed to the larger hydrogen adsorption energy of Ag compared to Cu [70].

In a study from 2017, the CO spillover theory (CO_2 to CO on Ag, followed by CO reduction on Cu) is not believed to be the reason behind the synergistic effect of Cu and Ag in CO_2RR [71]. Instead the authors attribute C_{2+} selectivity improvements of CuAg systems to compressive strain in Cu surface atoms, caused by the formation of surface CuAg alloys. Along with better C_{2+} selectivity, a drastic reduction in HER was seen in the study, which was also seen as a result of the lattice strain in the Cu surface atoms. This surface lattice strain is noted as the cause of lowered HER through less favourable hydrogen binding on the Cu atoms, which also leads to lowered oxophilicity and thereby lowered C-O bond breaking, consequentially leading to a higher degree of carbonyl products (containing -C=O) at the cost of hydrocarbons. A 2023 study also looked at the effects of lattice dynamics and strain on selectivity in CO_2 electrolysis [72]. They found that the selectivity is correlated with lattice strain, caused by applied voltage. Ag and Cu NP are found to agglomerate to distinct immiscible domains, the segregated structure and lack of Cu/Ag interfaces suppressing CO spillover and C-C coupling and therefore C_2H_4 formation, while promoting CH_4. However, in these two studies ([71, 72]) the CuAg catalyst was formed by melting and mixing the metals, forming the alloys with distinct crystal lattice structures. In the studies discussed above which cited the CO spillover from Ag to Cu theory, nanoparticles are mixed in ink and spray-coated onto carbon paper, either in layers [45] or mixed [56]. Lee et al. revealed with cross-sectional EDS (Energy Dispersive X-Ray Spectroscopy) mapping that the Ag and Cu remained in distinct layers [45], and Chen et al. showed with TEM (Transmission Electron Microscopy) measurements that the CuAg NP was very agglomerated with no distinct morphology [56], which should prevent any strain effects from occuring as the particles can move around under strain from the applied voltage. Indeed, Chen et al. note that the typically suppressed HER seen in Ag doped Cu alloys, not being the case in their study, might be because of Cu and Ag sites operating independently in their system. In the study by Wang et al., Ag and O was incorporated into the catalyst respectively via acid treatment and thermal annealing [64]. Although the researchers studied the atom distribution, which showed an even distribution of Ag, O and Cu atoms before reduction, they don't discuss possible changes in the

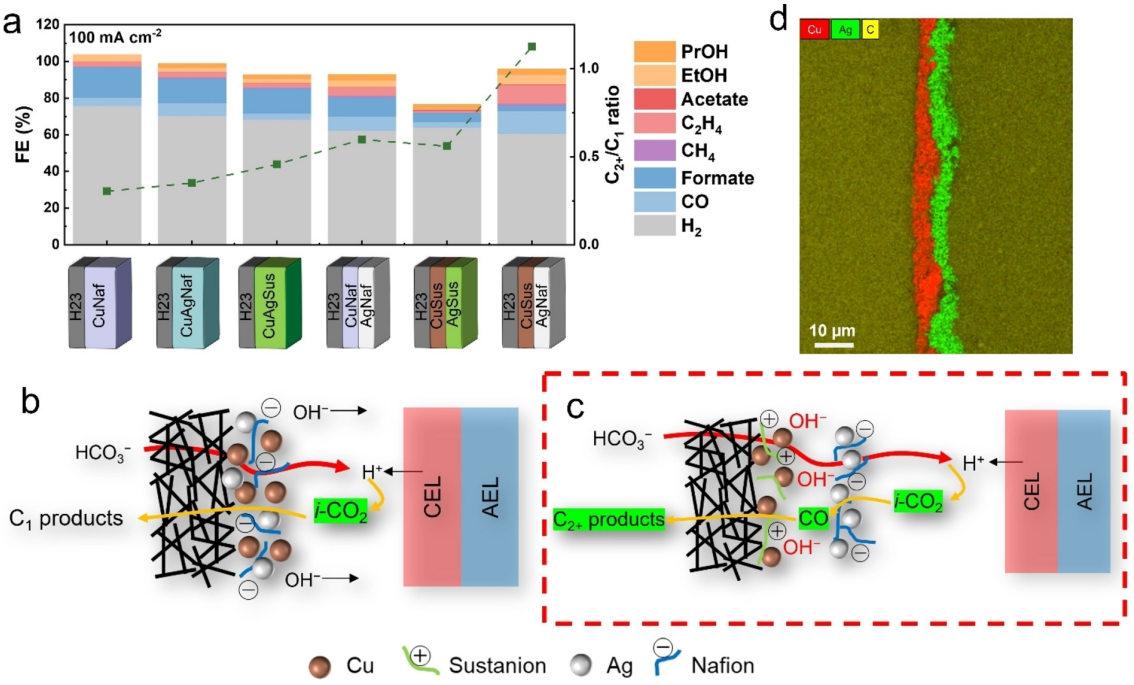

Figure 2.4: (a): Different catalyst/ionomer layer configuration variations, the best results are with carbon paper/CuSus/AgNaf layering. **(b)**: Illustration of species behaviour in CuAgNaf configuration. **(c)**: Illustration of species behaviour in CuSus/AgNaf bilayer configuration. **(d)**: Cross-sectional EDS mapping of the bilayer electrode, showing the distinct layers [45].

lattice during electroreduction. It would be an interesting area of research to look at changes in morphology - and possibly lattice - that tandem CuAg systems undergo during electrolysis, and to relate those changes to product selectivity.

An overview of the main results of the discussed literature on bimetallic CuAg systems can be seen in table 2.3, along with Cu catalyst system results.

Table 2.3: Main results of the literature discussed on Cu catalyst electroreduction to multicarbon products.

Source	Catalyst	C_{2+} FE	C_2H_4 FE	C_2H_5OH FE	J_{total} [mA/cm^2]	Catholyte	Separator	Other
[50]	Cu GDE	14.4	10.1	4.3	250	K_2CO_3	BPM	PVD film before coating, carbon black in ink
[54]	Naf/Sus/Cu GDE	90	25	50	13	CO_2 sat'd $CsHCO_3$	AEM	Pulsed
[21]	Cu/CoPc-CNT GDE	50	30	NA	300	K_2CO_3	CEM	
[45]	CuSus/AgNaf-P GDE	41.6	20	15	100	$KHCO_3$	BPM	
[56]	CuAgNaf GDE	40	20	NA	400	KOH	AEM	
[64]	Cu/CuO-Ag foam	52.5	40	12	20	NA	NA	H-cell

2.3. Electrode Types in Bicarbonate Electrolysis

2.3.1. Gas Diffusion Electrodes

Gas Diffusion Electrodes (GDEs) are porous electrodes with high surface area that are composed of a gas diffusion layer (GDL) and a catalyst layer (CL). The GDL has several purposes. Firstly, it serves as a structural support onto which the catalyst layer is deposited; secondly, it transports electrolyte to the CL as well as gaseous and liquid products away from the CL; thirdly, it conducts electrons from the current collector to the CL to drive the CO_2RR [73, 74]. GDEs are developed for gas-fed operation, wherein a 3-phase layer between the catalyst, liquid electrolyte and gaseous CO_2 exists and must be stable during operation. If the CO_2:H_2O ratio becomes too low and water covers the CL excessively, HER overpowers CO_2RR. This is called flooding of the CL. Most GDLs are composed of a highly porous carbon fibre layer. They often also include a microporous layer (MPL), which has been treated

with hydrophobic polymers, such as PTFE. Figure 2.5 shows the components of a GDE.

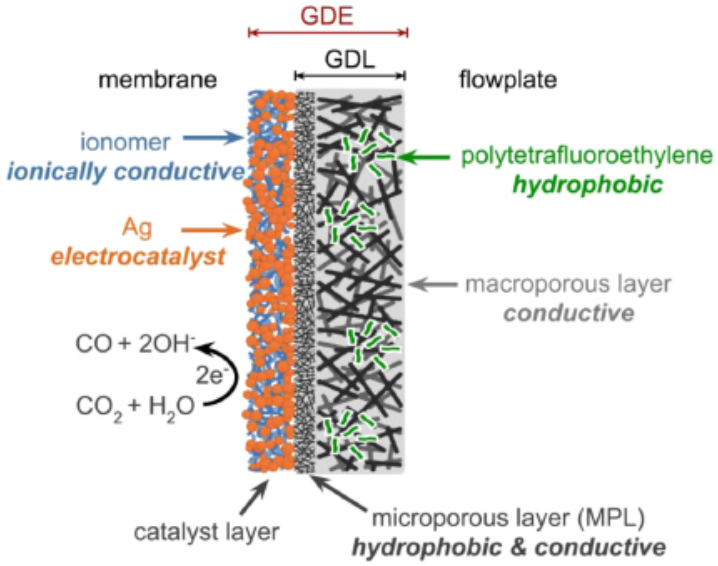

Figure 2.5: The components of a gas diffusion electrode (GDE) that is utilized for the reduction of CO_2 into CO using Ag catalyst [23].

Utilization of GDEs in (non gas-fed) bicarbonate electrolysis, where the carbon donor is the aqueous electrolyte, is a quite different application. Despite the name, diffusion of gases through the GDL is now not the focus, nor is maintaining a separate liquid and gas phase at the catalyst layer. Rather, the GDE must transport the aqueous electrolyte through it so that HCO_3^- can react with protons and form CO_2 for reduction. The GDL must therefore be conducive to aqueous transport and not hinder it such as in traditional gas-fed application of GDEs. Flooding is therefore not relevant in bicarbonate electrolysis, however the interplay of H_2O and CO_2(aq) and CO_2(g) at the CL is critical for efficiency. GDEs are by far the most commonly used electrodes in both gas-fed CO_2 electrolysis and (bi)carbonate electrolysis with the electrolyte as the carbon donor. Although GDEs are effective in gas-fed CO_2 electrolysis, it is not clear if that is the case when aqueous feed is the carbon source. For instance, hydrophobic constituents inhibit the transport of aqueous bicarbonate, reducing i-CO_2 formation, as was shown by Lees et al. from the Berlinguette group [23]. However, as mentioned previously, Lee et al. showed that including hydrophobic PTFE produced the best results in bicarbonate electrolysis on a GDE [45]. In that case, the PTFE can be assumed to act as both a promoter and a suppressor of CO_2RR, as it hinders aqueous transport but promotes CO_2:H_2O ratio thus decreasing HER, and depending on the application one or the other might prove to be more dominant. In addition, the carbon support has been known to degrade during operation [75], and reproducible and uniform CL can be difficult to achieve [76, 77], as previously mentioned. Other types of electrodes have been studied that might be better suited for non gas-fed operation, these are mainly free-standing porous metal electrodes (foams and meshes).

2.3.2. Porous Metal Electrodes

Free standing porous metal electrodes offer advantages over GDEs such as ease of fabrication and durability [78, 79]. Such electrodes are indeed in current industrial operation in processes that use aqueous liquid feedstocks similar to (bi)carbonate, for example in hydrogen production and the chloralkali process [79, 80]. Zhang et al. from the Berlinguette group compared bicarbonate electrolysis using a GDE and a foam in CO production on Ag catalyst in 2022 [37] (see section 2.2.1 above). Ease of fabrication, durability and resistance to impurities are some of the benefits the group mentioned for using a foam catalyst. A slightly lower cell voltage was however noticed with the GDE system, despite substantially higher conductivity of the metal foam electrode compared to the carbon based GDE. This the group believed to be because of electrolyte resistance caused by higher volumes of electrolyte being retained in the porous foam. Factors that can be tuned for lower voltage losses and product

selectivity are thickness, pore size distribution, and surface roughness [37]. Importantly, thickness and porosity are also parameters that can be modified in GDE for performance optimisation. Zhang et al. saw higher CO FE between applied current densities of 100 and 300 mA/cm^2, as can be seen in figure 2.6. The group also tested different inlet temperatures and pressures (section 2.7.3), and their overall conclusion was that a silver foam electrode was more efficient in bicarbonate electrolysis than GDEs. It should however be mentioned that the group had previously reached 82% CO FE at 100 mA/cm^2 using a Ag GDE in their study from 2020 [23], in which they also found that CO production on Ag GDE from bicarbonate benefitted from a GDL free of hydrophobic constituents, whereas in this electrode comparison study they utilized a GDE that included a hydrophobic MPL. It is therefore not conclusive from this comparison alone which electrode type is superior under optimum conditions for each electrode at STP.

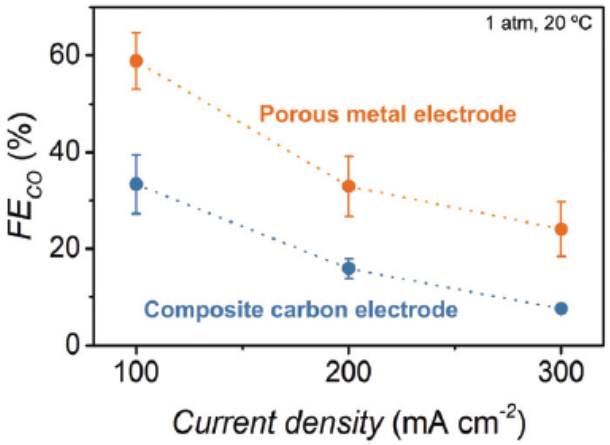

Figure 2.6: Comparison of a silver foam electrode and a silver GDE in bicarbonate electrolysis into CO [37].

Wang et al. used copper foam electrodes in their multicarbon CO_2RR study [64] (see section 2.2.4). They did not however compare foam electrodes with GDEs, but instead compared Cu foil electrode with CuO foam and CuO-Ag foam. Unsurprisingly, the foam catalysts had higher roughness factors than the foil, which has been linked with higher C_{2+} selectivity on Cu. Both foam catalysts also displayed higher current densities than the foil, indicating higher catalytic activity.

2.4. Ionomers

2.4.1. Nafion and Sustanion

Ion exchange polymers (Ionomers) are used in electrolysis with a GDE, both for their catalyst NP binding ability as well as for their ion selectivity and operating effects. High pH and high concentration of i-CO_2 are critical in achieving high C_{2+} FE, but these properties also increase the unwanted carbonation reactions, i.e. formation of HCO_3^- and CO_3^- from CO_2. Coating Cu catalysts with ionomers can overcome this trade-off, as water content and ion transport can be tailored [81]. The two most predominantly used ionomers are Nafion (a perfluorosulfonic acid, cation-conducting ionomer) and Sustanion (a polystyrene vinylbenzyl methylimidazolium, anion-conducting ionomer). Table 2.7 shows thermodynamic and CO_2 transport properties of Nafion and Sustanion, compared with an aqueous electrolyte (0.1M $CsHCO_3$). Water concentration is higher in Sustanion than Nafion, but CO_2 solubility in Sustanion is much higher, due to imidazolium groups which have a high CO_2 affinity [57]. It is then expected that the CO_2:H_2O is higher in Sustanion than in Nafion, which was shown by Kim et al. [54] (section 2.2.2). The ionic conductivity for a 3M $KHCO_3$ solution is about 128 mScm-1 at 20°C [82], more than double that of the aqueous electrolyte in the table, because of the higher molarity.

In addition to their other experiments, Lees et al. looked at the effect of Nafion loading on CO FE and CL morphology [23]. At constant Ag NP loadings, they varied the Nafion loading from 2.5 wt% to 11.5 wt%. At 100 and 200 mA/cm^2, they found that the optimum Nafion loading was 4 wt%. Nafion less than 2 wt% caused Ag particles to detach from the GDE, and too high loading caused some of the

Table 1 | Thermodynamic and transport properties of aqueous electrolyte, Nafion and Sustainion

		Aqueous solution	Nafion	Sustainion
Water concentration (M)	Reported for bulk ionomer membrane	55.6	22.1 (H^+ exchanged)[43] 4.8 (Cs^+ exchanged)[43]	48.9 (OH^- exchanged)[44]
	Measured for thin film on Cu		18.7 (H^+ exchanged) 4.4 (Cs^+ exchanged)	24.9 (OH^- exchanged) 19.7 (HCO_3^- exchanged)
Reported CO_2 solubility for bulk ionomer membrane (mM)		34	36.1 (ref. [45])	<703 (ref. [24])[a]
Mole CO_2/H_2O (a.u., $\times 10^{-4}$)		6.1	82.0 (Cs^+ exchanged)	<356.9 (HCO_3^- exchanged)
CO_2 permeability (10^{-16} mol cm^{-1} s^{-1} Pa^{-1})		64.94 (ref. [46])	8.70 (ref. [45])	<2.51 (ref. [24])[a]
Ionic conductivity (mS cm^{-1})		56.54[b]	70.1–200 (H^+ exchanged)[43,47] 1.1–20 (Cs^+ exchanged)[43,47]	64 (OH^- exchanged)[48] 24 (HCO_3^- exchanged)[48]

[a]Values taken from the literature for imidazolium-based anion-exchange membrane. [b]Value is for 0.1 M $CsHCO_3$ electrolyte.

Figure 2.7: CO_2 transport properties of Nafion and Sustanion, compared with an aqueous electrolyte. The table is taken from [54], primary sources used in the table can be found in the paper.

catalyst to be completely covered by the ionomer, decreasing catalytic activity. It is not clear from this study if this ionomer loading is optimal under different conditions, as the group only varied the Nafion loading and no other parameters. It would have been interesting to see the effect of Nafion loading paired with another parameter changed, such as the GDL or PVD film.

In the bicarbonate electrolysis study using CuAg GDE catalyst by Lee et al. (section 2.2.4), it was found that the optimum ionomer loading was 20 wt% [45]. This is almost double the highest loading that was previously explored by Lees et al. from the Berlinguette group. It is not clear which parameters are correlated here, since along with different catalysts many factors were different in the two studies, but it appears that the optimal ionomer loading strongly depends on system parameters. Lee et al. tested different compositions of the CuAg, Nafion and Sustanion, incorporating the catalysts and ionomers differently into layers on the GDL. They found that the optimum composition was CuSus on the GDL, with AgNaf there on top closest to the protons being released from the BPM. The group principally attributes the success of their bi-ionomer bi-metallic catalyst to the favorable CO production kinetics on Ag as well as to high local pH enabled by OH^- trapping in the Sustanion layer. Kim et al. also looked at the effect of different layering of Nafion and Sustanion with Cu catalyst [54]. In figure 2.8, the product distribution variability depending on ionomer stacking is clear, as is the effect on H_2 FE and C_1:C_{2+} production ratio. The OH^- affinity of the ionomers is also shown in the figure, explained by the background charge. It is therefore evident from the results of Lees et al. and Kim et al. that the catalyst microenvironment can be manipulated to favor CO_2RR by varying the order of the ionomers and their composition and loading in the GDE. The optimum conditions depend on the desired product and system properties.

2.4.2. PTFE - Effect of hydrophobicity

GDEs utilized in gas-fed electrolysers are hydrophobic in nature. This is so that the 3-phase boundary can be maintained and flooding prevented, as flooding of the pores of the GDE inhibit CO_2 diffusion and support HER [83], [73]. In bicarbonate electrolysers however the feed is aqueous, so the GDE must be hydrophilic in this application to ensure reactant supply at the catalyst layer. Lees et al. concluded that the addition of the hydrophobic constituents PTFE and an MPL were not beneficial to bicarbonate reduction [23]. They maintain that is because there is less in-situ CO_2 released when the GDL is hydrophobic, as there is less contact between bicarbonate ions from the electrolyte and protons released at the BPM. They confirmed this with experiments with catalyst free GDLs, measuring less CO_2 in the outlet stream from a hydrophobic GDL system than systems without PTFE and MPL. Many others that have studied bicarbonate reduction on Ag have opted for GDEs free of hydrophobic constituents, citing the work of Lees et al. [84, 49, 83].

However, there is some indication that hydrophobicity might be beneficial in bicarbonate electrolysis. That is based on the fact that suppressing the main competing reaction of HER is a key factor in improving product selectivity. By adding hydrophobic constituents to the GDE, the CO_2:H_2O ratio can be increased as well as CO_2 transport in the CL, improving efficiency. Lee et al. found that by substituting a simple carbon paper GDL with a hydrophobic one that had a MPL with 5wt% PTFE, they saw an

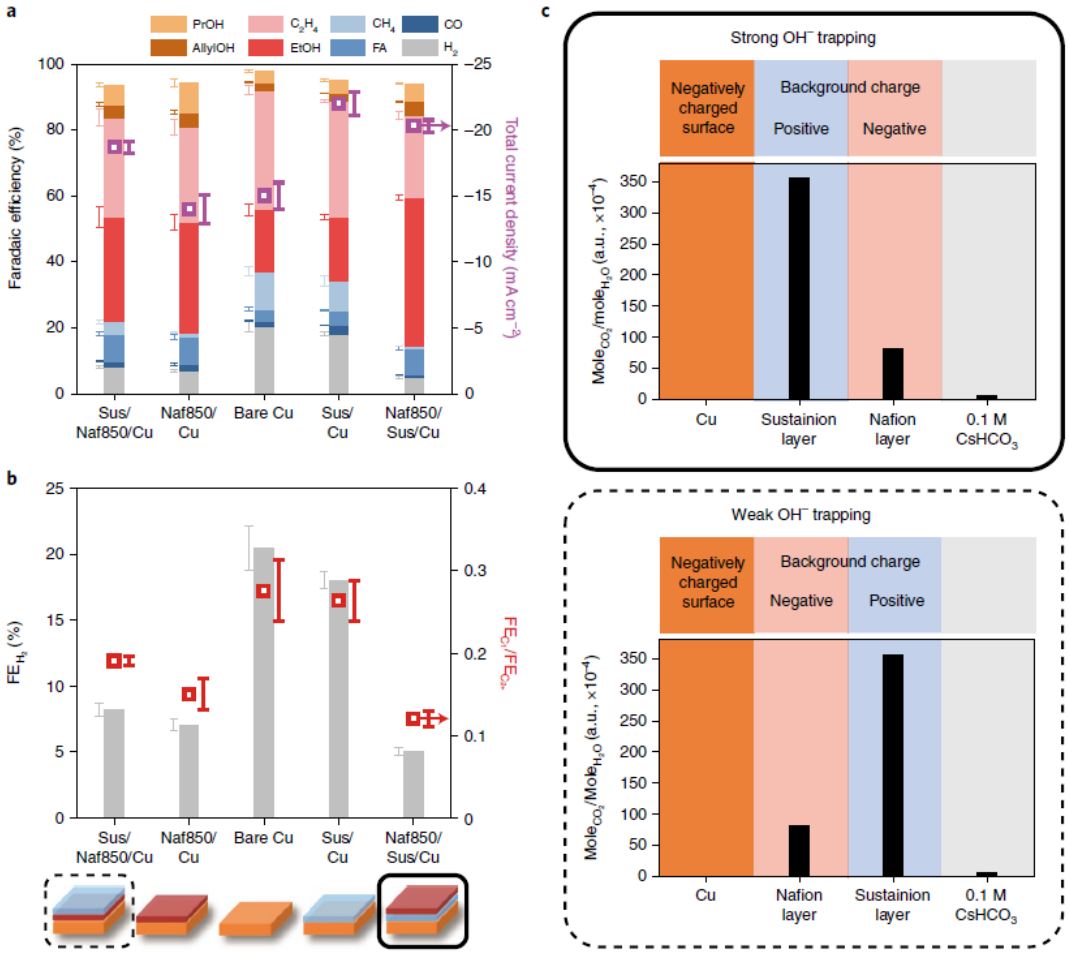

Figure 2.8: The product distribution is dependent on the catalyst/ionomer configuration, with the highest C_{2+} production in Naf/Sus/Cu (a), while HER is favored on pure Cu and the most suppressed on Naf/Sus/Cu (b). These results are correlated with the CO_2:H_2O ratio in the layers and the ionomers background charge (c and d), with the optimum Naf/Sus/Cu giving the highest ratio closest to the catalyst (c) [54].

increase in C_{2+} production along with a slight decrease in HER [45]. When they incorporated PTFE into the catalyst layer as well, specifically the Ag layer, they saw a further suppression in HER as well as an increase in C_{2+} selectivity, with an optimum PTFE addition of 50wt%. The group saw the most HER suppression when incorporating the PTFE only in the Ag layer, when compared to in the Cu layer or both layers, as can be seen in figure 2.9. They attribute this to a likely HER domination on the Ag layer, resulting from favourable H^+ trapping through the negatively charged Nafion polymer in the Ag layer, and the closer proximity to the BPM as they deposited the Ag layer on top of the Cu layer. However, the group only varied the PTFE loading in the Ag layer. In addition to increased efficiency due to suppressed HER, the authors mention that the hydrophobic microenvironment can increase the transport of i-CO_2 and CO through the GDE, thus increasing CO_2RR.

It is clear that an obstacle in CO_2RR is the competing HER. In theory, including hydrophobic components in the MEA should help combat the HER. However, the downside in aqueous electrolysis is the reduction in aqueous transport through the GDE. Ultimately, it seems to be the case that the inclusion of hydrophobic constituents will be a trade-off between the positive effect on CO_2RR by limiting water and proton contact with the catalyst and thus suppressing HER, and the negative effect of reducing the flow of the aqueous electrolyte through the GDE. The extent to which one or the other dominates and whether hydrophobic components can be beneficial in bicarbonate electrolysers most likely depends on the application, configuration of components and the intended products. No studies on hydrophobic constituents in other types of electrodes than GDEs was found in the literature. It is

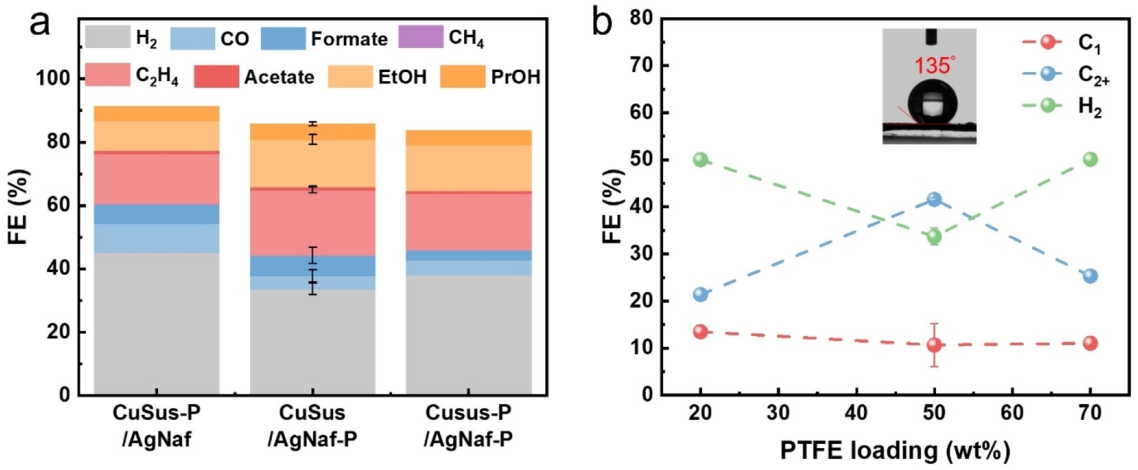

Figure 2.9: (a): The inclusion of hydrophobic PTFE in different layers, PTFE only in the AgNaf layer produced the best results (a).**(b)**: Different PTFE loading wt% in the AgNaf layer, 50wt% giving the best results [45].

clear hydrophobicity in bicarbonate electrolysers is somewhat of a contested topic, and thus presents an opportunity for further research.

2.5. The Role of the Catholyte Cation

Electrolyte cation identity affects product selectivity [54]. As such, its effect in CO_2 electrolysis has been the subject of research in recent literature, both in gas-fed and liquid bicarbonate electrolysis. The most used electrolyte cation in bicarbonate electrolysis is K^+. In 2021, Fink et al. from the Berlinguette research group studied the effect of electrolyte cation in bicarbonate electrolysis to CO [36]. They found that the cation identity does not impact the formation of i-CO_2, but that CO_2 reduction to CO increases as the cation ionic radius increases, with increasing CO selectivity in the order of $Li^+ < Na^+ < K^+ < Cs^+$. This indicates that catalyst activity is affected by the cation identity. The group tested different concentrations, the highest CO FE always being with the $CsHCO_3$. These results are in line with similar experiments in gas-fed CO_2 electrolysers [85, 86, 87, 88, 89, 90]. Importantly, at 3M electrolyte concentration, the CO FE of Cs^+ and K^+ electrolytes was nearly the same (see figure A.2 in appendix A). Additionally, the CO_2 utilization from Cs^+ and K^+ was nearly identical (see figure A.3 in appendix A). Potassium might be a better option in that case, as it is inexpensive compared to cesium, and more data exists in the literature on the use of K^+ in bicarbonate electrolysis. As there was no change in the i-CO_2 formation, which is highly pH dependent, most likely the pH is not affected by the cation identity [36].

Kim et al. tested the effect of cation identity on ionomer coated Cu catalysts, comparing $LiHCO_3$ with their catholyte of choice $CsHCO_3$ [54]. They found lower total current density and carbon product selectivity in Li^+ exchanged ionomer layers, in agreement with previous studies [85]. Yang et al. studied cation effects in a gas-fed CO_2 electrolyser [55]. Ion crossover in BPM electrolysers is usually an unwanted side-effect, but in this study the authors showed the benefits of K^+ crossover from the anolyte to the cathode. They varied the concentrations of the anolyte KOH from 0.2 to 3M, and saw increasing CO FE as a result, at the cost of reduced HER. At 200 mA/cm^2, the CO FE and H_2 FE are similar, but at a lower current density of 50 mA/cm^2, the CO selectivity reached 68%. To decouple the effects of K^+ and OH^- (pH), the researchers tested an anolyte mixture of 0.2M KOH and 0.4M K_2CO_3, which had the same pH as 0.2M KOH solution but a higher K^+ concentration (1M). The saw similar CO FE at lower current densities, but at 200 mA/cm^2, the CO selectivity was the highest with the anolyte mixture, which the group hypothesized to be because of higher K^+ crossover in the mixture than in 1M KOH.

Bui et al. have also studied the effect of alkali metal cations in bicarbonate electrolytes on product selectivities on Cu [91]. They found that the selectivity of formate, ethylene and ethanol increased with increasing alkali metal cation ionic radius, from Li^+ to Cs^+. It is not clear from the literature what mechanisms lie behind the observed increases in catalytic activity with larger cation ionic radii [92].

However, one theory explains them through the Donnan exclusion principle. The hydration radius is inversely proportional to ionic radius for alkali cations [93, 94]. The C_{2+} selectivity increases can then be attributed to the stabilized adsorption of reaction intermediates that have large dipole moments ($*CO_2$ and *OC-CO) to the catalyst surface, caused by a stronger electrostatic field in the Helmholtz double layer, which is a result of the smaller hydration radii of larger alkali metal cations [85, 94].

2.6. Bipolar Membranes (BPMs)

Bipolar membranes (BPM) are the most widely used in bicarbonate electrolysis [35], although cation exchange membranes (CEM) and anion exchange membranes (AEM) are also used. CEMs and AEMs facilitate the transport of either cations or anions, whereas BPMs are (ideally) non-permeable to ions due to their composition of both positively and negatively charged layers. They consist of a negatively charged cation-exchange layer (CEL), a positively charged anion-exchange layer (AEL), and between them an interface layer (IL), which contains a catalyst [95]. The bipolar charge of the membrane that occurs under applied voltage, along with the IL catalyst, drive the dissociation of water molecules into protons and hydroxide ions. Dissociation of water BPM operation is called reverse-bias operation. The CEL is then facing the negatively charged cathode, toward which the flux or protons is directed, while the AEL is facing the positively charged anode, attracting the OH^- ions [96]. Conversely, if either the BPM is reversed or the electric field is reversed by changing the flow of the current, the protons and anions flow towards the BPM where they recombine to form water. This mechanism is called forward-bias. BPM utilization in bicarbonate electrolysis can be seen in figure 2.10, which includes the flow-cell components. The HCO_3^- reacts with H^+ released from the BPM to form i-CO_2, which is then reduced at the cathode to form carbon products. The OH^- produced on the anode side drives the OER.

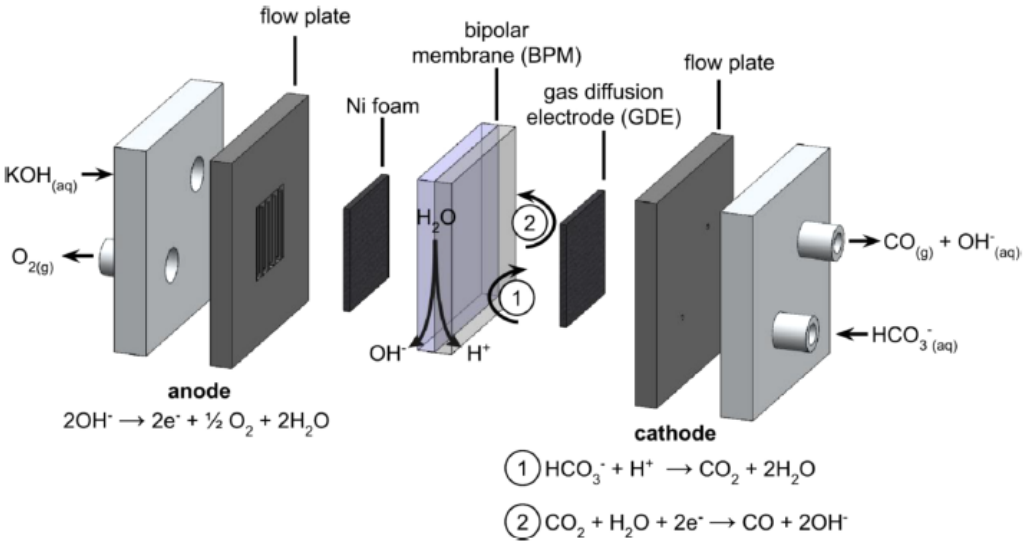

Figure 2.10: The components of a bicarbonate flow-cell operated by a BPM in reverse-bias [23]. Water disassociates at the BPM to form protons and hydroxide ions, which in turn drive the release of i-CO_2 for CO_2RR on the cathode side, and the OER on the anode side.

The benefit of using a BPM instead of a CEM or AEM is that it offers the possibility of creating separate, distinct environments on either side of the membrane [97]. This is beneficial in various scenarios where the optimal conditions differ for the reduction and the oxidation reactions. BPMs make it possible to use different electrolytes (catholyte and anolyte), and they make it possible to maintain a pH gradient across the membrane. Another advantage of BPMs is that the release of protons is proportional to the applied current density. This is a direct result of the fact that it is the voltage across the BPM, from the positively charged CEL to the negatively charged AEL, that causes the dissociation of water and proton production. Although this is beneficial in combating excessive HER, there is a certain energy loss involved due to this water dissociation overpotential. This overpotential is quite significant at high current densities, but an effective water dissociation catalyst can lower it, improving energy efficiency

[98]. The overpotential of BPM use remains a downside in their application, it is a reason many cite in opting for other membrane types. Research is being dedicated to combating the overpotential, and as such remains an active area of interest. BPMs have in addition been shown to block CO_2 cross-over and thereby reduce CO_2 losses [50, 99, 55].

Since BPM's conception in the 1950s they have mainly been used in acid/base reactions [100, 101]. In 2016 they were first used in CO_2RR [99, 102]. Since then there have been many advances made in their application. However, no energy conversion technology that utilizes a BPM has reached industrial scale yet [103]. To aid that development, BPMs with specifically tuned characteristics for each application must become commercially available. Understanding BPM function, effects on product selectivity and pH dependency is important because of CO_2RR high sensitivity to pH and contaminations [99].

2.7. Operating Conditions

2.7.1. Current density

Applied current density affects selectivity in CO_2 electrolysis, generally the higher the applied current, the lower the carbon product selectivity at the cost of increased HER, most likely because of faster H_2 kinetics including diffusion and mass-transport, adsorption and desorption. It is also known that the morphology of catalysts can undergo changes during electrolysis, changing the surface structure and oxidation state of the metal, thereby changing the selectivity. This is in part due to the applied voltage/current density, and becomes more apparent at high currents due to the increased strain on the catalyst as well as catalytic activity. At higher current densities in bicarbonate electrolysis, the selectivity of carbon products decreases and HER increases, dropping from about 40% at 100mA$/$cm^2 to about 15% at 300 mA$/$cm^2 due to the faster H_2 kinetics, as for example Lee et al. saw in their bimetallic CuAg study [45].

2.7.2. Electrolyte conditions

The effect of electrolyte flow rate on productivity was studied by Zhang et al. in their study using porous silver electrodes [37]. They conclude that by increasing the catholyte flow rate paired with an interdigitated flow pattern, CO selectivity improved. They attribute this to the higher convective mass transport resulting from the increased flow through the discontinuous channels of the flow plate. No study has been done on the effect of electrolyte flow rate and mass transport in (bi)carbonate electrolysis when using a GDE, to the author of this work's best knowledge. Most studies note their experimental setup, including the catholyte and anolyte flowrates, but usually do not specify why the values were chosen. Electrolyte volumes also vary depending on study, and are sometimes not mentioned. It is possible that volume also affects product selectivity, and that remains an open area of research.

2.7.3. Temperature and Pressure

Changing the operating temperature or pressure also affects selectivity in bicarbonate electrolysis. Zhang et al. showed that by increasing the inlet pressure of the 3M bicarbonate feed solution from 1 to 4 atm increased the CO FE from 55% to 95%, at 100 mA$/$cm^2 [37]. At higher pressures the solubility of CO_2 in the electrolyte increases [104], decreasing the unwanted carbonation back reactions between i-CO_2 as well as CO_2 breaking from the solution in gas form. They also saw that by raising the inlet temperature of the feed solution from 20°C to 70°C increased the CO FE from 59 to 78% at 100 mA$/$cm^2. The group expects the higher temperatures to increase the kinetics of HCO_3^- reaction to CO_2 and OH^-, increasing reactant availability for CO_2RR while simultaneously raising the pH, suppressing HER. Garcia et al. from the Sargent group also tested the effect of temperature on CO_2 electrolysis [105]. Using a Cu catalyst and gas-fed CO_2, they saw over 50% increase in C_{2+} selectivity at 60°C, compared with 20°C. They do however mention that despite higher temperatures increasing CO_2RR kinetics, they also cause lower CO_2 availability and thus productivity in alkaline electrolysers. The group does not cite a source for this, and it seems at odds with their own results, which clearly show higher CO_2 conversion rates at higher temperatures in their highly alkaline conditions of pH ≈ 15 (7M KOH electrolyte). Operating at higher pressures and temperatures involve more process complexity and higher energy cost, but the ulitmate effect on energy efficiency will depend on the ratio of the benefit of higher CO_2 conversion and product selectivity versus the higher energy cost. Indeed, Zhang et al. reported a rough 10% increase in cathodic energy efficiency when they raised the pressure from 1 to

4 atm. No other studies were found that studied the effect of temperature or pressure on selectivity in (bi)carbonate electrolysis. It should be kept in mind that increasing the temperature is not always possible and will depend on other parameters. For example, the maximum operating temperature of the hydrophilic porous membrane used by Lee et al. in their catalyst-membrane gap study [21], is 70°C.

2.7.4. Pulsed electrolysis

Pulsed electrolysis is a method that has surfaced as a way to improve product selectivity and electrolyser stability in CO_2 electrolysis. Pulsed electrolysis is generally carried out in rectangular potential pulse sequences. The cathode is then held at a cathodic potential for a fixed time period, and then the potential is switched to anodic for another fixed time period [106]. Several studies have been conducted in recent years on pulsed electrolysis in bicarbonate electrolysers using a Cu cathode, many of which reported increased C_{2+} selectivities and reduced HER under pulsed operation compared to static [106]. The reason for the increased efficiency during pulsed electrolysis is the transient access to optimal conditions on the Cu catalyst for CO_2RR [91]. These transient conditions and the positive effect are attributed in the literature to the formation of oxidized Cu species and reconstruction of the Cu surface, the removal of H_2 and carbon compounds from the Cu catalyst surface and the adsorption of OH^-, raising the local pH and CO_2 availability at the catalyst [107]. Often the cathode potentials have been chosen above and below the standard reduction potential of Cu (+0.42 vs RHE), in which case the catalyst morphology is under constant reconstruction due to its oxidation and reduction [91]. Importantly, higher carbon product selectivity and reduced HER has also been seen when the potentials chosen were both more negative than the standard reduction potential of the Cu catalyst. In these cases at least, it is not the catalyst´s structure or oxidation state that is the cause of the improvements, rather changes in the catalyst's microenvironment.

Kim et al. from the Bell research group have published 3 papers in recent years where they study among other things the benefits of pulsed electrolysis in CO_2RR on Cu. In 2020, they showed how the H_2 FE can be decreased from 22% to 11% and the C_{2+} product FE can be increased from 68% to 81%, which they attribute to the increased ratio of CO to H_2 adsorption on Cu during pulsed electrolysis [106]. In addition, they found that the ratio of oxygenated to hydrocarbon products increased, from 0.62 to 0.86. The group alternated between -1.15 V (vs RHE) and -0.8 V (vs RHE) at the cathode, holding the -1.15 V for 25s and varying the -0.8 V pulses. The optimum time for the -0.8 V pulses was found to be 10s. According to the authors, four variables need to be defined for pulsed electrolysis investigation, namely the potential and time duration of each potential [106]. In 2021, the group investigated ionomer coated Cu catalysts, optimizing the catalyst microenvironment (section 2.2.2). After optimizing the ionomer composition and layering, when coupled with pulsed electrolysis the group achieved 90% C_{2+} FE, with just 4% H_2 [54]. They alternated between the same potentials as in their previous study, but this time alternated every 10s. The success of the pulsed electrolysis the group attributes to the same mechanism that saw the optimum catalyst-ionomer layering being CuSusNaf, i.e. high pH in the CL caused by OH^- ion trapping (due to the anion conductive Sustanion and the anion repellive Nafion) and high CO_2:H_2O ratio, caused by Sustanion's high CO_2 solubility. These conditions were magnified under pulsed electrolysis, leading to the high C_{2+} production and low HER, according to the results. In 2022, the Bell group published another paper, where they detail their results from the 2021 study as well as developing a model to further explain the differences in the catalyst microenvironment between pulsed and static electrolysis [91].

Timoshenko et al. conducted pulsed electrolysis on a Cu_2O nanocube catalyst [107]. They alternated between oxidizing and reducing potentials of -1.0V (vs RHE) and +0.6V (vs RHE), with the duration of the restoring anodic pulse of +0.6V just 0.5s, producing Cu oxide species. Their main result was a twofold increase in ethanol production, when compared with static electrolysis. It is clear that pulsed electrolysis can be beneficial in improving C_{2+} product selectivity. However, the downtime during anodic potential pulses and the associated loss of production must be weighed against the selectivity benefits. This trade-off of higher selectivity and production downtime does not receive much attention in the literature on pulsed electrolysis, and so should be scrutinized thoroughly, especially for scale-up considerations.

Most of the pulsed electrolysis literature feeds gaseous CO_2 into the electrolyte, and uses Cu catalysts.

One study was found that performed pulsed electrolysis using purely (bi)carbonate as the carbon donor and Ag catalyst. Azumi et al. demonstrated similar improvements on selectivity and stability using Ag catalyst as have been observed with Cu catalysts [108]. Using a Ag plate electrode and carbonate electrolyte, they found up to 14% improved CO FE when periodically setting the potential at 0. Importantly however, they only did experiments at very low current densities, recording at most about 3 mA/cm^2 partial current density of CO. Such low current densities provide little insight into operation at meaningful production rates. The impact of pulsed electrolysis using Ag catalysts paired with (bi)carbonate electrolytes at meaningful current densities is thus as of yet unknown.

3

Methodology

3.1. Design of Experiments

The Design of Experiments (DoE) of this study refers to the planning, executing, results analysis and subsequent reevaluation during the experimental phase. Specifically, it incorporated the following parts:

1. Identification of key parameters for the process of CO production from bicarbonate
2. Planning experiments to test identified key parameters
3. Execution of experiments
4. Analysis and interpretation of results, including parameter interactions that positively affect performance and parameter interactions that negatively affect performance
5. Reevaluation of key parameters based on results, followed by repeating steps 2-5

Due to the highly experimental nature of the project, hypotheses were constantly under reevaluation based on findings. Experiments were performed in duplicates, occasionally triplicates, acquiring statistical data that granted information about the validity of the results. Due to time constraints towards the end of the experimental phase, some of the last executed experiments were not performed in duplicates.

3.2. Materials, Consumables and Equipment

In tables 3.1 and 3.2 information about the materials, consumables and equipment used in this study can be found, as well as the supplier for each item.

3.3. Methods

3.3.1. Electrode preparation

The electrodes used in this study were prepared by first cutting the carbon paper substrate (the GDL), either Freudenberg H23 or Sigracet 39BB (Fuelcell Store), into pieces of 3x2.5 cm^2 using a box cutter and ruler. The substrates were kept 3cm on one side to allow for extra space to keep them in place during spray-coating. The edges were then cut off post spray-coating to get the final 2.5x2.5 cm^2 electrodes. The 3x2.5 cm^2 carbon papers were sonicated in acetone for 10 minutes, and subsequently DIW (deionized water, milliQ water) for 10 minutes, rinsing thoroughly in between with DIW. The electrodes were then dried on an aluminum foil covered hot plate for about 15 minutes at 100°C, turned over once about half-way through to ensure complete drying. The electrodes were then weighed to determine their dry weight pre-spray-coating.

The catalyst-ionomer ink was prepared by pipetting 8 ml of IPA into an 8ml vial, 80 μL of ionomer binder (Nafion 1100W 5%, Sigma Aldrich or Sustanion XA-9 5%, Dioxide Materials) and 84 +/-5 mg of Ag catalyst NP (nanoparticles). The catalyst NP were weighed in a fume-hood using weighing paper, subsequently poured into the vial by folding the weighing paper and creating a funnel-type opening in the paper. For the PTFE containing ink, 10.9g of PTFE granules (>40μm, Sigma Aldrich) were weighed

Table 3.1: A list of the items and consumables used in the study. *The supplier for the silicone rubber gasket is unknown as it originated from a past PhD student.

Item/Consumable	Supplier
Peroxide cured EPDM sealing set, 0.5mm	ElectroCell
Silicone rubber gasket, 0.2mm	Unknown*
Polypropylene mesh for anolyte	ElectroCell
PTFE tubing, naturel 3.96x6.35 mm (IDxOD)	Polyfluor
LongerPump Platinum-cured Silicone Tubing	Darwin Microfluidics
Ni flow plate, 2.0mm	ElectroCell
Ti flow plates, 1.0mm	ElectroCell
Stainless-steel flow plate, 1.5mm	ElectroCell
BPM	Fumasep FBM-PK
Freudenberg H23 carbon paper	Fuelcell Store
Sigracet 39BB carbon paper, with 5%PTFE MPL	Fuelcell Store
Nickel foam, 2mm (approx 75 PPI)	ElectroCell
MCE hydrophilic 8.0um membranes	MF-Millipore
MilliQ water, 1.7 ppb TOC	NA
Acetone, 99%	VWR Chemicals
Isopropanol (IPA), 98%	VWR Chemicals
Ag Nanoparticles, 20-40nm	Thermo Fisher Scientific
Cu Nanoparticles, 25nm	Sigma Aldrich
Nafion 1100W 5wt% in water and propanol	Sigma Aldrich
Sustanion XA-9 5wt% in EtOH	Dioxide Materials
$KHCO_3$, 99.95%	Sigma Aldrich
K_2CO_3, 99.0%	Sigma Aldrich
KOH, 85.0%	Sigma Aldrich
NaCl, 99.5%	Sigma Aldrich
PTFE powder, 40um	Sigma Aldrich
Silica gel granulate 1-3mm (orange gel)	Sigma Aldrich
Argon gas	Linde
Nitrogen gas	Linde
Aluminum foil	Thermo Fisher Scientific

Table 3.2: Information about the equipment used in the study.

Equipment	Type/model	Supplier
Flow-cell	Micro Flow Cell 10 cm^2 MFC30010	ElectroCell
Potentiostat	SP-200	Biologic Science Instruments
Pump	BT100-3J Basic Peristaltic Pump	Darwin Microfluidics
Pump heads	LongerPump YZ1515X-B	Darwin Microfluidics
MFC/MFM	EL-FLOW	Bronkhorst High-Tech
GC	Compact GC 4.0	Interscience
HPLC	1260 Infinity II	Agilent Technologies
ICP-OES	Spectro Argos	Sysmex
SEM/EDS	JSM6500F	JEOL
Ultrasonic bath	2800 Ultrasonic cleaner 2.8L	Branson
Spray-gun	Custom Micron Absolute Precision	Iwata
Stirrers/heaters	UC152D	Stuart
Stirrers	Topolino	Ika
Scales	ME204/MS204S/PR8002	Mettler Toledo
Vortex	Vortex Genie 2	Scientific Industries
Pipettes	Finnpipette F1, 10-100ul/100-1000ul/1-10ml	Thermo Fisher Scientific

into 6 ml of IPA along with 44.9mg Ag NP and 30μL Nafion. For the bimetallic Ag-Cu experiments, 66 +/-5 mg of Ag or Cu NP were weighed into 6ml of IPA, and 360μL of ionomer (Nafion for the Ag ink, Sustanion for the Cu ink) added. For the PTFE Ag-Cu experiments, 27.5mg of PTFE was weighed into 8ml of IPA along with 88 +/- 5mg Ag NP and 480μL Nafion. The ink was sonicated for 40 minutes in an ultrasonic bath (2800 Ultrasonic cleaner 2.8L, Bransoln) and used within 30 minutes.

The carbon papers were spray-coated with the catalyst ink in a specially prepared fume-hood (picture ref.) using a spray-gun (Custom Micron Absolute Precision, Iwata). For coating, 2 ml of ink was pipetted into the aluminum ink cup at a time. Just prior to pipetting the ink was vortexed for 5 seconds to ensure complete mixing. Catalyst loading was kept at 1.0 - 1.8mg/cm2. During spray-coating of the catalyst ink the carbon papers were kept on an aluminum foil covered hot plate, which was set to 70°C to ensure rapid evaporation of the IPA and settling of the Ag-Nafion layering. Nitrogen gas was used for the spray-coating at a pressure of 0.6 barg. After applying the ink on the carbon papers, the electrodes were kept to dry on the 70°C hotplate for about 10 minutes to ensure all IPA had evaporated. They were then weighed and kept in petri dishes in a desiccator under vacuum.

For the catalyst surface coverage experiments, a thin layer of Ag catalyst was sputtered on top of the GDL (H23 Freudenberg or Sigracet 39BB) using direct current magnetron sputter deposition technique - a form of physical vapor deposition (PVD). A layer of 500nm was sputtered at a pressure of 3 μbar in Ar at a rate of 3.125 Å/s. Acknowledgement and appreciation go to Siddhartha Subramanian, PhD candidate, who performed the PVD.

For the anode Ni foam (2mm thick, about 75PPI (pores per inch), ElectroCell) was used. It was cut into 2.9x3.3 cm^2 using a box cutter and ruler. The Ni foam anode was sonicated in DIW for 10 minutes for cleaning, and kept in DIW until use. A picture of the Ni foam anode pre and post electrolysis can be seen in figure B.1 in appendix B.

For experiments using interposers (spacers), hydrophilic mixed cellulose ester (MCE) membranes were used (MF-Millipore). The membranes had a thickness of 135 μm and pore size of 8.0 μm, with a diameter of 47 mm. They were cut into 2.5x2.5 cm^2 using scissors. Prior to experiments the interposers were rinsed with DIW and wetted in 3M $KHCO_3$ for 5 minutes.

The BPM used in this study was Fumasep FBM-PK. It was cut into 4.6x9.6 cm^2 using a box cutter, matching the dimensions of the sealing gaskets. In order to always know which side was the cathodic, the bottom right part was cut off with the cathodic side facing up. The BPM was stored in 1M NaCl. BPMs were reused in this study multiple times but exchanged regularly.

3.3.2. Electrolyte preparation

The catholyte in this study was 3M $KHCO_3$. The 3M catholyte was prepared by first weighing 300.36 g (+/- 0.5g) of $KHCO_3$ (Sigma Aldrich, 99.95%) into a beaker. About 500 ml of DIW was then added to the beaker and the solution transferred to a 1 L volumetric flask using a funnel while stirring. The flask was then filled to the 1 L mark and the $KHCO_3$ dissolved by magnetic stirring for about 3-4 hours until completely dissolved. Low heat was applied while stirring to help with the dissolving, while still maintaining the solution temperature below or at room temperature. The average pH of the 3M bicarbonate buffer preparations was 8.07 (based on $[H^+]$, standard error of 0.06 based on pH measurements). For the bicarbonate/carbonate buffers of pH 8.5 and 9.5, with the cation K+ molarity maintained at 3M, 500ml of each buffer was prepared. For the pH 8.5 buffer 137.0g of $KHCO_3$ and 8.9g of K_2CO_3 (Sigma-Aldrich >/= 99% purity) were weighed and dissolved in 500ml of water. For the pH 9.5 buffer 77.45g of $KHCO_3$ and 50.24g of K_2CO_3 were weighed and dissolved in 500ml of water. For pH calculations refer to section 3.5.4.

The anolyte used in this study was 1M KOH. The anolyte was prepared by weighing 56.11 g (+/-0.1g) of KOH pellets (Sigma Aldrich, >85.0%) into a 1 L volumetric flask and filling to the mark with DIW. The average pH of the 1M KOH preparations was 13.72 (based on $[H^+]$, standard error of 0.03 based on pH measurements).

3.3.3. Flow-cell set up and electrochemical experiments

The flow-cell was assembled in-house. It was a Micro Flow Cell 10 cm^2 MFC30010 from ElectroCell. All the components of the flow-cell can be seen in figure 3.1, with numbers corresponding to each component. The cell was assembled from the anode side up by first placing the anode cell housing (1) on a small jar for ease of assembly. A 0.5mm EPDM sealing gasket (2) was placed on the anode cell housing followed by the anode current collector (3), which was made of Ni. Polypropylene meshes (5) were placed where the flow enters and exits the anode part of the cell to break up the flow into the anode (6), which was placed between the meshes in the middle of an EPDM sealing gasket (4). For the anode 2mm thick Ni foam was used (ElectroCell) The BPM (7) was placed on top of the anode. A thin silicone gasket (8) of thickness 0.2mm was placed on the BPM, with 2.5x2.5 cm^2 space in the middle for the cathode (9), which was placed there with the catalyst side face down. Next the cathode flow plate (10, cathodic current collector) was placed on top of the cathode. The cathode flow plate was made of Ti and had interdigitated flow pattern with channel dimensions of 1.0mm x 1.0 mm (depht x width). After the cathode flow plate another EPDM sealing gasket (11) was placed in the assembly, followed by the cathode cell housing (12). The flow-cell was then closed evenly with 6 bolts (13), tightening the bolts oppositely for even pressure application. The bolts were tightened with a torque wrench to a pressure of 3 Nm. Other flow plates used in this study had Serpentine flow pattern dimensions 1.0mm x 0.7mm and 1.0mm x 1.5mm (depht x width), and interdigitated of dimensions 1.0mm x 1.5mm (deph t xwidth). All cathode flow plates had thickness 1.0mm and were made of Ti, except for the 0.7mm channel dimension Serpentine flow plate, which was made of stainless steel. The anode Ni flow plate had thickness of 2.0mm. The flow-cell assembled along with an interior view showing the cathode placement in the silicone gasket can be seen in appendix B, figures B.2 and B.3.

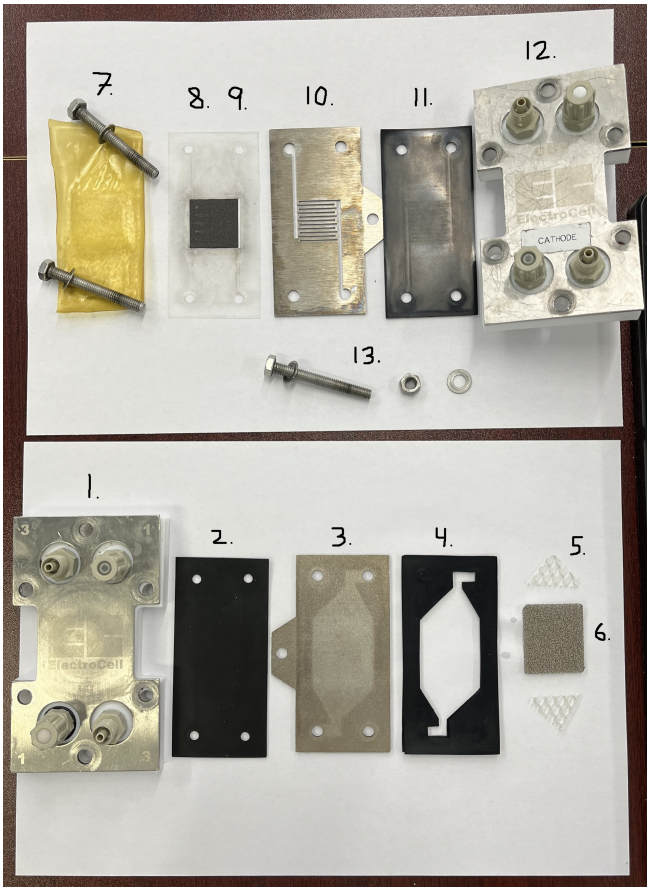

Figure 3.1: The components of the electrochemical flow-cell used in the study. 1 and 2: Flow-cell housings; 2, 4 and 11: EPDM sealing gaskets; 3: Ni anode flow plate; 5: PP flow meshes; 6: Ni anode; 7: BPM; 8: Silicone gasket; 9: Cathode; 10: Ti cathode flow plate; 13: bolt, nut and washer.

The 3M $KHCO_3$ catholyte volume was 70 ml, while the anolyte 1M KOH volume was 140 ml. For 14 hr overnight experiments the electrolyte volumes were 1L and 0.5L, respectively. The electrolyte reservoirs were connected to the flow-cell via tubings (material, vendor), passing through the pump (BT100-3J Basic Peristaltic Pump, Darwin Microfluidics). A secondary pump head (LongerPump YZ1515X-B, Darwin Microfluidics) was added for the anolyte so the same pump could be used for both electrolytes. The pump was set to 45.5 RPM which translates to 50 ml/min electrolyte flow.

The potentiostat used in this study was a SP-200 from Biologic Science. Leads equipped with alligator clips were used to connect the potentiostat to the cathode and anode flow plates (current collectors). The software to control the potentiostat was EC-lab. The experiments were operated in chronopotentiometric fashion, i.e. where the current was controlled. The current was set at 500 mA corresponding to 100 mA/cm^2 as the cathode active area was 5 cm^2 (Interdigitated 1.0mm flow plate).

The gas products formed on the cathode side of the flow-cell were analysed by a gas chromatograph (Compact GC 4.0, Interscience). It was equipped with two thermal conductivity detectors and one flame ionization detector. Samples were measured at 3 minute intervals during the experiments. Argon was used as carrier gas in this study, at a flow of 100 ml/min. The gasflow was controlled via an EL-Flow Bronkhorst mass-flow controller (MFC) through the software Flowsuite. The gas line was connected to the inlet tube of the catholyte reservoir (the outlet tube from the cell) where it passed through the tube and into the catholyte via a diptube. A second gas outlet line led from the catholyte reservoir to a liquid trap filled with silica beads, which was to protect the succeeding mass-flow meter (MFM, EL-Flow, Bronhorst) from moisture. The MFM preceded the GC and was used to determine the total gas output flow from the system to the GC. Both the MFC and the MFM used in this study were calibrated for CO_2. In order to convert the CO_2 flow to Ar flow, as well as the gas output reading to include the Ar and products, gas conversion factors were used (see calculations below, equations 3.8-3.10).

Experiments were run for between 30 minutes to 14 hours. The experiments were conducted in a fume-hood. An example of the electrochemical setup during operation can be seen in figure 3.2. Electrolyte samples were taken post experiments for pH measurement, liquid product detection and metal detection. The electrodes were kept for SEM/EDX testing post electrolysis.

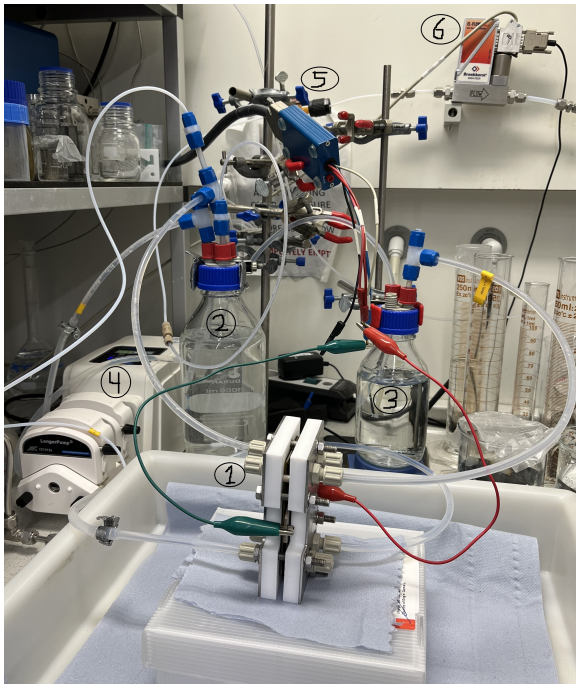

Figure 3.2: An example of the flow-cell in operation. Labeled in the picture are: 1: The flow-cell, 2: The 3M bicarbonate catholyte buffer, 3: The 1M potassium hydroxide anolyte, 4: The electrolyte pump, 5: The potentiostat connection, 6: The massflow-meter. In this picture the electrolyte volumes are 1L and 0.5L (catholyte and anolyte respectively), as this is from the overnight 14 hour CO stability set of experiments.

3.4. Chemical Reactions and Species

The carbonate equilibria system is an acid-base buffer system that involves the balance of carbonic acid, bicarbonate, carbonate and carbon dioxide. The reactions in a neutral water system are as follows, with the equilibrium constants noted for STP conditions:

$$CO_2 + H_2O \rightarrow H_2CO_3 \qquad K = 3.47 \cdot 10^{-2} \tag{3.1}$$

$$H_2CO_3 \rightarrow H^+ + HCO_3^- \qquad K = 4.37 \cdot 10^{-7} \tag{3.2}$$

$$HCO_3^- \rightarrow H^+ + CO_3^{2-} \qquad K = 4.68 \cdot 10^{-11} \tag{3.3}$$

$$CO_2 + H_2O \rightarrow H^+ + HCO_3^- \qquad K = 1.51 \cdot 10^{-8} \tag{3.4}$$

$$CO_2 + H_2O \rightarrow 2H^+ + CO_3^{2-} \qquad K = 7.08 \cdot 10^{-19} \tag{3.5}$$

The dissociation of water equilibrium was used to determine the concentration of protons and hydroxide ions based on the pH (reaction 3.6):

$$[H^+] \cdot [OH^-] = 1 \cdot 10^{-14} \tag{3.6}$$

3.5. Calculations

3.5.1. FE and GCFs

The Faradaic Efficiency (FE) of product i was calculated by dividing the partial current (i_c) of product i with the overall applied current I 3.7:

$$FE_i = \frac{i_{c_i}}{I} = \frac{c_i \cdot n_{e^-} \cdot P \cdot F \cdot Q_r}{R \cdot T \cdot I} \tag{3.7}$$

Where c is the concentration of product i (ppm); n_{e^-} is the amount of electrons transferred in the overall reduction reaction of product i, P is the pressure; T is the temperature; F is the Faraday constant (96485 $s \cdot A \cdot mol^{-1}$), R is the gas constant ($Pa \cdot m^3 \cdot mol^{-1} \cdot K^{-1}$) and Q is the total flow of gaseous species ($m^3 \cdot s^{-1}$). The concentration of the product was found by fitting the measured area (a.u., absorbance units) of the product, as measured in the GC, on a calibration curve for said product. All experiments in this study were performed at ambient pressure (101325 Pa), and room temperature (273 K). The flow of gases, Q, includes the gaseous products, unreacted CO_2 as well as the carrier gas Ar. As the GFC and MFM were calibrated for CO_2 flow, the measured output signal of the gas flow (Q_m) had to be corrected to represent the actual gas flow of Ar including products and CO_2 (Q_r). To do so the gas conversion factor of the mixture (GCF_{mix}) was calculated for each GC measurement, using the measured concentration and calculated gas conversion factor (GCF) of each component, then correcting the signal for the actual flow, as per equations 3.8-3.10. The GCF and signal correction calculations were based on the Bronkhorst manual, from the MFM supplier Bronkhorst [109].

$$GCF_i = \frac{\rho_{N_2} \cdot c_{pN_2}}{\rho_i \cdot c_{pi}} \tag{3.8}$$

Where ρ is the gas density ($g \cdot L^{-1}$) and c_p ($cal \cdot g^{-1} \cdot K^{-1}$) is the specific heat of the gas.

$$GCF_{mix} = \left(\frac{c_i}{GCF_i} + \frac{c_{i+1}}{GCF_{i+1}} + ... + \frac{c_n}{GCF_n} + \frac{10^6 - (c_i + c_{i+1} + ... + c_n)}{GCF_{Ar}} \right)^{-1} \cdot 10^6 \tag{3.9}$$

$$Q_r = Q_m \cdot \frac{GCF_{mix}}{GCF_{CO_2}} \tag{3.10}$$

3.5.2. CO_2 utilization

Amount of i-CO_2 (in-situ CO_2) generated was calculated via equation 3.11 and CO_2 utilization to product i via equation 3.12.

$$i - CO_2 = C_{CO_{2,unreacted}} + \sum (n \cdot C_i) \tag{3.11}$$

$$CO_{2,util,i} = \frac{C_i}{i - CO_2} \tag{3.12}$$

Where C_i is the concentration of product i in mmol/L and n is the amount of carbons in product i. When using Ag catalyst, the only products are C_1, but for the experiments with CuAg catalyst, C_2 products are also formed.

3.5.3. Mass and charge balance

A carbon mass balance was set up to check the validity of the measurements and calculations. Total carbon into the system equals total carbon that comes out:

$$C_{in} = C_{out} \tag{3.13}$$

The starting molarity of the bicarbonate is 3M, which in solution will be distributed among the carbonate species according to the equilibrium constants (see carbonate equilibria reactions 3.1-3.5):

$$C_{in} = [KHCO_3]_{in} = 3M = [H_2CO_3]_{in} + [HCO_3^-]_{in} + [CO_3^{2-}]_{in} \tag{3.14}$$

The concentration of carbon species coming out of the system will contain the carbonate species in equilibrium along with carbon products and CO_2.

$$\begin{aligned} C_{out} &= C_{Carbonate\ species} + C_{products} \\ &= [H_2CO_3]_{out} + [HCO_3^-]_{out} + [CO_3^{2-}]_{out} + C_{products} + CO_{2,unreacted} \end{aligned} \tag{3.15}$$

Where $C_{Carbonate\ species}$ is the concentration of carbonate species and $C_{products}$ is the concentration of carbon products. The concentrations of the carbon products were measured via GC and HPLC. To convert from unit ppm to molarity, the following formula was used (equation 3.16):

$$M_{gas} = \frac{ppm_{gas} \cdot \frac{1\mu L\ gas\ volume}{1 \cdot 10^6 \mu L\ air\ volume} \cdot \rho_{gas}}{MW_{gas}} \tag{3.16}$$

Where ρ [$g \cdot L^{-1}$] is the gas product density and MW_{gas} [$g \cdot mol^{-1}$] is the molar weight of the gas product. The concentrations of the carbonate species depends on the pH of the solution as the carbonate buffer system is an acid-base equilibrium. The relative concentrations of the carbonate species, pre and post electrolysis, were calculated based on the measured pH values. That was done by solving a system of equations in python, i.e. with 3 unknowns being the 3 carbonate species, and using 3 equations: carbonate reactions 3.2 and 3.3 along with the charge balance of the bicarbonate buffer (reaction 3.17):

$$[H_2CO_3] + [HCO3^-] + 2[CO_3^{2-}] = [H^+] + [K^+] \tag{3.17}$$

Where the concentration of potassium ions, $[K^+]$, is 3M, as per the initial concentration of $KHCO_3$. In these calculations the effect of CO_2 in the equilibria was neglected for simplicity.

3.5.4. pH calculations for buffers

The electrolyte pH was measured pre and post electrolysis. The theoretical pH of the 3M bicarbonate buffer was compared with measured values. To calculate the theoretical pH the average of the pK_a values for reactions 3.2 and 3.3 was taken. This simple calculation can be done since bicarbonate in water is amphiprotic, meaning it acts as both an acid and a base (equation 3.18):

$$pH = \frac{pK_{a,1} + pK_{a,2}}{2} \tag{3.18}$$

To prepare the bicarbonate-carbonate buffers of pH 8.5 and 9.5, the same 3 equations as above were solved with the same unknowns, with the addition of the fourth equation being the carbon mass balance (equation 3.15) and a fourth unknown being the total concentration of carbon species, C_{tot}, as the concentration of potassium was kept constant at 3M for the preparation of these buffers. It should be noted that for these calculations, the target pH of the buffers was 9.0 and 10.0 respectively, and the

resulting species concentrations used in the calculations were based on that. However the measured experimental pH values were lower, 8.5 and 9.5. This can be because of experimental variability compared to theory, but also because CO_2 equilibria were disregarded.

Python code for the calculations can be found in appendix B, figure B.4.

3.6. Liquid Product Detection

Post experiments, catholyte samples were analyzed for liquid products using a high-pressure liquid chromatograph (HPLC) (1290 Infinity II, Agilent). 5 µl of sample was injected into two Aminex HPX-87 H columns (Biorad) which were aligned in series. The columns were heated to 60 °C, the eluent was 1 mM H2SO4 in milliQ water and a refractive index detector (RID) was used for the detection of products.

3.7. Electrode Characterization

SEM (Scanning Electron Microscopy) and EDS (Energy Dispersive Spectroscopy) were performed to characterise the cathode surface areas pre and post electrolysis. The SEM/EDS was done using a JSM6500F from JEOL. For SEM the working distance was set at 10cm, the voltage used was 15kV and the resolution 1280x1024 pixels. For EDS the working distance was 25cm and the resolution 256x202 pixels.

3.8. Metal Detection

Post experiments, a sample of the catholyte was measured for metals using an ICP-OES (Inductively Coupled Plasma - Optical Emission Spectrometry, Spectro Argos from Sysmex).

4

Results and Discussion

4.1. Overview

In this chapter the results of the study are presented. First, a brief overview of the different parts of the experimental work is provided, outlining the goal of each segment, the variables studied and experiments conducted. Second, each segment is discussed in more detail. Here perspective on the study with regard to current literature is presented, explaining why the experiments were chosen. Next the experiments and conditions are outlined, followed by the results and finally discussion. Intermediate conclusions are provided at the end of each segment.

The experimental part of the study can be divided into five parts: Initial tests; Parameters for CO selectivity; CO stability; Effect of bulk pH and finally Bimetallic Cu-Ag electrolysis. The five parts are presented in a flowchart below (figure 4.1, which includes the goals of each segment and variables tested. The first experimental part aimed at gathering understanding on the system and establishing good working conditions and parameters for the remainder of the study. A few initial factors were tested to see if they had a significant impact on CO selectivity. In the second segment key factors that influence CO selectivity were examined, with the goal to improve CO selectivity. Here hydrophilic and hydrophobic carbon paper supports were compared in unison with surface coverage and flow patterns. A gap between the catalyst and bipolar membrane (BPM) was also introduced. The third part revolved around characterising the long-term stability of the process of bicarbonate reduction to CO, and examining ways to improve that stability. Stability is defined in this study as the change in selectivity over time. Here 3 hour and 14 hour runs were carried out, comparing the stability of systems with different catalyst-BPM spacing. Pulsed electrolysis was also tested. In the fourth segment of the experimental phase, the effect of catholyte pH on CO selectivity and stability was examined. Inlet (starting) pH was varied as well as studying constant (single-pass) pH. Finally, initial experiments using bimetallic Cu-Ag catalysts were carried out in part five, with the aim to see how the system optimisation carries over to bimetallic catalyst operation. This segment can be viewed as an addition to the main topic to serve as a reference for future outlook.

In total about 100 experiments were carried out in the course of this study. Experiments were performed in duplicates except otherwise mentioned, with error bars shown on graphs calculated as standard errors (via standard deviation). For each experiment electrodes were prepared as explained in the methodology (chapter 3). An overview of the experiment results presented here can be found in table C.2 in appendix C.7. Liquid products were not measured for all runs as the only product formed was formate, and always in low quantities ($\leq 4\%$). As such, formate was omitted when presenting and discussing the results. For reference, an overview of liquid product measurements can be found in table C.5 in appendix C.7. The potential profiles of the 100 mA/cm^2 controlled current operation showed little changes over time or when changing parameters, with the full cell potential measured between 3.4 and 3.7 V. As energy efficiency is outside of the scope of this project, emphasis was not placed on reporting potential trends. In the experiment result overview in table C.2, average cell potentials are recorded. In section C.6 in appendix C examples of potential profiles from experiments can be seen.

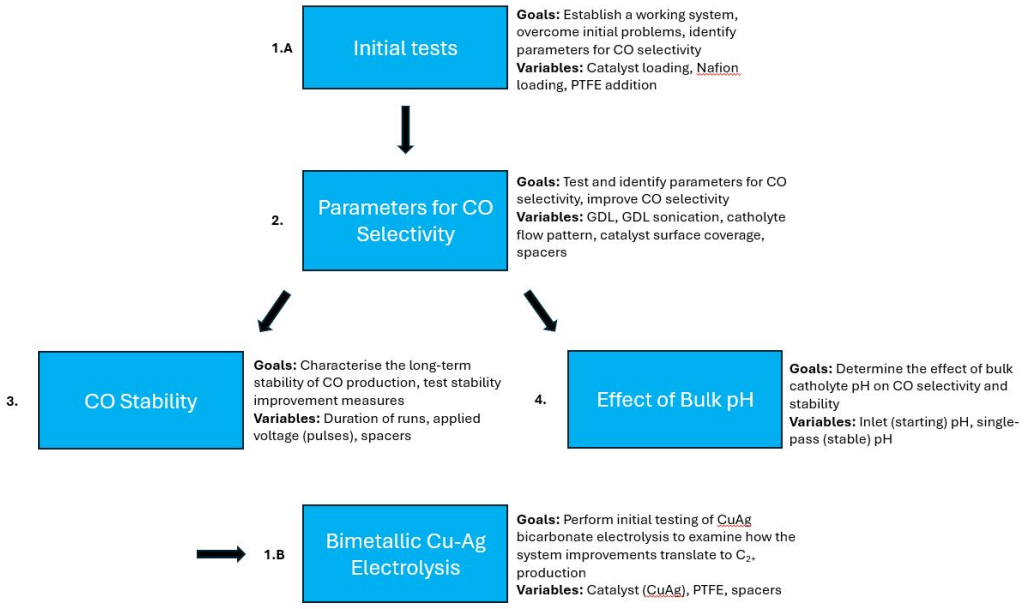

Figure 4.1: A flowchart showing the different parts of the experimental phase, includuing the goals and variables of each segment.

4.2. Initial Tests

4.2.1. Ag, Nafion and PTFE loading

The goal with the initial experimental phase was to establish the cell and operating parameters for the system and to achieve 30-40% CO FE, reproducing state-of-the-art literature results. This part included the process characterisation, i.e. defining electrode preparation methods and basic cell and operating parameters; and method of calculating results. This provided the basic process that was used in subsequent experiments for varying factors for process improvement in terms of CO selectivity and stability.

Factors that were varied in the initial part include the silver catalyst loading, Nafion loading and PTFE addition in the catalyst layer (CL). The catalyst loading experiments were performed to see whether CO selectivity was dependent on catalyst loading. It is hypothesised that there exists an optimum Ag catalyst loading, where too low loading would result in insufficient catalyst surface coverage of the gas diffusion layer (GDL) and thereby increased HER; and too high loading would result in increased HER through easier access by protons to active catalyst sites that are not reachable by CO_2, by virtue of diffusion distance and thickness of CL, as increased diffusion distance of CO_2 increases the rate of carbonation reactions. Nafion loading experiments were conducted based on results from Lees et al., who found that Nafion loading was optimal between 2.5 and 11.5 wt%, specifically 4wt%. The goal was to verify that Nafion loading is important in bicarbonate electrolysis, expecting lower CO selectivity at 30wt% due to more of the catalyst being covered by Nafion, reducing active surface area.

The results of the initial experiments discussed here can be found in appendix C, figure C.1. The results of these experiments were inconclusive, with no significant impact on CO production seen, as the CO FE remained around 30% for all variables, lower than reported literature results at the same current density of 100 mA/cm^2 (see 2.2), which are in the range of 30-80%, depending on system parameters. This does not prove that catalyst and ionomer loading does not affect CO selectivity, but in the range tested (1-3 mg/cm^2 Ag catalyst and 3-30wt% Nafion), for the system used in this study, there is no impact observed. The expectation was that the 30wt% Nafion would show lower CO selectivity, which was not the case. This might be due to different cell factors when compared to the study of Lees et al. Namely, interdigitated flow pattern and hydrophobic 39BB is used in this study compared to serpentine flow pattern and hydrophilic H23 in the Lees et al. study. These system differences prompted a closer look at the role of catholyte flow pattern and the GDL in bicarbonate electrolysis (see sections 4.3.1 and 4.3.2). As no difference was seen for catalyst and Nafion loading variations, for the remainder

of this study the catalyst loading was kept between 1 and 1.8 mg/cm^2 and the Nafion loading was kept 4wt%. That loading range is also in line with results from Lees et al., where the optimum Ag loading was found to be 1.3 mg/cm^2, and the Nafion content to be 4wt% [23]. The group did however first deposit a 500nm Ag film by PVD pre spray-coating, as discussed in section 2.2.3. The group did not test the effect of catalyst loading without a PVD film. The effect of catalyst surface coverage on CO selectivity is further examined in section 4.3.4. PTFE of 20wt% was included in the Ag catalyst layer for the PTFE experiments to examine whether increased hydrophobicity would lead to improved CO selectivity through HER suppression. However, as can be seen in graph c) in figure C.1, no effect was noted. It is possible that any improvement in CO selectivity is negated by reduced CO_2 to CO conversion as less catalyst active sites are available with the added PTFE covering much of the catalyst.

4.2.2. Troubleshooting - Defining how results are reported

During an investigation into system and operating conditions as well as literature to discover the cause of the limited CO production, it was uncovered that in the (bi)carbonate literature there seems to be a lack of explanation regarding how the results are reported, specifically whether they are single measurements or averages over time, and if they are averages, over which time periods. Through email correspondence with a member of the Berlinguette group, it was verified that the values reported are indeed single measurements, i.e. peak measurement values, taken after 5 minutes of electrolysis (Yong Wook Kim, email correspondence, 23FEB2024 - 06MAR2024). Following that discovery, the results of the initial experiments (catalyst, nafion loading and PTFE addition) were recalculated, averaging over the first 20 minutes of the experiments, giving around 35% CO FE, with peak values around 40%. Figure C.2 in appendix C.1 provides a view of the different results that can be optained by varying the calculation method. This discovery also highlighted what seems to be a trend in the (bi)carbonate literature to focus on peak production values, and to overlook stability of production over time. This prompted a separate stability study, which can be found in section 4.4. During this investigation into the cause of the limited CO production a table was prepared which provided a comparison of various cell and operating parameters between this study and comparable studies (table C.1 in appendix C.7).

During the investigation into the cause of lower CO production, it was also discovered that the pH of the catholyte was unusually high. It was measured at 9.45, significantly higher than the theoretical pH of a bicarbonate buffer of 8.35. It is unclear what caused this high pH, as the preparation of the buffer remained the same throughout the study. However, regular maintenance was carried out on the milliQ water dispenser around the same time, where a filter was exchanged, after which, the pH of the bicarbonate buffers were measured in the range of 8.0 - 8.26. It is possible the filter changing coincides with the variation of the catholyte pH, but as there is no record of when it was performed and no samples remain it cannot be verified. An average bicarbonate pH of subsequent preparations was 8.07 (based on $[H^+]$, with a standard error of 0.06 based on pH measurements). As pH was now suspected to be a factor in limited CO selectivity in the system, it was measured before and after each run for the remainder of the study for control, as well as for each electrolyte lot, and it's effect was studied specifically in a separate set of experiments (see section 4.5).

NiO_2 tends to form on the nickel (Ni) foam anode during operation. This can be noticed by the blackening of the Ni, which dissipates slowly over time if the Ni is kept in water, or if sonicated. However it is unlikely that NiO_2 formation on the anode affects CO selectivity or stability, rather it most likely contributes to increased overpotential due to the NiO_2 limiting the active surface area of the Ni as well as the conductivity of the anode due to NiO_2's insulating effect. As energy efficiency is outside of the scope of this study, it was not examined further. However, for sake of reproducibility, a fresh Ni foam anode was used for each experiment for the remainder of the study.

Intermediate conclusions from the initial tests segment of the study:

1. No effect of Ag or Nafion loading on CO selectivity observed in the range tested for the system used in this study
2. No effect of 20 wt% PTFE in CL on CO selectivity
3. CO stability is often overlooked in (bi)carbonate literature, with focus on peak values
4. The pH is a key parameter for CO selectivity

4.3. CO selectivity

4.3.1. Carbon paper support

An important factor on CO selectivity in bicarbonate electrolysis was hypothesized to be the carbon paper support (the GDL). GDLs can be distinguished by three main factors: thickness, porosity and hydrophobicity. In this study the effect of the hydrophobic nature of GDLs on CO selectivity was examined. It is mainly the presence of a microporous layer (MPL) that has been treated with PTFE, that determines the degree of hydrophobicity. Two different GDLs were tested in this study: hydrophilic Freudenberg H23 and hydrophobic Sigracet 39BB which containts a MPL that has been treated with to 5wt% PTFE, both from FuelCell Store. Table 4.1 outlines the characteristics of each GDL. Experiments were performed in duplicates for 45 minutes, according to the method described in methodology (chapter 3). Concomitantly with GDLs, the effect of GDL sonication pre spray-coating was studied. In the

Table 4.1: Information about the carbon paper supports tested in the experiments.

Carbon paper support (GDL)	Supplier	Base Material	Microporous Layer (MPL)	PTFE treatment	Thickness [um]
Freudenberg H23	Fuelcell Store	Carbon fiber	No	No	210
Sigracet 39BB	Fuelcell Store	Carbon fiber	Yes, one side	Yes, 5%	315

literature researchers often sonicate the carbon paper supports before ink deposition, but do not always explain why. It is likely that the main reason is to ensure that the GDL is clean of any contaminants. During initial experiments of this study it was noticed that during sonication of MPL containing 39BB it appears the MPL breaks down to some degree, as evidenced by darkening of the solution (acetone and water, separately). Following this observation, it was hypothesized that sonication of GDLs pre ink deposition could break down the MPL of the 39BB, improving aqueous flow through the GDL thus improving CO_2RR. Modifications and/or changes in aqueous flow in the H23 were not expected, but the effect of sonication was however also tested with the H23 for comparison. To the author of this work's best knowledge, the effect of GDL sonication has not been studied in (bi)carbonate electrolysis before. For the sonication experiments, electrodes were prepared in duplicates using both 39BB and H23 GDLs, that had been either sonicated for 20 minutes pre ink deposition (10 minutes in acetone, 10 minutes in water) or left untreated (non-sonicated).

Figure 4.2 shows the results of the GDL experiments including the GDL sonication experiments. The CO selectivity of the 39BB GDL was higher than that of the H23 (sonicated GDLs, graph a). In both cases the CO production is the highest at the beginning of the runs and then drops, a known trend in bicarbonate electrolysis. However, the drop is less for the 39BB than for the H23, or about 15 percentages compared to 20. CO production over time is examined more closely in the stability section of the results (see section 4.4). As with the sonicated GDLs, the CO FE of the 39BB is higher than that of the H23 for the non-sonicated carbon papers (graph b). The most likely reason for the observed improved CO production with the hydrophobic 39BB compared to the hydrophilic H23 is that the hydrophobic nature of the 39BB's MPL suppresses the HER - the main competing reaction. The hydrophobicity will increase the CO_2:H_2O ratio at the CL surface, promoting CO_2RR. In the (bi)carbonate electrolysis literature there seem to be different views on the optimum carbon support. The Berlinguette and Sargent groups prefer hydrophilic GDLs [23],[21], whereas Lee et al. have reported better results with hydrophobic GDLs [45]. It is likely that the optimum GDL depends on other cell parameters that influence the mass-transfer through the GDE or the catalytic activity. A reason cited for opting for hydrophilic GDLs over hydrophobic ones in the literature is that in (bi)carbonate electrolysis the aqueous electrolyte must pass through the GDE to reach the CL-BPM space, and the hydrophilicity improves that flow-through. It is likely that the flow pattern of the catholyte flow plate plays a key role in the electrolyte GDE flow-through. In this study, as mentioned, interdigitated flow pattern is used. In that case the flow is forced through the GDE with the mass-transfer being convection dominated. However, most studies in the literature where GDEs are used, opt for flow plates with serpentine flow pattern - if the flow pattern is mentioned at all. With serpentine flow pattern the mass transfer through the GDE is diffusion dominated. In that case it is likely that hydrophilic GDLs play a bigger part in carrying the electrolyte through to the CL-BPM space, whereas when interdigitated flow pattern is used and the electrolyte is forced through, hydrophobicity does not impact the electrolyte passing through the GDE, however still improves the ef-

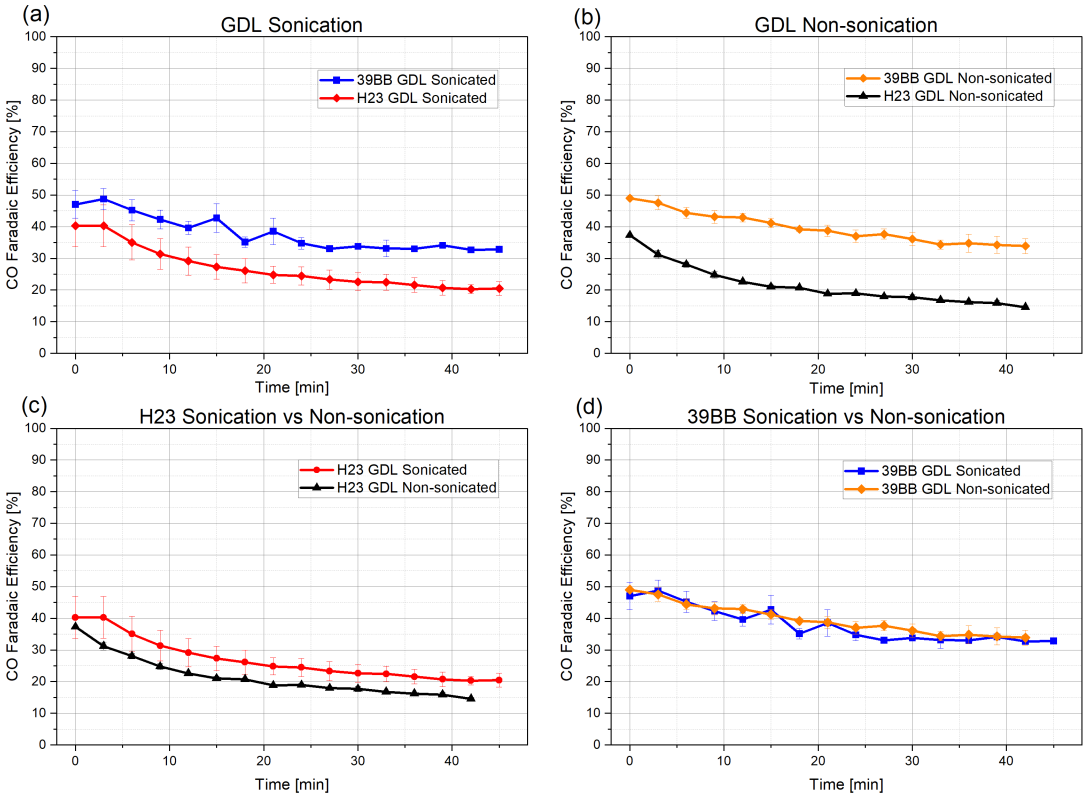

Figure 4.2: The CO FE results of the carbon paper support (GDL) experiments. a): H23 and 39BB sonicated GDLs, b): H23 and 39BB non-sonicated GDLs, c): H23 sonicated vs non-sonicated GDL, d): 39BB sonicated vs non-sonicated GDL.

ficiency by limiting HER and increasing CO_2:H_2O ratio on the CL. These results indicate that the trade off of reduced electrolyte flow through the GDE vs suppressed HER by using hydrophobic GDEs is irrelevant when using interdigitated flow pattern (see section 2.4.2). This difference in GDL/flow plate combination and results when compared with the literature led to the design of a study meant to shed light on the interplay of GDL and flow pattern (section 4.3.2).

Another difference between the system used in this study and in (bi)carbonate literature that prefers the H23 is that in those studies the GDL is covered with a Ag film by PVD prior to spray-coating, citing a less-than-perfect catalyst surface coverage without the film [21],[23]. It is possible that the effect of less than complete catalyst surface coverage would have more of a detrimental impact on CO selectivity with the H23 than the 39BB as the H23 is more susceptible to the HER due to it's hydrophilicity. The effect of catalyst surface coverage was thus examined also in this study, in the next section (section 4.3.4). When looking at the effect of sonication, the CO FE of the sonicated H23 is higher than that of the non-sonicated H23, but the difference is minimal and inconclusive (c in figure 4.2). This was expected, as the H23 is a simple carbon fiber paper, likely to be unaffected by sonication. Interestingly, no difference was seen between the sonicated and non-sonicated 39BB (d in figure 4.2), counter to what was expected. Three plausible reasons might explain these results. Firstly, it is possible that any observed breakdown of the PTFE-containing MPL during sonication and increase in electrolyte flow through the GDE is countered by a decrease in hydrophobicity accompanied by said MPL breakdown, increasing the HER. Secondly, it can be that the breakdown of the MPL is very little and thus has no measurable impact on the application. In that case, a third explanation might be that if the GDL was sonicated for longer an effect might be seen. Different time durations of sonication were however not tested in this study, and can be an avenue for future research. SEM/EDS testing of GDLs pre and post sonication might have shed some light on the degree of MPL breakdown, but was not performed in this study due to time constraints and to the SEM being decommissioned without notice to the author of this study. GDLs were not compared based on thickness or porosity in this study. Information on the GDL

porosity was not found, but the 39BB is thicker than the H23 (see table 4.1), which might also have an impact on the efficiency. It is recommended for future studies to examine these GDL factors as well as hydrophobicity. Contact angle measurements would also be a good further avenue of hydrophobic research, linking different levels of hydrophobicity to CO selectivity.

4.3.2. Catholyte flow pattern

The combination of GDL and catholyte flow pattern was examined in this study, with the goal to gather information on the effects of different mass transport on CO selectivity. To examine the effect of mass transport on CO selectivity, flow plates that had interdigitated and serpentine flow pattern of different channel dimensions, paired with either hydrophilic H23 or hydrophobic 39BB GDLs were studied. Three flow plates with serpentine flow pattern were tested, of width 0.7mm, 1.0mm and 1.5mm (depth 1.0mm). Two interdigitated flow pattern flow plates were tested, with channels of width 1.0mm and 1.5mm. Figure 4.3 shows the five flow plates that were compared. With interdigitated flow pattern, the mass transport through the GDE is convection dominated as the flow is forced through the channels, since the channels are not continuous. For serpentine flow pattern however, the flow will be more affected by diffusion with the continuous channels, although convective transport will also be present as the catholyte is forced through the channels and will thus encounter pressure resistance and pass through the GDE. Due to time constraints the 1.0mm serpentine and 1.5mm interdigitated flow plates were not performed in duplicates, as the rest of the experiments were, but were run singly. The experiments were run for a time period of 25-30 minutes, and the catholyte flow was kept constant at 50 ml/min. The effect of keeping the set point of the flow rate constant means that the velocity in the channels was not the same. The channel velocities as calculated (at the inlet channel) can be seen in table 4.2. As evident the velocities differed substantially, with the channel velocity in the 0.7mm plate 1.4 times that in the 1.0mm plate, and twice that in the 1.5mm plate. No flow pattern studies in the field of (bi)carbonate electrolysis using a GDE have been performed in the past to the author's best knowledge. However, Zhang et al. found that interdigitated flow pattern led to the highest CO selectivity compared to serpentine and parallel flow pattern, when using a porous silver electrode [37].

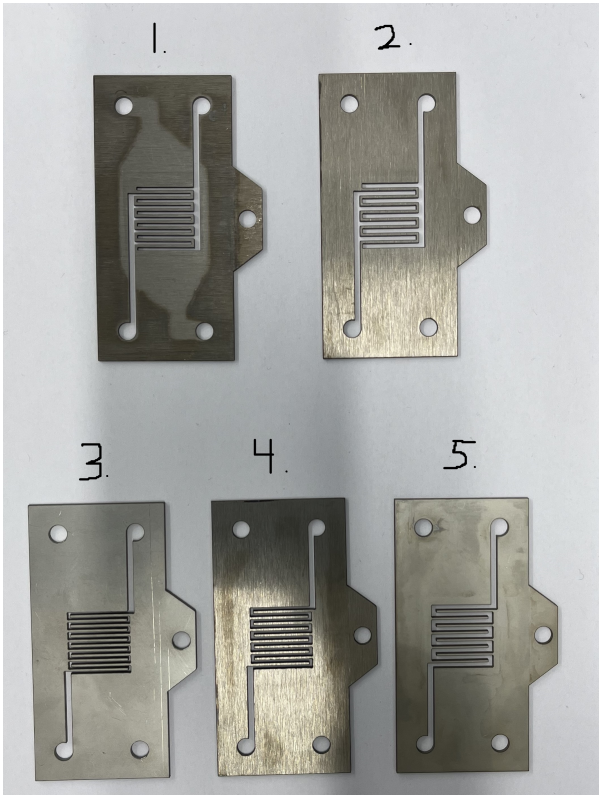

Figure 4.3: The flow plates tested in the flow pattern study. From left to right, top to bottom: 1:Interdigitated 1.0mm; 2:Interdigitated 1.5mm; 3:Serpentine 0.7mm; 4: Serpentine 1.0mm; 5: Serpentine 1.5mm. All flow plates had thickness of 1.0mm and were made of Ti, except for the 0.7mm Serpentine plate which was made of stainless steel.

Table 4.2: The different channel dimensions of the flow plates tested. The catholyte flow rate was kept constant, which meant the channel flow velocity varied depending on dimensions.

Flow plate (width x depth)	Catholyte flow set-point (ml/min)	Channel flow velocity (m/s)
0.7mm x 1.0mm	50	1.19
1.0mm x 1.0mm	50	0.83
1.5mm x 1.0mm	50	0.56

Figure 4.4 shows the results of the flow plate experiments. In both the serpentine and interdigitated cases, the 39BB outperforms the H23, showing higher CO selectivity. It is especially noticeable that the CO stability is better with the 39BB. Interestingly, for the serpentine flow pattern in the case of the H23 GDL, the CO selectivity does not scale with increasing dimensions. The 1.0mm channel dimensions gave the best results, followed by the 1.5mm and then the 0.7mm plates (a in figure 4.4). This indicates that there are at least two competing mechanisms at work. One could be increasing level of convective mass transport as channel dimensions decrease, due to higher pressure drop in the channels. Another could be the overall surface area of the channels, which increases with increasing channel dimensions. Diffusive mass transport will also increase with increasing channel surface area, but remain unaffected by channel flow velocity. The countering mechanisms could then be diffusive and convective mass transport. In that case by increasing the channel surface area to the GDE, CO FE increases via increased diffusion but convective mass transport is reduced. Thus the optimum lies somewhere between the largest channel surface area (the 1.5mm) and the highest convective transport (0.7mm), i.e. the 1.0mm (H23 Serpentine, a in figure 4.4).

For the 39BB GDL however, the best serpentine channel dimension proved to be the 1.5mm, followed by the 1.0mm and then the 0.7mm (b in figure 4.4), the CO selectivity scaling with increasing channel dimensions. This could then mean that for the 39BB the channel surface area (diffusion) has more impact on CO FE than convection, or that both forms of mass transport are more inhibited with the smaller channel dimensions for the 39BB compared to the H23 due to the hydrophobicity. As the PTFE treated MPL is only on the GDL side facing the BPM, if the aqueous flow cannot pass through the GDE the dominant reaction will likely be HER on the back side of the electrode.

There seems to be less of an impact of the channel dimensions (channel velocity) for the interdigitated flow plates (c and d in figure 4.4). Due to the interdigitated pattern, the mass transfer through the GDE is convection dominated, with little to no effect from diffusion. The 50 ml/min flow can then be thought to more or less completely cross over to the CL-BPM side regardless of channel dimensions. It is then likely that there is no change in the diffusion and convection mass transfer with interdigitated flow pattern as a function of channel dimension. A change in the flow and mixing behaviour in the CL-BPM space can though be expected to occur. The narrower channel dimensions of the 1.0mm flow plates now represent a higher pressure drop across the GDE than with the 1.5mm flow plates or with the serpentine flow plates. As previously mentioned, this should not affect the amount of catholyte passing through, rather it likely varies the pressure gradient across the 3-dimensional CL-BPM area and possibly causes more turbulent flow in that space. Turbulent flow in the CL-BPM space would likely not be beneficial for CO_2RR, as a pH gradient across the space is required for the release of i-CO_2, i.e. low pH at the BPM for proton release and high pH at the CL for improved CO_2RR. However in the case of the 39BB, the 1.0mm interdigitated flow plate gave better results than the 1.5mm flow plate, contrary to the previous theory. It can then be hypothesised that the increase in mixing in the CL-BPM space when going from 1.5mm to 1.0mm channels is insufficient to have a detrimental effect on CO FE. A modelling study of the mixing in the CL-BPM area as a function of convective mass transport through the GDE (varying flow patterns as well as channel dimensions) would be an interesting topic for future research. Ansarul Huq performed a one dimensional modelling study examining the effect of electrolyte inlet velocity in a bicarbonate electrolyser [110]. However, as electrolyte flow boundary conditions are illdefined in one dimension, the simulation did not converge. A 2 or 3 dimensional study is required to define the flow in the catalyst-membrane space adequately, as recommended by Ansarul Huq and furthered by the author of this work. In the case of the H23 interdigitated flow plates, no conclusive difference was noted. It is not clear why that is. The higher flow velocity in the narrower channels could

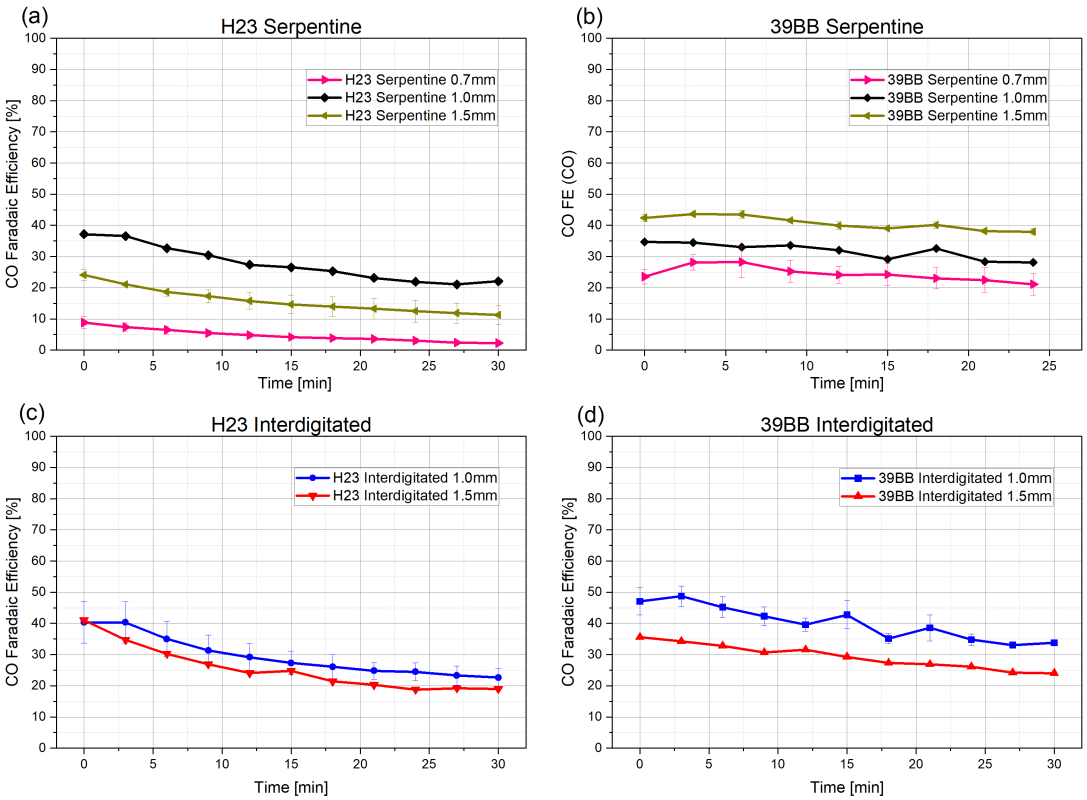

Figure 4.4: The CO FE results of the flow pattern experiments. a): H23 Serpentine flow pattern, b): 39BB Serpentine flow pattern, c): H23 Interdigitated flow pattern, d): 39BB Interdigitated flow pattern.

indicate a higher pressure drop and thus more convective transport, but to which degree is unclear. It should also be mentioned that the 1.0mm interdidigated results are from the same runs as in the previous GDL comparison basecase experiments.

4.3.3. Electrolyte flow rate

To examine the effect of catholyte flow rate on CO selectivity and stability, specifically the effect of convective mass transport of bicarbonate through the GDE, an experiment was performed where bicarbonate flow rate was increased periodically. The flow rate was increased from 20 to 40 to 70 and finally 100 ml/min, keeping each flow set-point for 15 minutes. The results can be seen in figure C.3 in appendix C.2. The CO FE did not drop over time as is the usually observed trend, but remained stable. This indicates that higher bicarbonate convective transport can lead to higher CO selectivity. Zhang et al. also tested the effect of catholyte flow rate on CO FE, using a a porous Ag electrode. They saw an increase in CO FE of about 25% when increasing the flow of bicarbonate from 30 to 100 ml/min. They however used a serpentine flow plate which also includes diffusive mass transport more so than interdigitated. The group also tested different flow patterns and found that interdigitated flow pattern was optimal for CO production, when compared to serpentine and parallel flow patterns [37]. The results of their study can be seen in figure A.1 in appendix A. It is not clear if starting with a higher flow rate and maintaining it would lead to the same improvements in selectivity. Due to time constraints it was not possible to test this parameter further. It is recommended for future studies to verify if a higher bicarbonate flow rate leads to higher CO selectivity.

Based on these results the optimum GDL is the 39BB. The 1.5mm serpentine flow pattern and the 1.0mm interdigitated flow pattern give similar CO FE values, with the interdigitated reaching higher selectivity but the serpentine showing better stability. However, the 1.5mm serpentine flow plates were added to the study at a later stage and as such, were not available throughout the experimental phase.

Thus, the chosen flow plate for future experiments was the 1.0mm interdigitated flow pattern, paired with the 39BB GDL.

4.3.4. Surface coverage

A factor thought to influence the CO FE is catalyst surface coverage on the carbon paper. Lees et al. found in 2020 that without depositing a Ag film pre spray-coating, they were unable to achieve complete silver surface coverage [23]. This promted a study to see whether the CO selectivity could be improved by depositing a silver film on the carbon paper before spray-coating. Catalyst surface coverage was again tested in unison with GDL, comparing the H23 and 39BB once more. 500nm Ag nanoparticle layers were deposited on H23/39BB GDLs by PVD, after which the electrodes were spray-coated with Ag nanoparticles, reaching a loading of 1.3 - 1.5 mg/cm^2. Experiments were performed in duplicates for a duration of 45 minutes. Figure 4.5 shows the results of the catalyst surface coverage experiments. The first graph compares the PVD prepared H23 electrodes with the H23 basecase (a in figure 4.5), the second graph shows the results of the 39BB tests (b in figure 4.5), while the third graph compares the two PVD treated GDLs (c in figure 4.5). As can be seen there is no substantial difference between the PVD treated electrodes and the basecase electrodes with only spray-coated Ag catalyst, with the non-PVD treated electrode giving slightly higher CO FE for the 39BB, while for the H23 it was the PVD treated electrode that had a slightly higher CO FE. When comparing the two GDLs, the 39BB shows better CO FE stability while the H23 has a higher peak value in the beginning but then drops faster. It can be concluded from these tests that catalyst surface coverage is not a limiting factor in this system.As such, it is not necessary to deposit a Ag film on electrodes pre spray-coating, which costs time and money and complicates the process.

Lees et al. however did see an improvement in Ag surface coverage by depositing a Ag film on the GDE [23]. The difference between their results and the ones from this work is likely because of the fact that they covered the GDE on both sides with a Ag film. Additionally, the group only tested the hydrophilic H23 for CO selectivity based on surface coverage. With the H23 GDL the HER will be more present than with the hydrophobic 39BB, and by completely covering the electrode with Ag catalyst they can suppress the HER to a high degree. The researchers also used different a different flow pattern, serpentine instead of interdigitated, which will affect the mass transport through the GDE as discussed above (section 4.3.2. These differences could explain why in this study we did not see a higher CO selectivity with the Ag film electrodes.

4.3.5. Spacing (interposers)

As discussed in section 2.2.2, a factor believed to impact carbon product efficiency in (bi)carbonate electrolysis is the spacing between the catalyst and the membrane separating the anode and cathode, specifically the CL-BPM spacing for the system used in this study. For an efficient CEM or BPM electrolyser low pH is required for proton release at the membrane, while the pH must be high for CO_2RR at the CL. High pH at the membrane suppresses proton release and i-CO_2 generation, while low pH supports HER and suppresses CO_2RR at the CL. Based on the study discussed in section 2.2.2 and done by Lee et al. [21], it was hypothesised that by increasing the CL-BPM space, CO selectivity could be improved in a BPM based bicarbonate system using Ag catalyst.

To test this theory, experiments were performed where an interposer membrane was inserted between the cathode and the BPM. The interposer membranes were made of hydrophilic and porous mixed cellulose ester (MCE), with each membrane having a thickness of 135 μm and pore size of 8.0 μm, supplied by MF-Millipore. Experiments were performed with one and two interposers inserted, resulting in a CL-BPM spacing of 135 and 270 μm, which were compared with zero gap system. These CL-BPM gap lengths were chosen as Lee et al. have determined the optimal spacing to be 135 - 270 μm [21]. The MCE interposer membranes were also chosen based on the Lee et al. study, who had found that it was optimal based on its high porosity. The experiments were done in duplicates, except for the 2 interposer (270 μm) runs which was done in triplicates. This was done because of a relatively large error between the first two experiments.

The results of the CL-BPM spacing experiments can be seen in figure 4.6. As can be seen, the CO FE was improved by increasing the CL-BPM space. At a spacing of 135 μm, the CO FE was 51%,

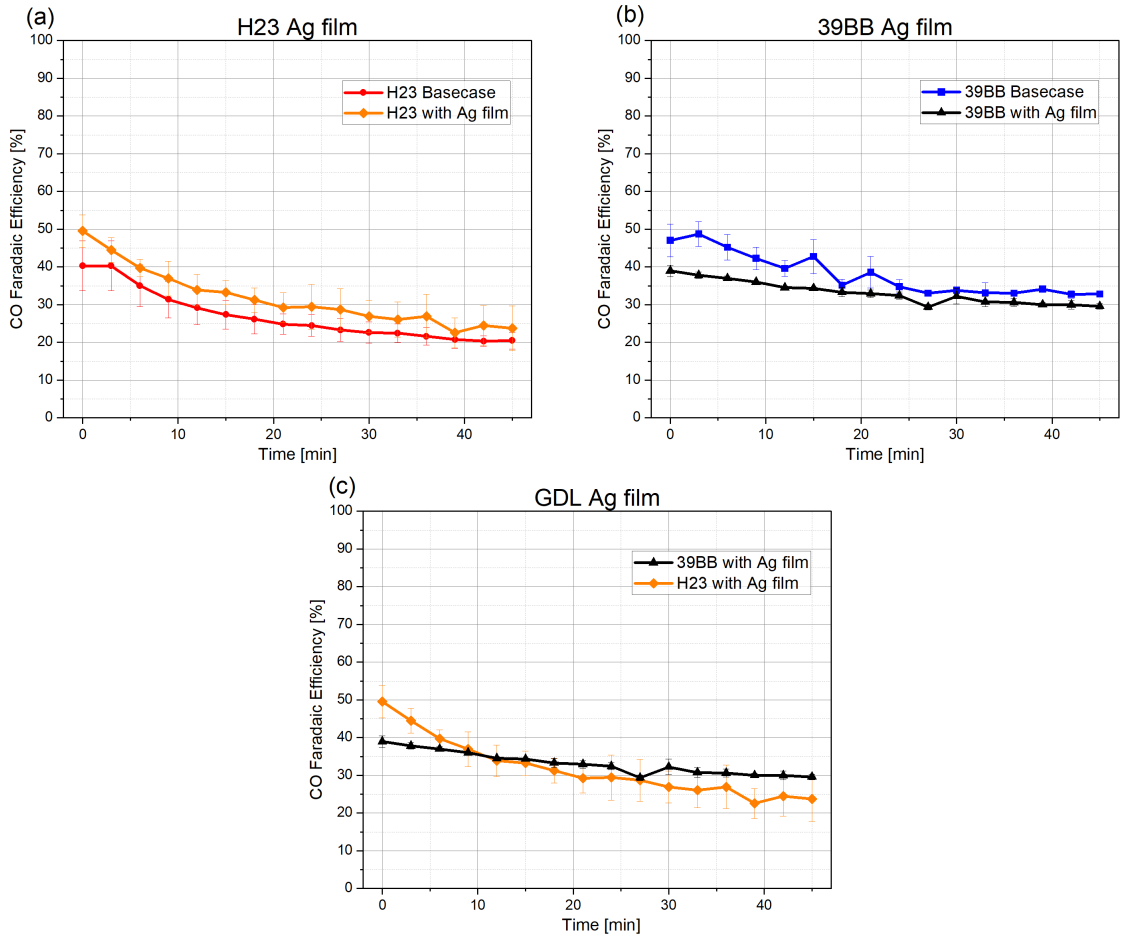

Figure 4.5: The CO FE results of the catalyst surface coverage experiments. For the Ag films a 500nm Ag layer was deposited via PVD, which was then coated with Ag nanoparticles. The basecase refers to normal Ag nanoparticle spray-coating directly on the GDL. a): H23 basecase vs Ag film, b): 39BB basecase vs Ag film, c): H23 vs 39BB Ag film GDL comparison.

while with 270 μm space the FE CO was 66%, averaged over the course of the experiment. Both CL-BPM spacings offer improvements in CO selectivity when compared to the zero gap basecase. When comparing the results to the results obtained by Lee et al. [21], the improvement in carbon product selectivity is similar. The group achieved an increase of about 25% (from 14% to 40%) for C_{2+} products when increasing the gap length from 60 μm to 135 μm. Similar improvements were observed in this study, with the CO FE increasing from about 47% to 75%, with the higher CO FE resulting from the 270 μm gap length (when looking at peak CO values). The large difference between the 135 μm and 270 μm gap length can possibly stem from the fact that the experiments were performed using different catholyte batches, with slightly different pH values. The pH of the catholyte for the 135 μm runs had a pH of 8.26 while for the 270 μm the pH was 8.02. As it is suspected that a higher bulk pH limits i-CO_2 generation and thus CO_2RR, it cannot be verified from these experiments that the 270 μm space is better than the 135 μm. However the importance of the CL-BPM spacing is confirmed. Moreover, the improvement by inserting a CL-BPM gap is proven for a system that uses a Ag catalyst forming CO as a product. The study by Lee et al. used Cu catalyst making C_{2+} products, paired with a CEM (for their experimental part). Another difference is that Lee et al. used a carbonate electrolyte, while in this study the electrolyte is a bicarbonate buffer. The pH of a carbonate buffer is higher than that of a bicarbonate buffer, or around 11.70 compared to 8.35. The high pH of the carbonate electrolyte explains that at a gap length of 0 μm they record no C_{2+} products. The high pH here limits the i-CO_2 generation at the CEM significantly, or rather ensures that any CO_2 liberated rapidly reconverts to carbonate species.

Another difference is that Lee et al. used current densities in the range of 200 - 350 mA/cm^2 (seeing the best results with 250 mA/cm^2), while in this study the current density was fixed at 100 mA/cm^2. Bicarbonate CO electrolysis studies that look at the effect of CL-BPM spacing at higher current densities are recommended for future work, as the importance of efficient production at higher current densities is essential for scale-up and industrial considerations, although outside of scope for this project.

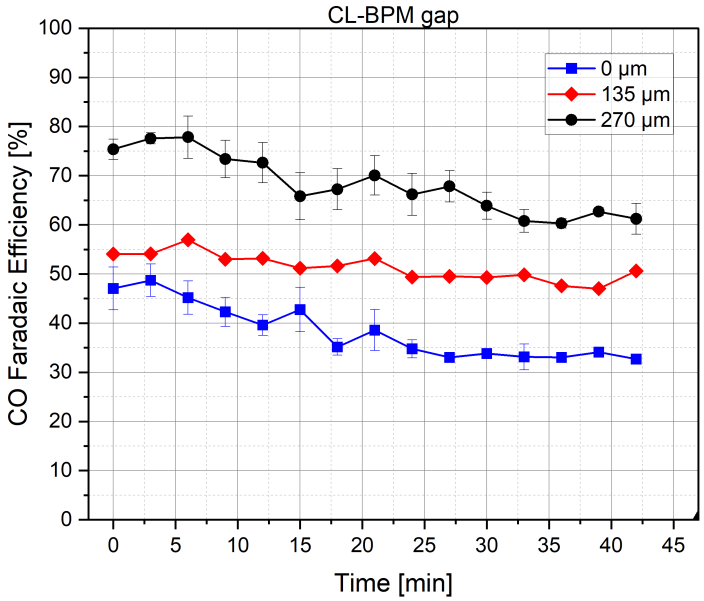

Figure 4.6: The effect of introducing a CL-BPM gap using spacers. CO FE increases from the zero gap case as a result of a pH gradient introduced by the gap.

Intermediate conclusions from Parameters for CO selectivity part:

1. Hydrophobic 39BB GDL is preferable to hydrophilic H23 for CO selectivity and stability when using interdigitated flow pattern.
2. Competing mechanisms are observed for serpentine flow pattern: Increasing channel dimensions likely increase diffusive mass transport due to higher surface area, while reducing convective mass transport as channel flow velocity and pressure drop reduce.
3. Optimum by balancing the two factors, here 1.0mm channel width for the H23, 1.5mm for the 39BB with the difference possibly due to hydrophobic effects and HER taking place on the back side of the electrode for the smaller channels.
4. Little to no impact of diffusive and convective mass transport changes when changing channel dimensions for interdigitated flow pattern, possibly caused by already fully convective dominated mass transport.
5. The CO selectivity is not limited by catalyst surface coverage of the GDL.
6. CL-BPM spacing improves CO selectivity in a BPM based bicarbonate electrolyser using Ag catalyst.

4.4. CO Stability

As previously mentioned, there is a general tendency in the (bi)carbonate electrolysis literature to focus on peak production values and overlook production stability. Lee et al. likely report peak values solely in their bicarbonate work [45], as no mention of average production values can be found in their work and in email correspondence with the authors there was no definitive answer given to the question of single values versus averages (Wenzhen Li, email correspondence, 08MAR2024-23FEB2024). As

discussed previously, the Berlinguette group also mainly reports single measurements in their bicarbonate work [18],[23],[37], as was verified in email correspondence with a member of the group (Yong Wook Kim, email correspondence, 23FEB2024 - 06MAR2024). Although not specifically stated which studies are being referred to, for the purpose of this study if no mention is found of whether single or average values are being reported, it is assumed they are single measurements. While important to keep the scope of a study limited and concise, and improving product selectivity is a necessary first step before working on improving product stability, it is recommended that when reporting results it is made clear what is being reported to avoid confusion, especially for reproducibility. Full appreciation and gratitude is extended to the cooperation of the above mentioned researchers for their swift replies and helpful advice, whose work and answers provided valuable information for the purpose of this study.

With this discovery in mind, a CO stability characterisation study was designed. It began by further examination into the effects of CL-BPM spacing, characterizing the CO stability over a period of 3 hours. Next a long-term CO stability characterization study was performed for a duration of 14 hours with in-line pH measurements, followed by pulsed experiments with start/stop potentials, attempting to improve the stability.

4.4.1. 3 hour CO stability with spacing

With the effect of the CL-BPM gap on CO selectivity established, it was set out to further characterise the difference based on gap length without the effect of inlet pH (using the same catholyte lot, initial pH: 8.26), with a focus on CO stability over time as well. With the optimal spacing identified as 130 - 270 μm, 405 μm was also tested with the goal to verify the aforementioned spacing range as the optimum, expecting a decrease in CO selectivity at the larger gap length. Although the introduction of the CL-BPM space offers a pH segmentation - low at the BPM while high at the CL, if the space is too large a competing mechanism is expected to counter the pH division benefits, i.e. carbonation reactions (reactions 1.6, 1.7). The longer the diffusion path of the i-CO_2 from generation at the BPM to conversion at the CL, the higher the rate of CO_2 reacting with OH^-, forming bicarbonate and carbonate. These competing mechanisms explain why there exists an optimum CL-membrane spacing, as shown by Lee et al. for their system [21], and examined in this study for a Ag catalyst, BPM bicarbonate electrolyser. The second set of experiments based on CL-BPM gap was performed using gap lengths of 0 μm, 135 μm, 270 μm and 405 μm (0, 1, 2 and 3 interposers) were tested over time periods of 3 hours. The results of these experiments are presented in figure 4.7.

While the 270 μm spacing from the first CL-BPM gap experiments (figure 4.6) showed higher CO selectivity than that of 135 μm, it was less stable, dropping by about 16 percent over the course of the runs. In contrast, the 135 μm system showed great stability over time, dropping by only 4 percent, albeit displaying lower selectivity. However for the 3 hour CL-BPM experiments (figure 4.7), there is marginal and inconclusive difference in stability between the 135 and 270 μm gap lengths. As the only difference between these two sets of experiments, other than the time duration, was that in the previous experiments the inlet pH of the 270 μm was 8.02 compared to 8.26 for the 135 μm runs, it might well be the reason for the higher CO selectivity and lower stability of the 270 μm in the first set of experiments. Most likely the main positive impact of lower pH on CO selectivity is higher i-CO_2 liberation and less carbonation backreactions, since lower pH also supports the HER combating CO_2RR. It is then likely that lower initial pH provides more i-CO_2 for more CO production, giving rise to faster alkalinization through the OH^- byproduct, when compared to the higher initial pH of the 135 μm runs. The higher alkalinity then begins to suppress i-CO_2 liberation and increase carbonation, leading to lower stability.

The lower CO selectivity (0 μm gap) and CO stability (405 μm gap) are most likely the cause of the already mentioned competing mechanisms of improved i-CO_2 release as a result of the introduced gap, and the increased diffusion path causing higher carbonation of the i-CO_2. With no gap, i-CO_2 liberation is too limited for considerable CO_2RR, and if the gap is too wide, the diffusion path from the site of release at the BPM to the site of conversion at the CL is too long and too much of the i-CO_2 converts to (bi)carbonate. Graph c in figure 4.7 shows how the stability of CO drops with increasing CL-BPM gap lengths. In the same figure is the pH of the catholyte measured at the end of the runs. The pH rise is the most for the 135 and 270 μm gap lengths, explained by the higher CO_2RR and thus OH^- production. Already discussed is the possibility of higher CO production (and OH^- ions) leading to the

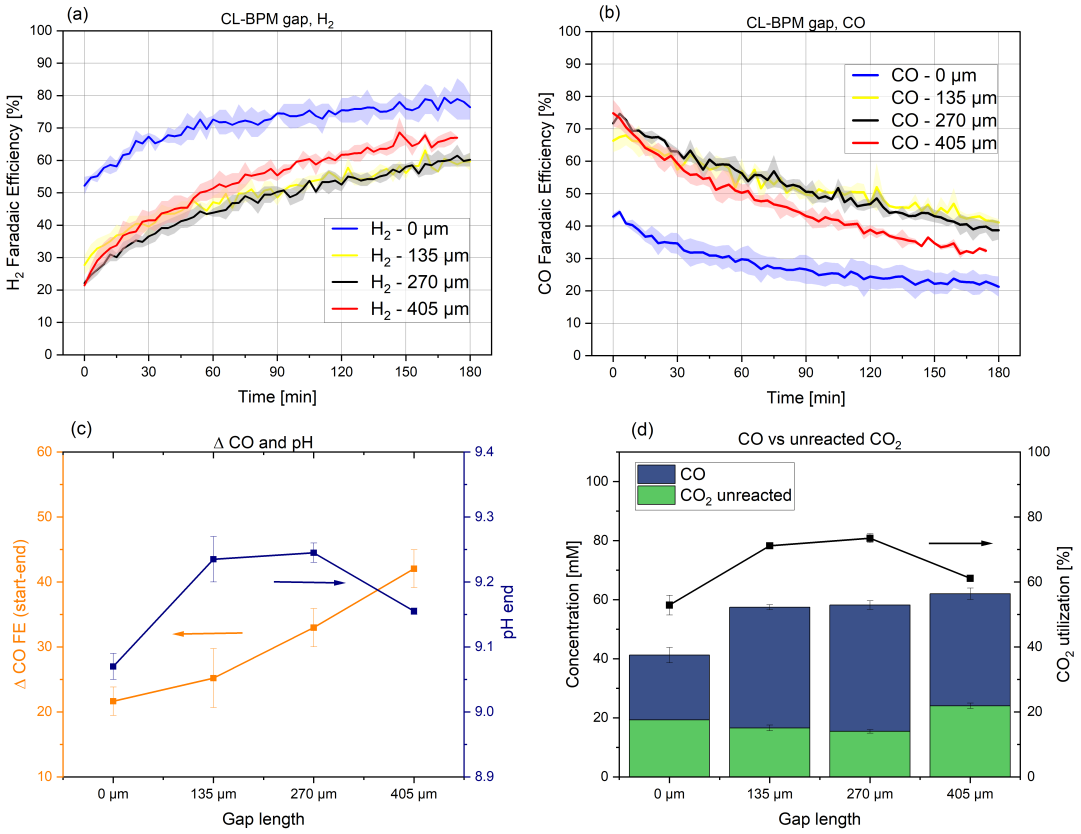

Figure 4.7: CL-BPM gap experiments performed for 3 hours. a): H_2 FE, b): CO FE, c): Drop in CO FE (Stability) and the increase in catholyte pH (initial pH: 8.26), d): CO_2 utilization to CO (as per calculation in section 3.5.2). CO_2 unreacted is CO_2 measured by the GC.

reduced CO selectivity over time, but that does not explain why the stability drop is the highest for the largest gap width. This observation indicates there is another mechanism than rise in pH causing the drop in stability. It is possible that there are changes in the local CL microenvironment causing the drop in stability. This is examined in section 4.4.3. Another possibility is changes in the CL itself, which is discussed in the same section.

Graph d in figure 4.7 shows how the CO_2 utilization is improved with the 135 and 270 µm gap lengths. The lower CO_2 utilization of the 0 µm gap system is likely not only caused by lower i-CO_2 liberation but also lower conversion due to the lack of a defined pH gradient across the CL-BPM space. If it were only a result of less i-CO_2 liberation, the CO:CO_2 ratio would be higher despite less CO_2 being available. The CO_2 utilization at the 405 µm gap is interesting, as more CO_2 and less CO is measured in the output compared to the 135 and 270 µm gap runs. Moreover, the combined CO_2 and CO is the highest for the 405 µm gap run. This behaviour must be caused by lower CO_2 conversion at the CL rather than lower CO_2 availability, albeit in this case the pH gradient will not be the reason, rather the mechanism mentioned before, which might be changes in the CL microenvironment or catalyst degradation. The higher CO_2 in the 405 µm gap case therefore indicates that more CO_2 is being liberated here based on the better defined pH gradient, only to be largely reconverted to carbonates, which stands to reason. The CO_2 utilization here is calculated based on the approach outlined in the Methodology chapter, section 3.5.2.

The 135 and 270 µm CL-BPM gap systems gave the best results, with the 270 µm system reaching higher peak CO values but the 135 µm system showing slightly albeit inconclusively better stability

over time. With the insignificant difference between the results in mind, the 135 μm system was chosen for future testing and improvements, due to it being simpler in preparation and operation having only 1 interposer membrane compared with 2 in the 270 μm case. It is likely that an as yet undiscovered optimum gap length exists, possibly between 135 and 270 μm. It is recommended for future studies to search for that optimum.

4.4.2. Long-term (14 hour) CO stability

Having chosen the 1 interposer (135 μm) system as the optimal CL-BPM spacing, it was set out to map CO production over extended time periods. Basecase (no gap) and 1 interposer system experiments were run overnight for 14 hours. With the pH having been identified as an important parameter in CO selectivity and possibly stability, it was measured in-line during the experiments. For these experiments electrolyte volumes of 1 and 0.5 L (catholyte and anolyte, respectively) were used, to ensure a sufficient supply of bicarbonate and to lower the impact on bulk pH during the extended operation. The results of the 14 hour stability characterisation runs can be seen in figure 4.8. The improvement in CO selectivity

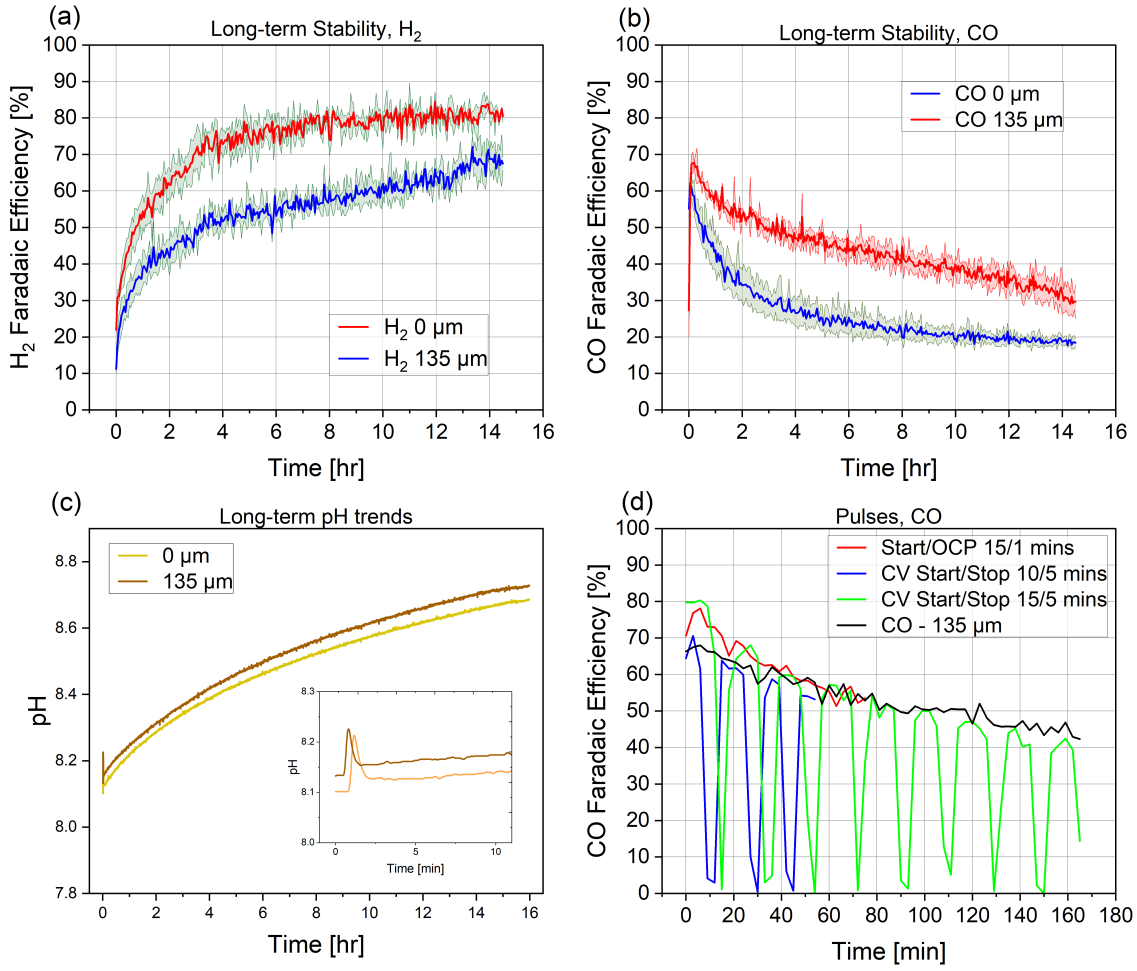

Figure 4.8: a) and b): Stability characterization overnight (14 hours), H_2 and CO FE. c) pH inline measrurements during the overnight experiments. d): Effect of start/stop pulsed experiments on CO FE.

in the 135 μm system is also evident in the overnight experiments, however the CO production drops over time. As shown in the 3 hour experiments and now confirmed for longer time periods, the CL-BPM spacing shows an improvement on CO selectivity but not stability. The pH of the bulk catholyte increases over time for both systems, inversely proportional to the CO FE (c in 4.8). This is mainly because of the formation of hydroxide ions as a byproduct of the CO_2RR, which build up over time in the catholyte. Interestingly, despite the higher CO production of the 135 μm system the rise in alkalinity

follows the same trend, only marginally higher for the 135 μm system. While the difference in CO production is about double, the rise in pH is quite similar, suggesting there is something other than just the formation of OH^- as a byproduct of CO_2RR that is causing the increase in pH. The high initial CO FE of the zero gap (basecase) system can likely be traced to high CO_2 values seen, probably a result of the higher electrolyte volumes. For the zero gap and 135 μm gap systems much higher CO_2 was recorded. To compare with the unreacted CO_2 measured in the 3 hour runs (figure 4.7), the unreacted CO_2 for the first 3 hours of the overnight runs were 135 mM and 80 mM for the zero gap and 135 μm gap systems respectively. About 6 times more CO_2 is thus measured from the 1L catholyte basecase, and 4 times more for the 135 μm gap run. The higher initial CO FE values seen are therefore likely due to the higher CO_2 availability. The reason for the increased i-CO_2 liberation with the higher electrolyte volume is unclear, but it is an important observation as electrolyte volume used in studies varies quite significantly, and is sometimes unreported (see table C.1 in appendix C.7). As such, effect of electrolyte volume on product selectivity and stability could be interesting to examine in future research. The pH rise is also lower compared to shorter runs, or about 8.1 to 8.7 compared to 8.26 to about 9.1-9.2 for the 3 hours runs, which is likely due to the increased buffering capacity of the higher electrolyte volume. The effects of bulk pH on CO selectivity and stability is examined more closely in section 4.5, and local pH as well as catalyst stability in the following section (4.4.3).

4.4.3. Pulsed electrolysis

Having characterised the stability of CO overnight (a and b in figure 4.8), the focus was placed on improving the stability. As discussed in section 2.7.4, a method that has been studied with regard to product stability is pulsed electrolysis. The theory is that changes in the local catalyst microenvironment are causing the drop in stability, and that this microenvironment can be affected by momentarily turning off the potential or switching to anodic potentials at the catalyst, resetting the conditions to close-to-original. To test this theory, a set of experiments based on pulsed electrolysis were designed. Three experiments were done using start/stop potentials. For the first experiment the current was controlled (100 mA/cm^2) and run for 15 minutes, after which OCP (open cell potential) was set for 1 minute. The other two experiments were thus run using set potential at -3.60 V, the voltage most commonly seen for the process, as using this configuration it was possible to set the potential to 0 at certain intervals. These two experiments were run as start/stop potential experiments for 10/5 minutes (on/off) for 54 minutes (3 pulses), and for 15/5 minutes for 3 hours. All runs had a 135 μm CL-BPM gap.

The results of the start/stop experiments can be seen in figure 4.8, graph d. Setting the potential to OCP for 1 minute was not enough time for the potential to reach 0, as can be seen in the voltage profile in figure C.4, appendix C.3. When compared with the basecase example from the 3 hour stability experiments (section 4.4), it is clear there is no effect on the selectivity or stability of CO FE when using the start/stop configuration. As discussed in section 2.7.4, most of the research on pulsed electrolysis has been focused on Cu catalysts, with only one study found that used Ag catalyst. That study saw improvements, yet they only applied very low current densites of 3 mA/cm^2. As such, the results of that study have very little significance when compared to operation at 100 mA/cm^2 or more. Thus selectivity improvements based on pulsed potentials are yet unconfirmed for bicarbonate reduction to CO on Ag catalysts.

The main discussed changes in the catalyst microenvironment that varying the potential theoretically addresses are changes in the local pH and changes in the catalyst itself [106],[54],[91]. The local catalyst pH is expected to rise faster than the bulk pH as OH^- are formed in CO_2RR and H^+ are consumed in HER (and i-CO_2 liberation), which scales with current density [111]. The local pH should increase even more with Ag catalyst than Cu, as Nafion is usually preferred over Sustanion as ionomer binder when using Ag catalyst (including in this thesis). The negative background charge of Nafion reduces their passing through the GDE, accumulating OH^- at the catalyst surface, raising the pH (see ionomer discussion in section 2.4). Thus the local pH gradient could in theory be higher in a Ag Nafion system compared to Cu systems preferring Sustanion. If the drop in stability were due to changes in local pH levels, it is likely that an impact would be seen in the start/stop experiments. However, as no impact is observed, it can be that the drop in CO production is due to irreversible changes in the electrode.

4.4.4. Electrode stability

Catalyst stability in terms of breakdown or metal detachment was examined by analysing post electrolysis catholyte samples in ICP-OES for metals. A table showing the results of ICP-OES measurements can be seen in appendix C.7, table C.4. Very little Ag was measured ($\leq$ 0.26 ppm or below detection limit), suggesting low CL breakdown. No trace metals were found (similar levels as a blank sample). However, some visible changes can be seen in the Ag electrodes post electrolysis. In figure 4.9 a Ag electrode can be seen pre and post electrolysis. Discoloration is notable along with markings from the flow plate. It is possible that during electrolysis the CL undergoes changes that reduce it's reduction capacity. It is recommended for future research that any changes in the cathode during electrolysis are examined. Changes in terms of rearrangement or agglomeration of the nanoparticles, which could reduce the active surface area of the catalyst, could be relevant in this regard.

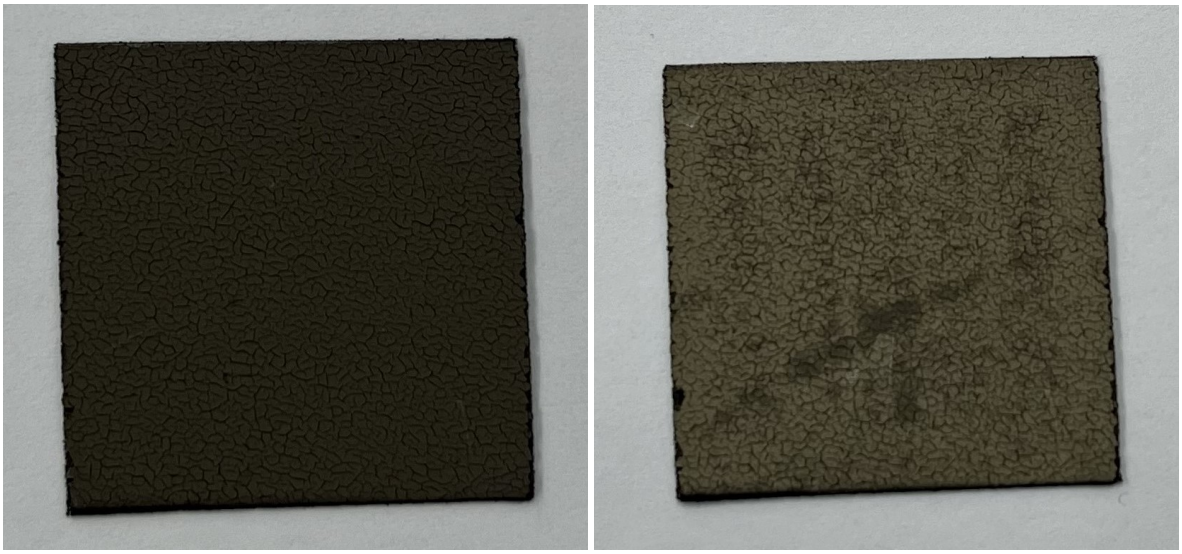

Figure 4.9: Effect of electrolysis on Ag electrode. Left: Ag electrode pre electrolysis. Right: Ag electrode post electrolysis. This electrode was used in an overnight 14 hr basecase experiment (no gap).

Intermediate conclusions from CO stability part:

1. The system shows a decrease in stability as characterised in experiments over 3 and 14 hours.
2. CL-BPM gap does not improve CO stability.
3. Zero gap reduces efficiency through limiting i-CO_2 liberation, while too large gaps reduce efficiency through large CO_2 diffusion path and carbonation reactions.
4. An optimum CL-BPM spacing likely exists in the 0 - 405 μm range, probably between 135 - 270 μm.
5. 135 μm spacing was chosen for subsequent experiments for simplicity.
6. Pulsed start/stop potentials do not improve CO stability in a bicarbonate electrolyser producing CO at 100 mA/cm^2.

4.5. Effect of pH

The pH of the catholyte was noticed to be a likely factor on CO selectivity early in the experimental phase (section 4.2.1). In the long-term stability characterisation part, the pH trend over 14 hours was characterised for the basecase (zero gap) and 135 μm gap systems (section 4.4). In this part of the experimental phase it was first set out to examine the effect of inlet catholyte pH (starting pH) on CO selectivity, and next to examine whether rising catholyte pH is a cause of decreasing CO stability.

4.5.1. Effect of bicarbonate pH

To test the effect of catholyte pH on CO selectivity, bicarbonate buffers of different pH values were prepared (as described in Methodology, section 3.3.2). Buffers of pH: 8.5 and 9.5 were prepared by including carbonate in different quantities, while maintaining the concentration of potassium ions constant. Due to time constraints, the experiments in this phase were performed singly, i.e. not in duplicates. It should be noted that in these experiments CL-BPM spacers were not included.

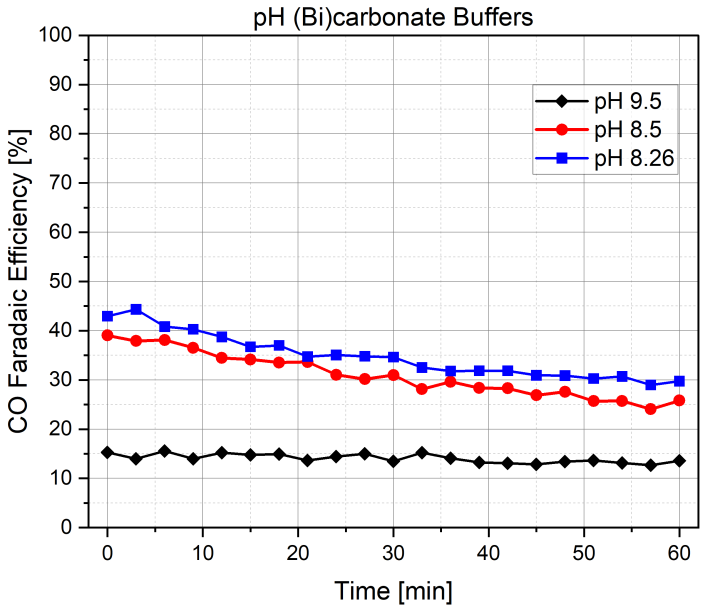

Figure 4.10: The effect of bicarbonate catholyte (starting) pH on CO selectivity. In these experiments a CL-BPM gap was not included, explaining the lower CO FE of the basecase 8.26 pH run.

The results of the experiments are shown in figure 4.10, also included is a basecase run with pH of 8.26 (regular 3M bicarbonate buffer). The CO selectivity is inversely proportional to rising pH of the catholyte, with the 9.5 pH buffer measuring just 15% CO FE. Interestingly, at the higher pH the CO stability is improved, dropping by barely 2 percentages over one hour. This might be because of lower CO_2RR producing less OH^-, causing a lower rise in pH; or because of less catalyst deterioration during electrolysis, since less CO_2RR is taking place. Lees et al. also found a correlation between reduced bicarbonate electrolyte pH and higher CO selectivity [23]. They studied the effect of pH over 8 hours, periodically adding H_2SO_4 and replenishing the catholyte, seeing a rise in CO selectivity coinciding with the decrease in pH (see figure A.4 in appendix A). However, the effect of purely the pH can not be concluded from their study as the addition of the H_2SO_4 is another variable unaccounted for. Based on the observations of the inlet pH experiments of this thesis, it is however likely that the conclusion drawn from the group's stability study holds.

4.5.2. Effect of constant pH (single-pass)

With the catholyte pH effect on CO selectivity established (figure 4.10), the focus was placed on stability over time. Following the observation from their 8 hour pH stability study, the Lees et al. group hypothesized that if the catholyte pH can be maintained, the CO FE would remain stable [23]. Based on the findings so far in this study, this hypothesis seemed likely. To test the theory, experiments were performed single-pass with different catholyte pH values, again prepared as before. The single-pass refers to the fact that instead of recycling the catholyte through the flow-cell back to the reservoir, it was passed only once through the cell and collected in a separate reservoir. This way, the pH and composition of the (bi)carbonate buffer remained the same throughout the duration of the experiments. (Bi)carbonate buffers were prepared of pH values 9.0 and and 10.0 and tested along with the buffers

of pH 8.5 and 9.5.

The results of the single-pass pH experiments can be seen in figure 4.11. Interestingly, the same trend as before is observed. The selectivity is again the highest for the lowest pH buffer of 8.5, dropping as the pH increases, with the opposite being true for the stability, which improves with the higher pH. The hypothesis that by keeping the bulk pH fixed the CO FE can be stabilised therefore is not proven. Other factors must be causing the drop in CO production over time. When examining the CO_2 availability and CO_2 utilization (c and d in 4.11), the first thing to notice is that the CO_2 is the lowest for the highest pH buffers. This stands to reason as the high pH increases the rate of carbonation reactions of the i-CO_2 as well as limiting its liberation. Importantly however, the CO_2 availability is quite high for the pH 8.5 run and even increases over time as CO selectivity decreases. This trend can best be seen in graph b (figure 4.11) which shows how the CO_2:CO ratio rises over time. This indicates that the CO_2 reactant is present in plentiful amounts and yet is being converted less and less. With the external factors constant (pH and bicarbonate concentration), this observation leads to the likely conclusion that there are indeed unwanted changes taking place in the cathode during electrolysis that are causing the drop in stability, as has already been suggested. Two types of changes are possible: changes in the catalyst microenvironment or changes in the catalyst structure itself. As already examined in the previous section (section 4.4.3), it remains inconclusive which factor is more influential, as no effects were seen from start/stop experiments. With no Ag catalyst or trace metals measured in the catholyte post electrolysis, changes other than catalyst breakdown are most likely, as conjectured before.

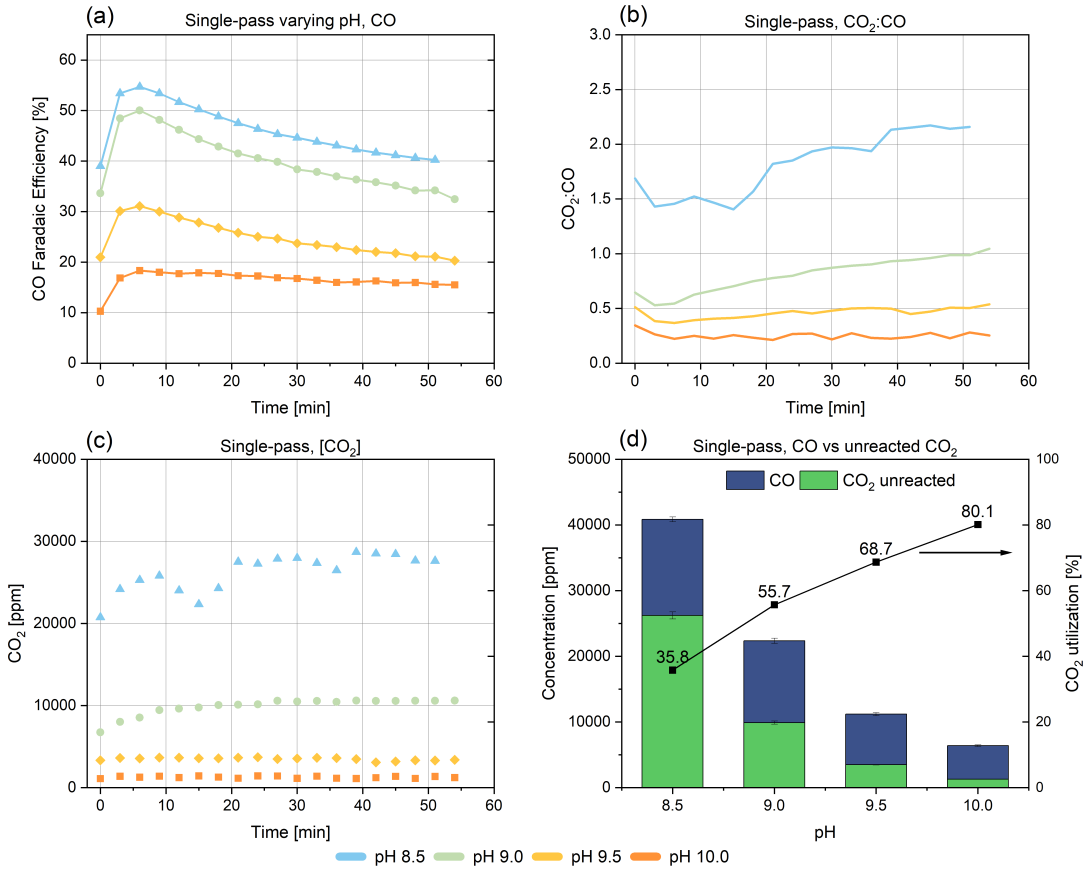

Figure 4.11: The results of the single-pass (constant) pH experiments. a): CO FE resulting from the different pH bicarbonate buffers, with the highest selectivity from the lowest pH buffer, but dropping over time. b) CO_2:CO ratio for the 4 bicarbonate buffer runs. c): CO_2 concentration over time, while low for the higher pH buffers it remains high for the low pH. d): CO_2 utilization increasing as pH and CO production decrease, while CO_2 and CO decrease in concentration.

Another implication of these results is that CO selectivity at lower bulk pH and CO stability at higher bulk pH are trade-off factors. Unless local pH levels can be optimized (and maintained), these two factors might have to be balanced against each other for best overall performance. In this study only the pH of the bulk catholyte was measured. It is recommended for future studies that the changes in CL-BPM gap pH profile are measured in operando, using techniques such as FLIM (Fluorescence Lifetime Imaging Microscopy). The pH gradient introduced by the spacing can then be studied with regard to its effect on stability, as well as differences in said space compared to the bulk environment. It is the opinion of the author of this work that understanding of changes in the CL-BPM microenvironment during electrolysis would provide valuable insight into improving the stability of CO production over time.

Intermediate conclusions from the Effect of bulk pH experimental segment:

1. Higher starting catholyte pH reduces CO selectivity, while improving stability.
2. Constant bulk catholyte pH does not lead to improved CO stability.
3. Higher bulk catholyte pH improves CO_2 utilization, although likely it is through increased carbonation reactions.
4. The results indicate that the primary cause of declining CO stability is undesirable changes taking place in the cathode during electrolysis.

4.6. Bimetallic CuAg Electrolysis

Based on the success of the CL-BPM spacing experiments, it was also examined how the improvements translate into multicarbon (C_{2+}) production. The goal was to provide initial insight into C_{2+} production using a bimetallic CuAg catalyst system, that could serve as a basis for future research. This part can be considered a side branch for future outlook reference.

As discussed in section 2.2.4, Lee et al. have demonstrated C_{2+} selectivity improvements in a similar system as the one used in this study, based on catalyst/ionomer layering and engineering, hydrophobic GDL and PTFE inclusion [45]. Building on those results, a set of experiments was designed using bimetallic CuAg catalyst with Sustanion and Nafion ionomers. The electrode was constructed with Cu/Sustanion layer first coating the GDL, with a Ag/Nafion layer on top, using 15wt% ionomers. This arrangement in theory facilitates the CO_2 reduction to CO intermediary, and subsequent CO reduction to C_{2+} products mechanism, as proposed by various authors and discussed in section 2.2.4. The hydrophobic 39BB carbon paper was used, based on earlier results of this study. Two factors were examined with regard to their impact on carbon products selectivity: The inclusion of 20wt% PTFE in the Ag/Nafion layer, and the inclusion of CL-BPM spacing of 270 μm (2 interposers). 2 interposers were used for the spacing case as when this set of experiments was performed the 3 hour stability experiments had not yet been done and it was not yet concluded which spacing was optimal. The 270 μm CL-BPM gap experiment was performed singly due to time constraints, while the 20wt% PTFE and basecase CuAg (no spacing, no PTFE) were performed in duplicates. An overview of the CuAg experiments discussed here can be found in table C.3 in appendix C.

The results of these experiments can be seen in figure C.5 in appendix C. As expected, the CO FE increases when going from basecase CuAg to the CL-BPM gap, increasing from about 8% to 20%. The 20wt% PTFE run also shows an increase in CO FE compared to the basecase, measuring about 15%. This is inline with results reported by Lee et al. [45], who also reported a roughly 15% CO FE using 20wt% PTFE. The group however reports quite higher C_{2+} production, or about 20% at the same PTFE loading, constituting mainly ethanol and ethylene (C_2H_4). In graph c in figure C.5 it can however be seen that C_2H_4 FE only increased from about 4 to 5% by including the PTFE. No conclusive impact can be seen on C_2H_4 FE by the addition of the CL-BPM gap, suggesting that although more CO is available it is not being reduced on the Cu as hypothesized by the CO intermediary theory (as discussed in section 2.2.4). This may suggest that the dominating C_{2+} production mechanism is in fact CO_2 reduction, not CO reduction. Indeed, good results have already been demonstrated using different types of monometallic Cu catalysts in C_{2+} production (section 2.2.2), albeit limited studies have been performed using (bi)carbonate electrolytes. The Sargent group reported 56% C_2H_4 FE in 2023 using carbonate electrolyte and Cu catalyst [21], the highest to date, although they also report no CO_2 in the gas stream, which although at first seeming implausible could potentially be because of the high

pH of the carbonate electrolyte. Lee et al. reported 40% C_{2+} products at 100 mA/cm^2, using 50wt% PTFE [45]. Surprisingly, with the same PTFE loading as in this study of 20wt% they still saw 20% C_{2+} products. That is four times more than what is observed in this study. With that in mind, the results of the Lee et al. work should be viewed cautiously until reproduced elsewhere.

CO_2 utilization to CO increases when going from basecase to 20wt% PTFE to 270 μm gap (d in figure C.5). Similar improvement in i-CO_2 liberation is therefore seen in a bimetallic CuAg system as was seen in a Ag catalyst system (figure 4.7). Interestingly, i-CO_2 liberation does not seem to be improved by the PTFE addition, suggesting that the improvement seen there in CO selectivity compared to the basecase is due to HER suppression and improving i-CO_2 transport through the GDE, which agrees with the literature on the benefit of hydrophobic constituents (see section 2.4.2). The stability of CO and C_2H_4 is quite good, with no drop in CO FE and an increase in C_2H_4 production over time. The stable CO FE is likely due to the lower CO_2RR taking place, which as seen in the pH experiments is connected to more stable CO production, albeit as yet unconcluded if is caused by less bulk pH rise or less electrode degradation. The increase in C_2H_4 FE can be explained by the rise in pH observed during operation, as C_{2+} production is favored at higher pH levels due to improved C-C coupling [112]. The lower pH of the pure bicarbonate buffer is likely limiting the C_{2+} production in this study. As mentioned the Sargeant group used carbonate electrolyte, which generally has a pH of about 11. A carbonate-bicarbonate buffer similar to the ones used in the pH study in this work is likely to increase the selectivity of C_{2+} products, and can be an avenue for future research. Surprisingly, no C_{2+} liquid products were detected in these experiments, with the only liquid product being formate (2-4% FE, table C.5). The 20wt% PTFE with 270 μm gap experiment was not measured for liquid products due to sample misplacement (human error).

Intermediate conclusions from Bimetallic CuAg Electrolysis experimental part:

1. PTFE in AgNafion layer increases CO selectivity but not C_{2+} in a bimetallic CuAg system.
2. CL-BPM gap improves i-CO_2 liberation and CO production in a bimetallic CuAg system.
3. The improved CO_2 and CO production does not seem to lead to higher C_{2+} production in a bimetallic CuAg system, contrary to the CO intermediary theory.

5

Conclusions and Recommendations

5.1. Conclusions

This thesis examines a novel version of CO_2 electrolysis known as bicarbonate electrolysis. Through the process value-added chemicals that are normally sourced from oil and gas can be produced using renewable energy sources and sustainably sourced CO_2. Importantly, bicarbonate electrolysis can be integrated with carbon capture which effectively bypasses the energy intensive steps of CO_2 recovery and compression associated with gaseous-fed operation, making the process even more sustainable. The focus of this work is on CO_2 reduction to CO, with the goal to identify factors that can improve the selectivity and stability of CO. Special emphasis is placed on the role of pH in the process. With that in mind, the following research question was posed:

How can CO selectivity and stability be improved in bicarbonate electrolysis?

Three sub-research questions were also stated to assist in covering the topic:

1. **What are the parameters that influence CO selectivity in bicarbonate electrolysis?**
2. **What is the long-term stability of CO in bicarbonate electrolysis?**
3. **What is the effect of pH on CO selectivity and stability over time?**

In order to address the posed research questions a variety of reactor and operational parameters from the (bi)carbonate literature were evaluated for their effect on CO selectivity. It was concluded that in current bicarbonate electrolysis peak values of CO selectivity are reported mostly. Therefore, this thesis focused on shedding light on the stability of CO production, reporting trends of CO selectivity over time as well as peak values.

The selectivity of CO was improved substantially by introducing a catalyst-membrane gap using a hydrophilic and porous spacer. CO selectivity increased from 50% to 78% in peak production, recording 55% averaged over 3 hour operation. These results compare with the previously highest reported value in the (bi)carbonate literature, when working at ambient conditions with the current density of 100 mA/cm^2. In this work the selectivity improvement was accomplished in an economic and time efficient manner by inserting a relatively cheap spacer in between the membrane and electrode. The stability of CO was however not improved with the addition of the spacer. pH was shown to impact both CO selectivity and stability, with higher bicarbonate pH leading to decreased selectivity while improving the stability. Furthermore, it was shown that by maintaining a constant bicarbonate pH the stability does not improve, contrary to previous suggestions as well as indications of results from this study. This observation along with the increased CO_2 measured in the output points to cathode changes as the main cause of decreased CO stability in bicarbonate electrolysis.

The conclusions of this thesis are as follows:

1. CL-BPM spacing improves CO selectivity in a bicarbonate electrolyser using Ag catalyst.
2. The system shows a decrease in stability as characterised in experiments over 3 and 14 hours.
3. CL-BPM spacing does not improve stability.
4. An optimum CL-BPM spacing likely exists in the 0 - 405 μm range, probably between 135 - 270 μm.
5. Higher bicarbonate catholyte pH reduces CO selectivity, while improving stability.
6. Constant bicarbonate pH does not lead to improved CO stability.
7. Higher bicarbonate catholyte pH improves CO_2 utilization, although likely it is through increased carbonation reactions.
8. The results indicate that the primary cause of declining CO stability is undesirable changes taking place in the cathode during electrolysis.
9. No effect on CO selectivity is seen for changing Ag or Nafion loading, or adding PTFE to the CL, for the system used in this study.
10. Hydrophobic GDL (39BB) is preferable to hydrophilic GDL (H23) for CO selectivity and stability when using interdigitated flow pattern.
11. Flow pattern, channel dimensions and GDL interplay matter, with diffusive and convective mass transfer depending on these parameters, as well as the prevalence of the HER.
12. The CO selectivity is not limited by catalyst surface coverage of the GDL.
13. Pulsed start/stop potentials do not improve CO stability in a bicarbonate electrolyser producing CO at 100 mA/cm^2
14. PTFE in AgNafion layer in bimetallic CuAg electrolysis increases CO selectivity but not C_{2+}.
15. CL-BPM spacing improves i-CO_2 liberation and CO production in a bimetallic CuAg system.
16. In a bimetallic system, the improved CO_2 and CO production does not seem to lead to higher C_{2+} production, contrary to the CO intermediary theory.

5.2. Recommendations

There are a number of opportunies for improving upon the work of this thesis. Based on the conclusions outlined above, the following research is recommended for future studies:

1. An undefined optimum spacing for CO selectivity likely exists in the 0 - 405 μm range, probably between 135 - 270 μm. It is recommended for future studies to perform experiments within that range to search for that optimum, as well as search for factors that can improve the stability when accompanied with spacing. Longer gap lengths to identify the point of decreased effect are also advised.
2. It is likely that the drop in stability is related to changes taking place in the cathode during electrolysis. It is recommended for future research that any changes in the cathode, specifically the catalyst layer are examined. Rearrangement of the catalyst crystal structure or particle agglomeration, which could reduce the catalyst activity, could be relevant in this regard. Also to be explored is the effect of contamination of the catalyst from salts which can be introduced in the system from less than 100% pure bicarbonate salt.
3. pH measurements in the CL-BPM gap microenvironment in operando are recommended, with spacers present, to map the pH gradient in that space and any changes taking place during electrolysis with regard to CO selectivity. Techniques such as FLIM (Fluorescence Lifetime Imaging Microscopy) can be used to that effect.
4. There are many variables involved in the electrode preparation process. Sonication time of GDL (if sonicated), sonication time of ink and composition, ink vortexing pre coating, coating variables such as gas pressure, the temperature of the hot plate for drying the electrode during coating and more can play a role. It is unclear how these factors influence CO selectivity, and so could be an avenue for future research.
5. As limiting the HER is a key factor in improving CO selectivity in bicarbonate electrolysis, and in this study hydrophobic GDL was shown to be superior to a hydrophilic, it is recommended that a study be devoted to exploring the effect of hydrophobicity on CO selectivity. Testing electrodes of varying levels of hydrophobicity, quantified by contact angle measurements, and showing the relationship with CO selectivity would provide valuable information to the field.

6. When choosing flow pattern, channel dimensions of flow field, and the GDL for an experimental study it is recommended that the interplay of these factors is kept in mind. Although a certain flow pattern shows optimal results in one study for example, it might not be optimal for a system with different parameters.
7. It is recommended that a 2 or 3 dimensional modelling study be done on the electrolyte flow in the catalyst-membrane gap of a bicarbonate electrolyser, which uses interdigitated flow pattern. It is possible that the mixing has an impact on CO selectivity, as for desired operation a pH gradient must be maintained across the space, and although mixing is beneficial to distribute the reactant to the catalyst and remove the products, excessive turbulent mixing could be detrimental to the efficiency of the system.
8. There are indications that increasing bicarbonate flowrate (convective mass transport) improves CO selectivity, based on the results of an experiment in this work as well as the work of Zhang et al. [37]. However, as only one experiment was performed in this work due to time constraints, and the study by Zhang et al. was based on a different electrode, the implications cannot be confirmed. It is therefore recommended that the effect of convective mass transport on CO selectivity when using a GDE is examined in a separate study.
9. A substantially higher initial CO selectivity was seen when using increased electrolyte volumes in the long-term stability experiments of this study. It seems to be a result of the increased volume, although the reasons behind that are not clear. A study where the effect of electrolyte volume on CO selectivity is examined would provide insight to the field and help to explain this observation.
10. Bicarbonate CO electrolysis studies that look into the effect of CL-BPM spacing on CO selectivity and stability at higher current densities are recommended for future work, as the importance of efficient production at higher current densities is essential for scale-up and industrial considerations.

References

[1] United Nations. *What is Climate Change?* 2023. URL: https://www.un.org/en/climatechange/what-is-climate-change (visited on 09/12/2023).

[2] Intergovernmental Panel on Climate Change. *Climate Change 2021: Summary for all*. Intergovernmental Panel on Climate Change, 2021. URL: https://www.ipcc.ch/report/ar6/wg1/downloads/outreach/IPCC_AR6_WGI_SummaryForAll.pdf (visited on 11/12/2023).

[3] Yale School of Environment. *Why We Won't Know When We've Passed the 1.5-Degree Threshold*. 2023. URL: https://e360.yale.edu/digest/1.5-degrees-scientific-consensus#:~:text=Warming%20surpassed%20the%201.5%2Ddegree,expected%20to%20surpass%201.5%20degrees..

[4] A.G. Olabi and Mohammad Ali Abdelkareem. "Renewable energy and climate change". In: *Renewable and Sustainable Energy Reviews* 158 (2022), p. 112111.

[5] Jaime Nieto, Óscar Carpintero, and Luis J Miguel. "Less than 2 C? An economic-environmental evaluation of the Paris Agreement". In: *Ecological Economics* 146 (2018), pp. 69–84.

[6] International Energy Agency. *The role of CCUS in low-carbon power systems*. International Energy Agency, 2020. URL: https://iea.blob.core.windows.net/assets/ccdcb6b3-f6dd-4f9a-98c3-8366f4671427/The_role_of_CCUS_in_low-carbon_power_systems.pdf (visited on 11/12/2023).

[7] Pierre Friedlingstein et al. "Global carbon budget 2022". In: *Earth System Science Data Discussions* 2022 (2022), pp. 1–159.

[8] International Energy Agency. *Carbon capture, utilization and storage*. 2023. URL: https://www.iea.org/energy-system/carbon-capture-utilisation-and-storage (visited on 11/12/2023).

[9] International Energy Agency. *Direct air capture*. 2023. URL: https://www.iea.org/energy-system/carbon-capture-utilisation-and-storage/direct-air-capture (visited on 11/12/2023).

[10] Yale Climate Connenctions. *Covering Ocean Acidification: Chemistry and Considerations*. 2008. URL: https://yaleclimateconnections.org/2008/06/covering-ocean-acidification-chemistry-and-considerations/ (visited on 12/12/2023).

[11] David L. Chandler. *How to pull carbon dioxide out of seawater*. 2023. URL: https://news.mit.edu/2023/carbon-dioxide-out-seawater-ocean-decorbonization-0216 (visited on 11/12/2023).

[12] Wan Yun Hong. "A techno-economic review on carbon capture, utilisation and storage systems for achieving a net-zero CO2 emissions future". In: *Carbon Capture Science & Technology* 3 (2022), p. 100044.

[13] Goetheeer, Earl. CTO at High Tech XL, Part time full professor at Technical University of Delft. Personal communication, 25APR2024.

[14] European Commission. *Carbon capture, storage and utilisation*. 2022. URL: https://energy.ec.europa.eu/topics/oil-gas-and-coal/carbon-capture-storage-and-utilisation_en.

[15] International Energy Agency. *Putting CO2 to Use*. International Energy Agency, 2019. URL: https://iea.blob.core.windows.net/assets/50652405-26db-4c41-82dc-c23657893059/Putting_CO2_to_Use.pdf.

[16] Bas Fransen. *Carbon Capture and Utilization (CCU)*. 2020. URL: https://www.ecomatcher.com/carbon-capture-and-utilization-ccu/ (visited on 06/05/2024).

[17] Sumit Verma, Shawn Lu, and Paul JA Kenis. “Co-electrolysis of CO2 and glycerol as a pathway to carbon chemicals with improved technoeconomics due to low electricity consumption”. In: *Nature Energy* 4.6 (2019), pp. 466–474.

[18] Tengfei Li et al. “Electrolytic conversion of bicarbonate into CO in a flow cell”. In: *Joule* 3.6 (2019), pp. 1487–1497.

[19] Alex J Welch et al. “Bicarbonate or carbonate processes for coupling carbon dioxide capture and electrochemical conversion”. In: *ACS Energy Letters* 5.3 (2020), pp. 940–945.

[20] Jared Sisler et al. “Ethylene electrosynthesis: a comparative techno-economic analysis of alkaline vs membrane electrode assembly vs CO2–CO–C2H4 tandems”. In: *ACS Energy Letters* 6.3 (2021), pp. 997–1002.

[21] Geonhui Lee et al. “CO2 electroreduction to multicarbon products from carbonate capture liquid”. In: *Joule* 7.6 (2023), pp. 1277–1288.

[22] Emily Jeng and Feng Jiao. “Investigation of CO 2 single-pass conversion in a flow electrolyzer”. In: *Reaction Chemistry & Engineering* 5.9 (2020), pp. 1768–1775.

[23] Eric W Lees et al. “Electrodes designed for converting bicarbonate into CO”. In: *ACS Energy Letters* 5.7 (2020), pp. 2165–2173.

[24] Donald S Ripatti, Thomas R Veltman, and Matthew W Kanan. “Carbon monoxide gas diffusion electrolysis that produces concentrated C2 products with high single-pass conversion”. In: *Joule* 3.1 (2019), pp. 240–256.

[25] R Kortlever et al. “Electrochemical carbon dioxide and bicarbonate reduction on copper in weakly alkaline media”. In: *Journal of Solid State Electrochemistry* 17 (2013), pp. 1843–1849.

[26] Narayanaru Sreekanth and Kanala Lakshminarasimha Phani. “Selective reduction of CO 2 to formate through bicarbonate reduction on metal electrodes: new insights gained from SG/TC mode of SECM”. In: *Chemical Communications* 50.76 (2014), pp. 11143–11146.

[27] Marco Dunwell et al. “The central role of bicarbonate in the electrochemical reduction of carbon dioxide on gold”. In: *Journal of the American Chemical Society* 139.10 (2017), pp. 3774–3783.

[28] Shuyu Liang et al. “Electrolytic cell design for electrochemical CO2 reduction”. In: *Journal of CO2 Utilization* 35 (2020), pp. 90–105.

[29] Lei Fan et al. “Strategies in catalysts and electrolyzer design for electrochemical CO2 reduction toward C2+ products”. In: *Science advances* 6.8 (2020), eaay3111.

[30] Bhanu Chandra Marepally et al. “Enhanced formation of> C1 Products in Electroreduction of CO2 by Adding a CO2 Adsorption Component to a Gas-Diffusion Layer-Type Catalytic Electrode”. In: *ChemSusChem* 10.22 (2017), pp. 4442–4446.

[31] Danielle A Salvatore et al. “Electrolysis of Gaseous CO2 to CO in a Flow Cell with a Bipolar Membrane”. In: *ACS Energy Letters* 3.1 (2017), pp. 149–154.

[32] David Sebastián et al. “CO2 reduction to alcohols in a polymer electrolyte membrane co-electrolysis cell operating at low potentials”. In: *Electrochimica Acta* 241 (2017), pp. 28–40.

[33] Wonhee Lee et al. “Catholyte-free electrocatalytic CO2 reduction to formate”. In: *Angewandte Chemie International Edition* 57.23 (2018), pp. 6883–6887.

[34] Paula Sebastián-Pascual et al. “Structure-sensitivity and electrolyte effects in CO2 electroreduction: from model studies to applications”. In: *ChemCatChem* 11.16 (2019), pp. 3626–3645.

[35] Oriol Gutiérrez-Sánchez et al. “A State-of-the-Art Update on Integrated CO2 Capture and Electrochemical Conversion Systems”. In: *ChemElectroChem* 9.5 (2022), e202101540.

[36] Arthur G Fink et al. “Impact of alkali cation identity on the conversion of HCO3- to CO in bicarbonate electrolyzers”. In: *ChemElectroChem* 8.11 (2021), pp. 2094–2100.

[37] Zishuai Zhang et al. “Porous metal electrodes enable efficient electrolysis of carbon capture solutions”. In: *Energy & Environmental Science* 15.2 (2022), pp. 705–713.

[38] Linde Engineering. *Carbon Monoxide*. 2024. URL: `https://www.linde-engineering.com/en/process-plants/hydrogen_and_synthesis_gas_plants/gas_products/carbon_monoxide/index.html` (visited on 06/05/2024).

[39] Alexander Bagger et al. “Catalytic CO2/CO reduction: gas, aqueous, and aprotic phases”. In: *ACS Catalysis* 12.4 (2022), pp. 2561–2568.

[40] Stephanie Nitopi et al. “Progress and perspectives of electrochemical CO2 reduction on copper in aqueous electrolyte”. In: *Chemical reviews* 119.12 (2019), pp. 7610–7672.

[41] Allied Market Research. *Carbon Monoxide Market to Reach* $8.2Billion, Globally, by 2032 at 4.1\% CAGR : Allied Market Research$. 2024. URL: https://www.prnewswire.com/news-releases/carbon-monoxide-market-to-reach-8-2-billion-globally-by-2032-at-4-1-cagr-allied-market-research%20302043143.html#:~:text=According%20to%20the%20report%2C%20the,4.1%25%20from%202023%20to%202032. (visited on 06/05/2024).

[42] Allied Market Research. *Carbon Monoxide Market*. 2024. URL: https://www.alliedmarketresearch.com/carbon-monoxide-market-A311694 (visited on 06/05/2024).

[43] Mariana CO Monteiro et al. “Efficiency and selectivity of CO2 reduction to CO on gold gas diffusion electrodes in acidic media”. In: *Nature communications* 12.1 (2021), p. 4943.

[44] Bingjie Zha, Chunxiang Li, and Jinjin Li. “Efficient electrochemical reduction of CO2 into formate and acetate in polyoxometalate catholyte with indium catalyst”. In: *Journal of Catalysis* 382 (2020), pp. 69–76.

[45] Jungkuk Lee, Hengzhou Liu, and Wenzhen Li. “Bicarbonate Electroreduction to Multicarbon Products Enabled by Cu/Ag Bilayer Electrodes and Tailored Microenviroments”. In: *ChemSusChem* 15.22 (2022), e202201329.

[46] Cornelius A Obasanjo et al. “High-rate and selective conversion of CO2 from aqueous solutions to hydrocarbons”. In: *Nature Communications* 14.1 (2023), p. 3176.

[47] Alexander Bagger et al. “Electrochemical CO2 reduction: a classification problem”. In: *ChemPhysChem* 18.22 (2017), pp. 3266–3273.

[48] Seoin Back, Min Sun Yeom, and Yousung Jung. “Active sites of Au and Ag nanoparticle catalysts for CO2 electroreduction to CO”. In: *Acs Catalysis* 5.9 (2015), pp. 5089–5096.

[49] Yongwook Kim, Eric W Lees, and Curtis P Berlinguette. “Permeability Matters When Reducing CO2 in an Electrochemical Flow Cell”. In: *ACS Energy Letters* 7.7 (2022), pp. 2382–2387.

[50] Yuguang C Li et al. “CO2 electroreduction from carbonate electrolyte”. In: *ACS Energy Letters* 4.6 (2019), pp. 1427–1431.

[51] Yoshio Hori, Katsuhei Kikuchi, and Shin Suzuki. “Production of CO and CH4 in electrochemical reduction of CO2 at metal electrodes in aqueous hydrogencarbonate solution”. In: *Chemistry letters* 14.11 (1985), pp. 1695–1698.

[52] J Albo et al. “Towards the electrochemical conversion of carbon dioxide into methanol”. In: *Green Chemistry* 17.4 (2015), pp. 2304–2324.

[53] Yao Zheng et al. “Understanding the roadmap for electrochemical reduction of CO2 to multi-carbon oxygenates and hydrocarbons on copper-based catalysts”. In: *Journal of the American Chemical Society* 141.19 (2019), pp. 7646–7659.

[54] Chanyeon Kim et al. “Tailored catalyst microenvironments for CO2 electroreduction to multi-carbon products on copper using bilayer ionomer coatings”. In: *Nature Energy* 6.11 (2021), pp. 1026–1034.

[55] Kailun Yang et al. “Cation-driven increases of CO2 utilization in a bipolar membrane electrode assembly for CO2 electrolysis”. In: *ACS Energy Letters* 6.12 ().

[56] Chubai Chen et al. “Cu-Ag tandem catalysts for high-rate CO2 electrolysis toward multicarbons”. In: *Joule* 4.8 (2020), pp. 1688–1699.

[57] Mahsa Sadeghpour, Rozita Yusoff, and Mohamed Kheireddine Aroua. “Polymeric ionic liquids (PILs) for CO2 capture”. In: *Reviews in Chemical Engineering* 33.2 (2017), pp. 183–200.

[58] Justin C Bui et al. “Dynamic boundary layer simulation of pulsed CO2 electrolysis on a copper catalyst”. In: *ACS Energy Letters* 6.4 (2021), pp. 1181–1188.

[59] Ying Chuan Tan et al. “Modulating local CO2 concentration as a general strategy for enhancing C- C coupling in CO2 electroreduction”. In: *Joule* 4.5 (2020), pp. 1104–1120.

[60] Jiaqi Wang et al. “Silver/copper interface for relay electroreduction of carbon dioxide to ethylene”. In: *ACS applied materials & interfaces* 11.3 (2019), pp. 2763–2767.

[61] Youngkeun Jeon et al. “Electrodeposition of Cu-Ag films in ammonia-based electrolyte”. In: *Journal of Alloys and Compounds* 775 (2019), pp. 639–646.

[62] Seunghwa Lee, Gibeom Park, and Jaeyoung Lee. “Importance of Ag–Cu biphasic boundaries for selective electrochemical reduction of CO2 to ethanol”. In: *Acs Catalysis* 7.12 (2017), pp. 8594–8604.

[63] Yuguang C Li et al. “Binding site diversity promotes CO2 electroreduction to ethanol”. In: *Journal of the American Chemical Society* 141.21 (2019), pp. 8584–8591.

[64] Chong Wang et al. “Silver modified copper foam electrodes for enhanced reduction of CO 2 to C 2+ products”. In: *Materials Advances* 3.12 (2022), pp. 4964–4972.

[65] Andrew A Peterson et al. “How copper catalyzes the electroreduction of carbon dioxide into hydrocarbon fuels”. In: *Energy & Environmental Science* 3.9 (2010), pp. 1311–1315.

[66] Jeremy T Feaster et al. “Understanding selectivity for the electrochemical reduction of carbon dioxide to formic acid and carbon monoxide on metal electrodes”. In: *Acs Catalysis* 7.7 (2017), pp. 4822–4827.

[67] Ryan P Jansonius et al. “Strain engineering electrocatalysts for selective CO2 reduction”. In: *ACS Energy Letters* 4.4 (2019), pp. 980–986.

[68] Kendra P Kuhl et al. “Electrocatalytic conversion of carbon dioxide to methane and methanol on transition metal surfaces”. In: *Journal of the American Chemical Society* 136.40 (2014), pp. 14107–14113.

[69] Federico Calle-Vallejo and Marc TM Koper. “Theoretical considerations on the electroreduction of CO to C2 species on Cu (100) electrodes”. In: *Angewandte Chemie* 125.28 (2013), pp. 7423–7426.

[70] Jens Kehlet Nørskov et al. “Trends in the exchange current for hydrogen evolution”. In: *Journal of The Electrochemical Society* 152.3 (2005), J23.

[71] Ezra L Clark et al. “Electrochemical CO2 reduction over compressively strained CuAg surface alloys with enhanced multi-carbon oxygenate selectivity”. In: *Journal of the American Chemical Society* 139.44 (2017), pp. 15848–15857.

[72] Marvin L Frisch et al. “Unraveling the synergistic effects of Cu-Ag tandem catalysts during electrochemical CO2 reduction using nanofocused X-ray probes”. In: *Nature Communications* 14.1 (2023), p. 7833.

[73] David Wakerley et al. “Gas diffusion electrodes, reactor designs and key metrics of low-temperature CO2 electrolysers”. In: *Nature Energy* 7.2 (2022), pp. 130–143.

[74] Lien-Chun Weng, Alexis T Bell, and Adam Z Weber. “Modeling gas-diffusion electrodes for CO 2 reduction”. In: *Physical Chemistry Chemical Physics* 20.25 (2018), pp. 16973–16984.

[75] Balázs Endrődi et al. “Operando cathode activation with alkali metal cations for high current density operation of water-fed zero-gap carbon dioxide electrolysers”. In: *Nature energy* 6.4 (2021), pp. 439–448.

[76] Eric W Lees et al. “Linking gas diffusion electrode composition to CO 2 reduction in a flow cell”. In: *Journal of Materials Chemistry A* 8.37 (2020), pp. 19493–19501.

[77] Benjamin AW Mowbray et al. “How catalyst dispersion solvents affect CO2 electrolyzer gas diffusion electrodes”. In: *Energy & Fuels* 35.23 (2021), pp. 19178–19184.

[78] Chengxiang Xiang, Kimberly M Papadantonakis, and Nathan S Lewis. “Principles and implementations of electrolysis systems for water splitting”. In: *Materials Horizons* 3.3 (2016), pp. 169–173.

[79] Kai Zeng and Dongke Zhang. “Recent progress in alkaline water electrolysis for hydrogen production and applications”. In: *Progress in energy and combustion science* 36.3 (2010), pp. 307–326.

[80] Filipa Franco et al. “A systematic performance history analysis of a chlor-alkali membrane electrolyser under industrial operating conditions”. In: *Applied Sciences* 9.2 (2019), p. 284.

[81] Andrew R Crothers et al. “Theory of multicomponent phenomena in cation-exchange membranes: Part I. Thermodynamic model and validation”. In: *Journal of The Electrochemical Society* 167.1 (2020), p. 013547.

[82] D.R. Lide. *CRC Handbook of Chemistry and Physics, 90th Edition*. Taylor & Francis, 2009. ISBN: 9781420090840. URL: https://books.google.nl/books?id=OmkbNgAACAAJ.

[83] Eric W Lees et al. “Gas diffusion electrodes and membranes for CO2 reduction electrolysers”. In: *Nature Reviews Materials* 7.1 (2022), pp. 55–64.

[84] Tengfei Li et al. “Conversion of bicarbonate to formate in an electrochemical flow reactor”. In: *ACS Energy Letters* 5.8 (2020), pp. 2624–2630.

[85] Joaquin Resasco et al. “Promoter effects of alkali metal cations during electrocatalytic carbon dioxide reduction”. In: *J. Am. Chem. Soc* 139.11277.10 (2017), p. 1021.

[86] Meenesh R Singh, Ezra L Clark, and Alexis T Bell. “Effects of electrolyte, catalyst, and membrane composition and operating conditions on the performance of solar-driven electrochemical reduction of carbon dioxide”. In: *Physical Chemistry Chemical Physics* 17.29 (2015), pp. 18924–18936.

[87] Meenesh R Singh et al. “Hydrolysis of electrolyte cations enhances the electrochemical reduction of CO2 over Ag and Cu”. In: *Journal of the American chemical society* 138.39 (2016), pp. 13006–13012.

[88] Onagie Ayemoba and Angel Cuesta. “Spectroscopic evidence of size-dependent buffering of interfacial pH by cation hydrolysis during CO2 electroreduction”. In: *ACS applied materials & interfaces* 9.33 (2017), pp. 27377–27382.

[89] Michael R Thorson, Karl I Siil, and Paul JA Kenis. “Effect of cations on the electrochemical conversion of CO2 to CO”. In: *Journal of the Electrochemical Society* 160.1 (2012), F69.

[90] Saket S Bhargava et al. “System design rules for intensifying the electrochemical reduction of CO2 to CO on Ag nanoparticles”. In: *ChemElectroChem* 7.9 (2020), pp. 2001–2011.

[91] Justin C Bui et al. “Engineering catalyst–electrolyte microenvironments to optimize the activity and selectivity for the electrochemical reduction of CO2 on Cu and Ag”. In: *Accounts of chemical research* 55.4 (2022), pp. 484–494.

[92] Marilia Moura de Salles Pupo and Ruud Kortlever. “Electrolyte effects on the electrochemical reduction of CO2”. In: *ChemPhysChem* 20.22 (2019), pp. 2926–2935.

[93] Divya Bohra et al. “Modeling the electrical double layer to understand the reaction environment in a CO 2 electrocatalytic system”. In: *Energy & Environmental Science* 12.11 (2019), pp. 3380–3389.

[94] Stefan Ringe et al. “Understanding cation effects in electrochemical CO 2 reduction”. In: *Energy & Environmental Science* 12.10 (2019), pp. 3001–3014.

[95] Vincent J Frilette. “Preparation and characterization of bipolar ion exchange membranes”. In: *The Journal of Physical Chemistry* 60.4 (1956), pp. 435–439.

[96] R Pärnamäe et al. “Bipolar membranes: A review on principles, latest developments, and applications”. In: *Journal of Membrane Science* 617 (2021), p. 118538.

[97] Patrick K Giesbrecht and Michael S Freund. “Recent advances in bipolar membrane design and applications”. In: *Chemistry of Materials* 32.19 (2020), pp. 8060–8090.

[98] Zishuai Zhang et al. “Conversion of reactive carbon solutions into CO at low voltage and high carbon efficiency”. In: *ACS Central Science* 8.6 (2022), pp. 749–755.

[99] David A Vermaas and Wilson A Smith. “Synergistic electrochemical CO2 reduction and water oxidation with a bipolar membrane”. In: *ACS Energy Letters* 1.6 (2016), pp. 1143–1148.

[100] J Balster, DF Stamatialis, and Matthias Wessling. “Electro-catalytic membrane reactors and the development of bipolar membrane technology”. In: *Chemical engineering and processing: process intensification* 43.9 (2004), pp. 1115–1127.

[101] Carolina Fernandez-Gonzalez et al. “Electrodialysis with bipolar membranes for valorization of brines”. In: *Separation & Purification Reviews* 45.4 (2016), pp. 275–287.

[102] Xinghao Zhou et al. “Solar-driven reduction of 1 atm of CO2 to formate at 10% energy-conversion efficiency by use of a TiO2-protected III–V tandem photoanode in conjunction with a bipolar membrane and a Pd/C cathode”. In: *ACS Energy Letters* 1.4 (2016), pp. 764–770.

[103] Marijn A Blommaert et al. “Insights and challenges for applying bipolar membranes in advanced electrochemical energy systems”. In: *ACS Energy Letters* 6.7 (2021), pp. 2539–2548.

[104] Niko Kampman et al. “Fluid flow and CO2–fluid–mineral interactions during CO2-storage in sedimentary basins”. In: *Chemical Geology* 369 (2014), pp. 22–50.

[105] F Pelayo García de Arquer et al. “CO2 electrolysis to multicarbon products at activities greater than 1 A cm- 2”. In: *Science* 367.6478 (2020), pp. 661–666.

[106] Chanyeon Kim, Lien-Chun Weng, and Alexis T Bell. “Impact of pulsed electrochemical reduction of CO2 on the formation of C2+ products over Cu”. In: *ACS Catalysis* 10.21 (2020), pp. 12403–12413.

[107] Janis Timoshenko et al. “Steering the structure and selectivity of CO2 electroreduction catalysts by potential pulses”. In: *Nature Catalysis* 5.4 (2022), pp. 259–267.

[108] Toshi Oguma and Kazuhisa Azumi. “Improvement of electrochemical reduction of CO2 using the potential-pulse polarization method”. In: *Electrochemistry* 88.5 (2020), pp. 451–456.

[109] Bronkhorst. *General instructions digital Mass Flow / Pressure instruments laboratory style / IN-FLOW*. 2021. URL: https://www.bronkhorst.com/getmedia/50bed9ce-0445-4eba-9d37-f113ec53cb34/917022-Manual-general-instructions-digital-laboratory-style-and-IN-FLOW.pdf (visited on 05/12/2023).

[110] Fathaah Ansarul Huq. *Multiphysics Modeling of Electrochemical Conversion of Potassium Bicarbonate in Porous Electrode Flow Cell*. 2023.

[111] Giulia Marcandalli et al. “Electrolyte effects on CO2 electrochemical reduction to CO”. In: *Accounts of chemical research* 55.14 (2022), pp. 1900–1911.

[112] Cao-Thang Dinh et al. “CO2 electroreduction to ethylene via hydroxide-mediated copper catalysis at an abrupt interface”. In: *Science* 360.6390 (2018), pp. 783–787.

[113] Estela Ruiz-López et al. “Electrocatalytic CO2 conversion to C2 products: Catalysts design, market perspectives and techno-economic aspects”. In: *Renewable and Sustainable Energy Reviews* 161 (2022), p. 112329.

[114] Alejandro J Garza, Alexis T Bell, and Martin Head-Gordon. “Mechanism of CO2 reduction at copper surfaces: pathways to C2 products”. In: *Acs Catalysis* 8.2 (2018), pp. 1490–1499.

[115] Ki Dong Yang et al. “Current status and bioinspired perspective of electrochemical conversion of CO2 to a long-chain hydrocarbon”. In: *The Journal of Physical Chemistry Letters* 8.2 (2017), pp. 538–545.

[116] Polaris Market Research. *Ethylene Market Share, Size, Trends, Industry Analysis Report, By Feedstock (Naphtha, Ethane, Propane, Butane, Other Feedstock); By Application; By End-Use; By Region; Segment Forecast, 2023 - 2032*. Polaris Market Research, 2023. URL: https://www.polarismarketresearch.com/industry-analysis/ethylene-market#:~:text=The%20global%20Ethylene%20market%20was,across%20various%20end%2Duse%20industries..

[117] Precedence Research. *Ethanol Market (By Source: Second Generation, Grain-based, and Sugar Molasses Based; By Purity: Denatured and Undenatured; By Application: Industrial Solvents, Fuel Fuel Additives, Beverages, Disinfectant, Personal Care, and Others) - Global Market Size, Share, Trends Analysis, Segment Forecasts, Regional Outlook 2023 - 2032*. Precedence Research, 2023. URL: https://www.precedenceresearch.com/ethanol-market.

[118] Fortune Business Insights. *Carbon Monoxide Market Size, Share and Covid-19 Impact Analysis*. Fortune Business Insights, 2023. URL: https://www.fortunebusinessinsights.com/carbon-monoxide-market-105343.

[119] Data Bridge Market Research. *Global Methanol Market – Industry Trends and Forecast to 2030*. Data Bridge Market Research, 2023. URL: https://www.databridgemarketresearch.com/reports/global-methanol-market#:~:text=Data%20Bridge%20Market%20Research%20analyses,4.8%25%20during%20the%20forecast%20period..

[120] Sumit Verma et al. “A gross-margin model for defining technoeconomic benchmarks in the electroreduction of CO2”. In: *ChemSusChem* 9.15 (2016), pp. 1972–1979.

[121] Dong Dong Zhu, Jin Long Liu, and Shi Zhang Qiao. “Recent advances in inorganic heterogeneous electrocatalysts for reduction of carbon dioxide”. In: *Advanced materials* 28.18 (2016), pp. 3423–3452.

[122] Joshua A Rabinowitz and Matthew W Kanan. “The future of low-temperature carbon dioxide electrolysis depends on solving one basic problem”. In: *Nature Communications* 11.1 (2020), p. 5231.

A

Literature Supplementary Information

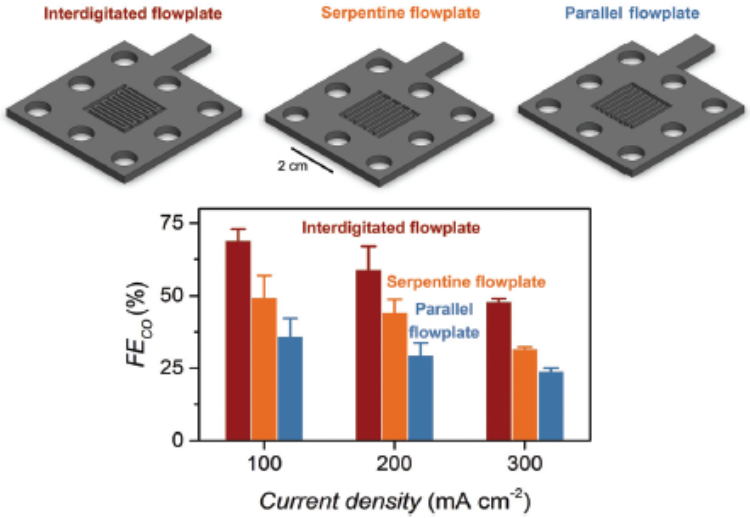

Figure A.1: Zhang et al. did experiments with three types of flow patterns in bicarbonate electrolysis: parallel, interdigitated and serpentine. They found that the faradaic efficiency of the intended product, CO, was the highest in the case of interdigitated flow channels [37].

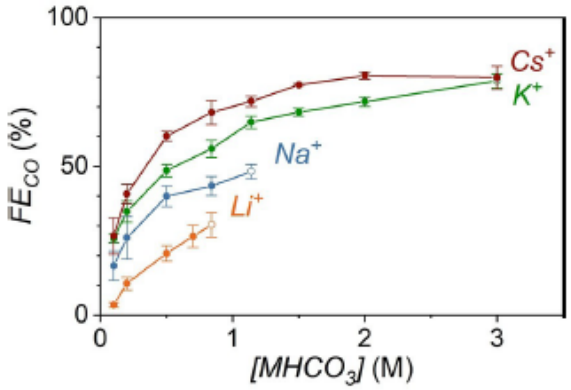

Figure A.2: The results from the study by Fink et al. show how CO selectivity is affected by the cation of the bicarbonate [36].

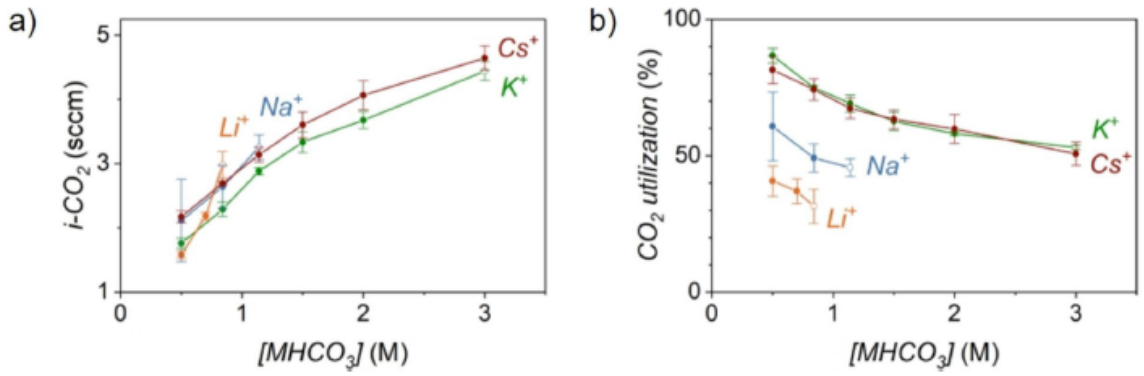

Figure A.3: Comparison between bicarbonate electrolyte cations for a) i-CO_2 formation and b): CO_2 utilization [36].

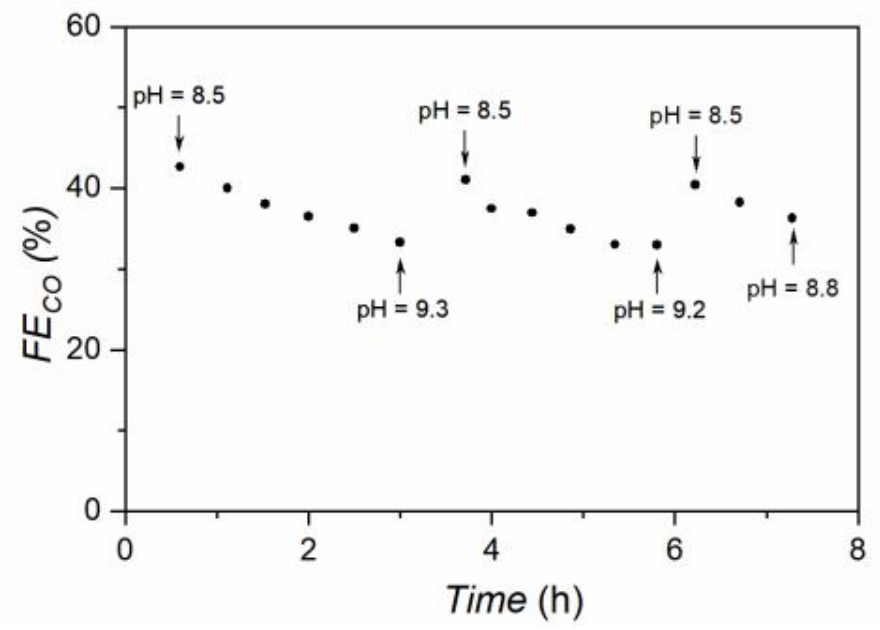

Figure A.4: 8 hour stability experiment performed at 100 $mAcm^{-2}$ by Lees et al. [23]. 3M $KHCO_3$ electrolyte was replenished after 3 and 6 hours, and H_2SO_4 was added at intervals to lower the pH.

B

Methodology Supplementary Information

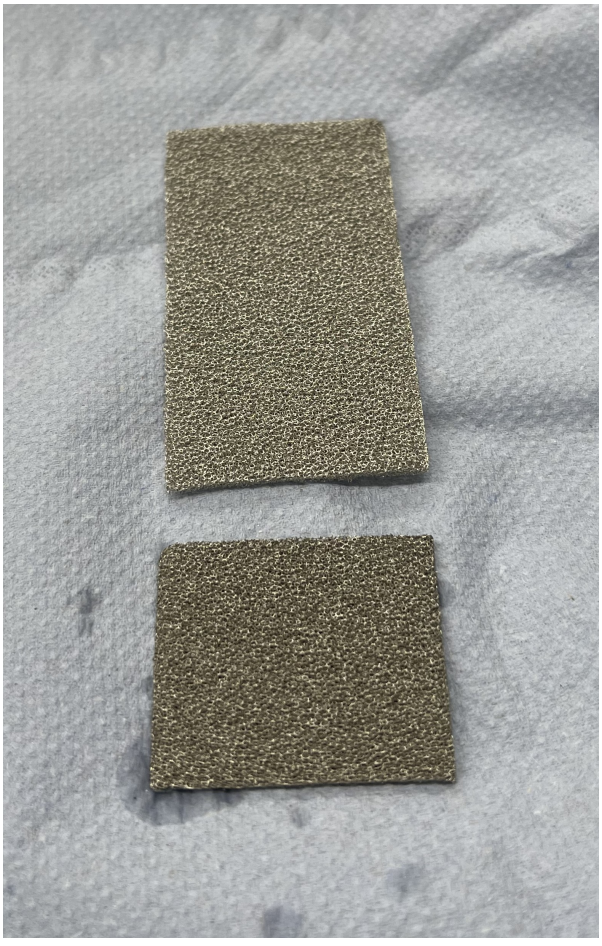

Figure B.1: The Ni foam anode used in the study. Above: an uncut piece of Ni foam sheet, below: a post-electrolysis Ni anode. Some darkening can be seen in the post-electrolysis anode, which is most likely NiO_2.

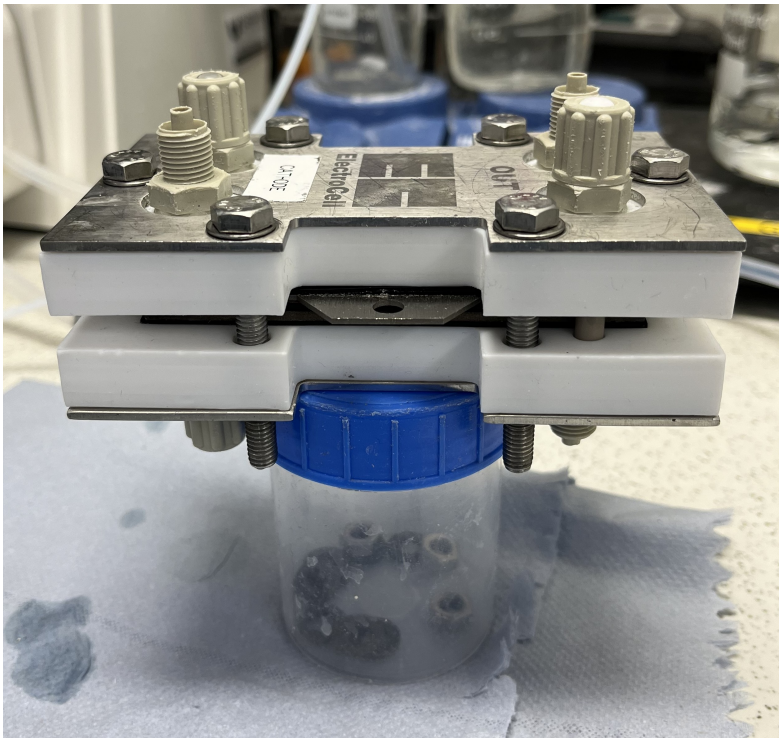

Figure B.2: The assembled flow-cell used in electrochemical experiments in the study.

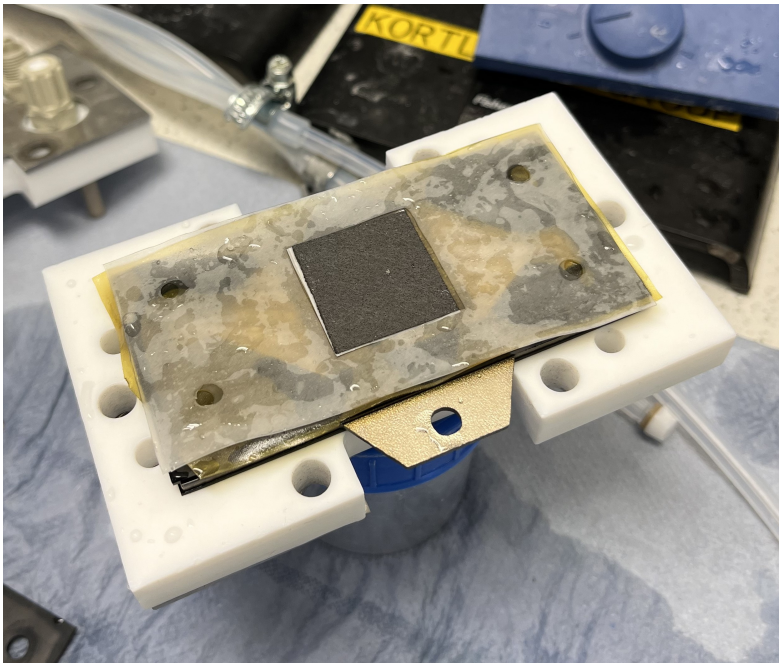

Figure B.3: An open view of the flow-cell used in electrochemical experiments in the study, showing the cathode placed in the silicone gasket, catalyst face down. Sandwiched between the cathode and the BPM is in this case an interposer, used to add CL-BPM spacing for a set of experiments.

```
# Bicarbonate buffer pH
Ka1=4.3e-7
Ka2=4.7e-11
pKa1 = -np.log10(Ka1)
pKa2 = -np.log10(Ka2)
print(pKa1,pKa2)
pH_2 = np.average([pKa1,pKa2])
print(pH_2)
# Bicarbonate carbonate buffer ph 8.5
Ka1=4.3e-7
Ka2=4.7e-11
def fall(ph,K):
    H=10**(-ph)
    OH=1e-14/H
    H2CO3,HCO3,CO32,Ctot = symbols('H2CO3,HCO3,CO32,Ctot')
    f1= H*HCO3/H2CO3 - Ka1
    f2= H*CO32/HCO3 - Ka2
    f3= H2CO3+HCO3+2*CO32 - H - K       # Charge balance
    f4= H2CO3+HCO3+CO32 - Ctot          # Carbon mass balance
    matrx =
nsolve((f1,f2,f3,f4),(H2CO3,HCO3,CO32,Ctot),(0.005,2.78,0.167,3.11))
    h2co3=matrx[0]
    print('For pH:',ph,'and K+:',K, ', H2CO3:',matrx[0],'HCO3-
:',matrx[1],'CO3_2-:',matrx[2],'Ctot:',matrx[3])
    return matrx
y=fall(9.0,3)
sumK = y[0]+y[1]+2*y[2]
print('Check:, K+ is',sumK)
# Bicarbonate carbonate buffer ph 9.5
Ka1=4.3e-7
Ka2=4.7e-11
def fall(ph,K):
    H=10**(-ph)
    OH=1e-14/H
    H2CO3,HCO3,CO32,Ctot = symbols('H2CO3,HCO3,CO32,Ctot')
    f1= H*HCO3/H2CO3 - Ka1
    f2= H*CO32/HCO3 - Ka2
    f3= H2CO3+HCO3+2*CO32 - H - K       # Charge balance
    f4= H2CO3+HCO3+CO32 - Ctot          # Carbon mass balance
    matrx =
nsolve((f1,f2,f3,f4),(H2CO3,HCO3,CO32,Ctot),(0.00035,1.55,0.73,2.27))
    h2co3=matrx[0]
    print('For pH:',ph,'and K+:',K, ', H2CO3:',matrx[0],'HCO3-
:',matrx[1],'CO3_2-:',matrx[2],'Ctot:',matrx[3])
    return matrx
y=fall(10.0,3)
sumK = y[0]+y[1]+2*y[2]
print('Check:, K+ is',sumK)
```

```
# Mass balance - S24 1xInterposer - Pre run carbonates concentrations
# [HCO3-] pH pre : pH:8.26
# With theoretical pH of 8.347 we have C total = 3.0000
pH=8.26
H=10**(-pH)
OH=1e-14/H
def func(X):
    # The components
    # H_+, CO3_2-, OH_-, HCO3_-, H2CO3 = A,B,C,D,E
    B,D,E = X
    # The acid-base equilibria
    eq1= H*D/E - 4.3e-7
    eq2= H*B/D -4.7e-11
    # Electrical neutrality expr. - charge balance
    eq4= D+2*B+OH - H -3
    return eq1,eq2,eq4
x0=[0.025,2.95,0.038]
roots = fsolve(func,(x0))
print(roots)
print(H,OH)
tes1=np.sum(roots)
print(tes1)
# Mass balance - S24 1xInterposer - Post run carbonates concentrations
# [HCO3-] pH post:9.27
# Overall [C] is now <3 (experimental + some C to gas products and i-CO2).
Product M from excel masterfile.
pH=9.27
H=10**(-pH)
OH=1e-14/H
def func(X):
    # The components
    # H_+, CO3_2-, OH_-, HCO3_-, H2CO3, CO2 = A,B,C,D,E,F
    B,D,E = X
    # The acid-base equilibria
    eq1= H*D/E - 4.3e-7
    eq2= H*B/D -4.7e-11
    # Electrical neutrality expr. - charge balance
    eq4= D+2*B+OH - H - (3-0.06005)
    return eq1,eq2,eq4
x0=[0.2,2.5,0.003]
roots = fsolve(func,(x0))
print(roots)
tes2=np.sum(roots)
print(tes2)
print(H,OH)
```

Figure B.4: The python code that was used to calculate the pH of the 8.5 and 9.5 carbonate-bicarbonate buffers, as well as for carbonates concentration for the mass balances.

C

Results and Discussion Supplementary Information

C.1. Initial Tests

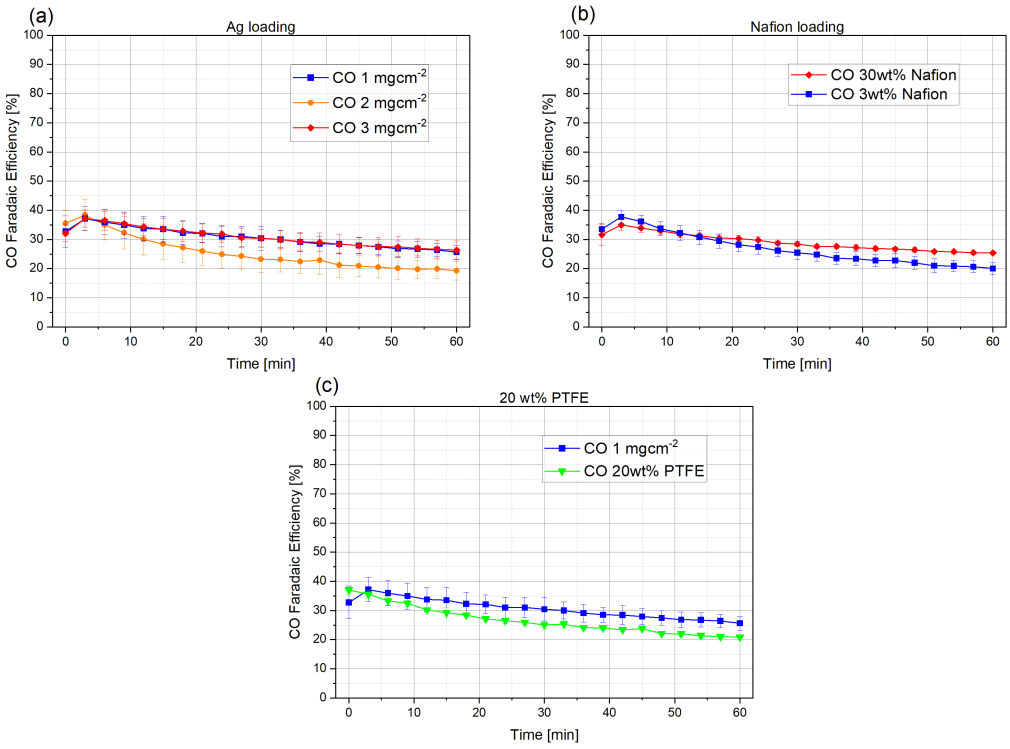

Figure C.1: Results of initial experiments. a): Ag loading experiments, b): Nafion loading experiments, c): PTFE addition to CL.

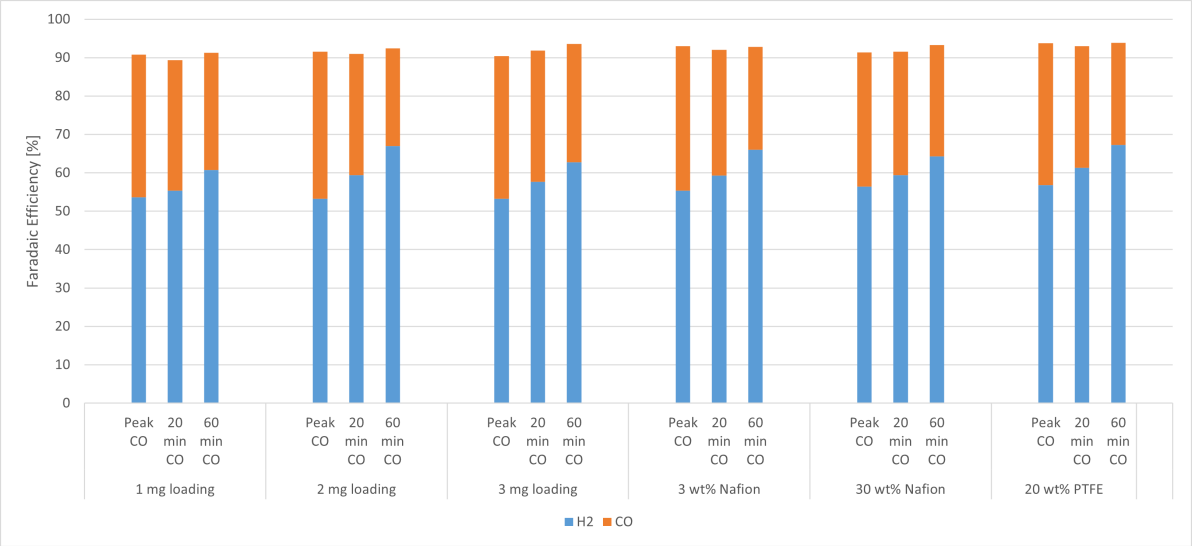

Figure C.2: CO FE results of initial experiments. How results are reported is important in interpreting results and putting them in context with literature results.

C.2. CO Selectivity

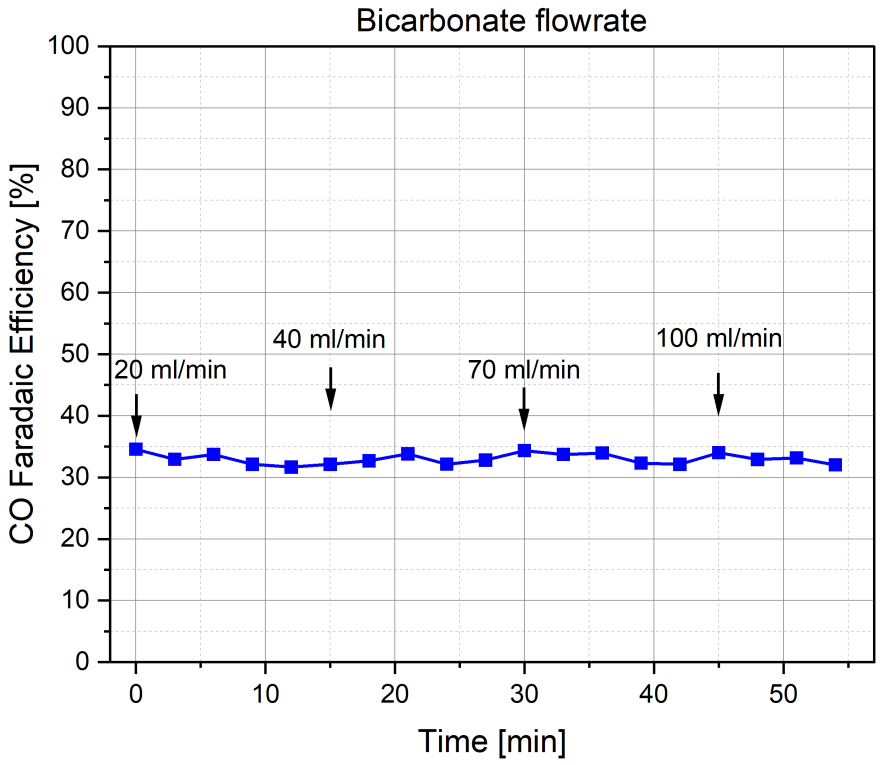

Figure C.3: The results from the bicarbonate flowrate experiment suggest that when increasing the convective mass transport the CO selectivity improves, as the usual drop in stability is not observed here.

C.3. CO Stability

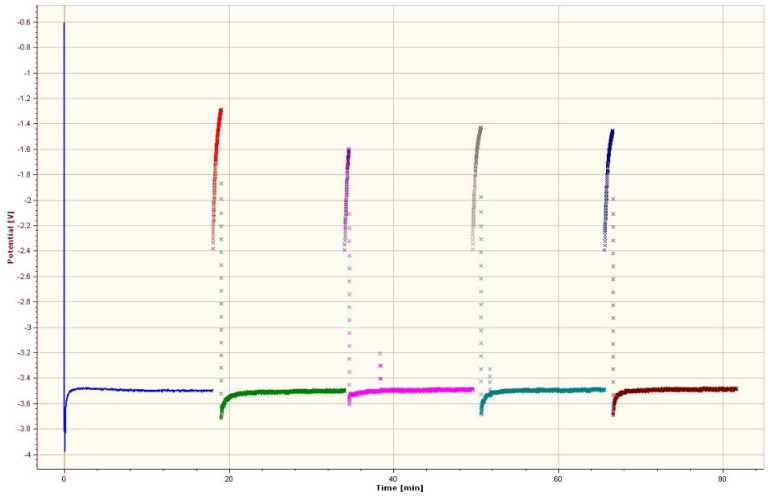

(a) OCP 15/1 mins

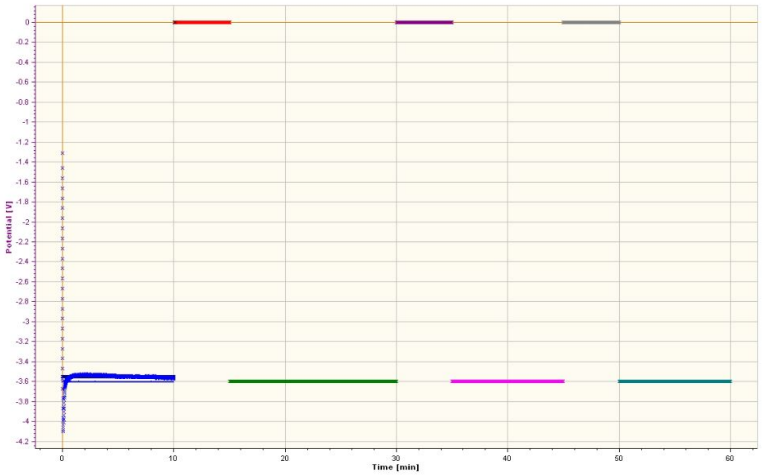

(b) CV 10/5 mins 1hr

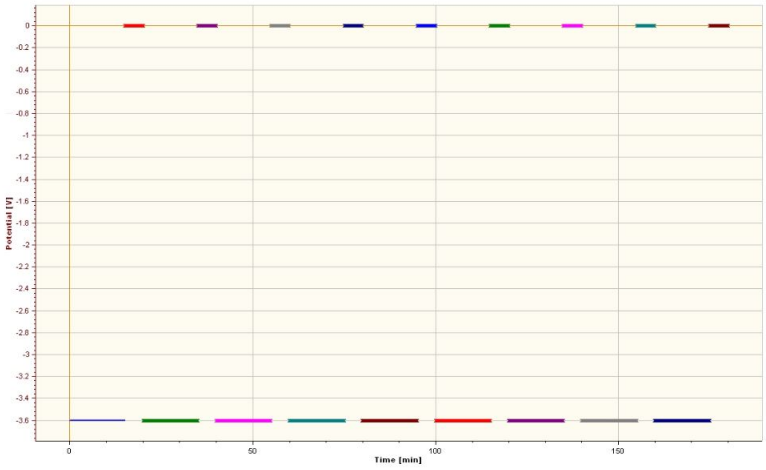

(c) CV 15/5 mins 3 hrs

Figure C.4: The potential profiles for the start/stop experiments. a): With open cell potential (OCP) for one minute pulses the voltage did not reach 0, with no effect on CO selectivity seen. b): By running set start/stop potential operation and setting the pulses at 0 V for 5 minute pulses, an effect on CO selectivity was seen albeit no improvement. c): In longer applied start/stop potential operation (15/5 minutes), no improvement of CO selectivity was seen.

C.4. Bimetallic CuAg Electrolysis

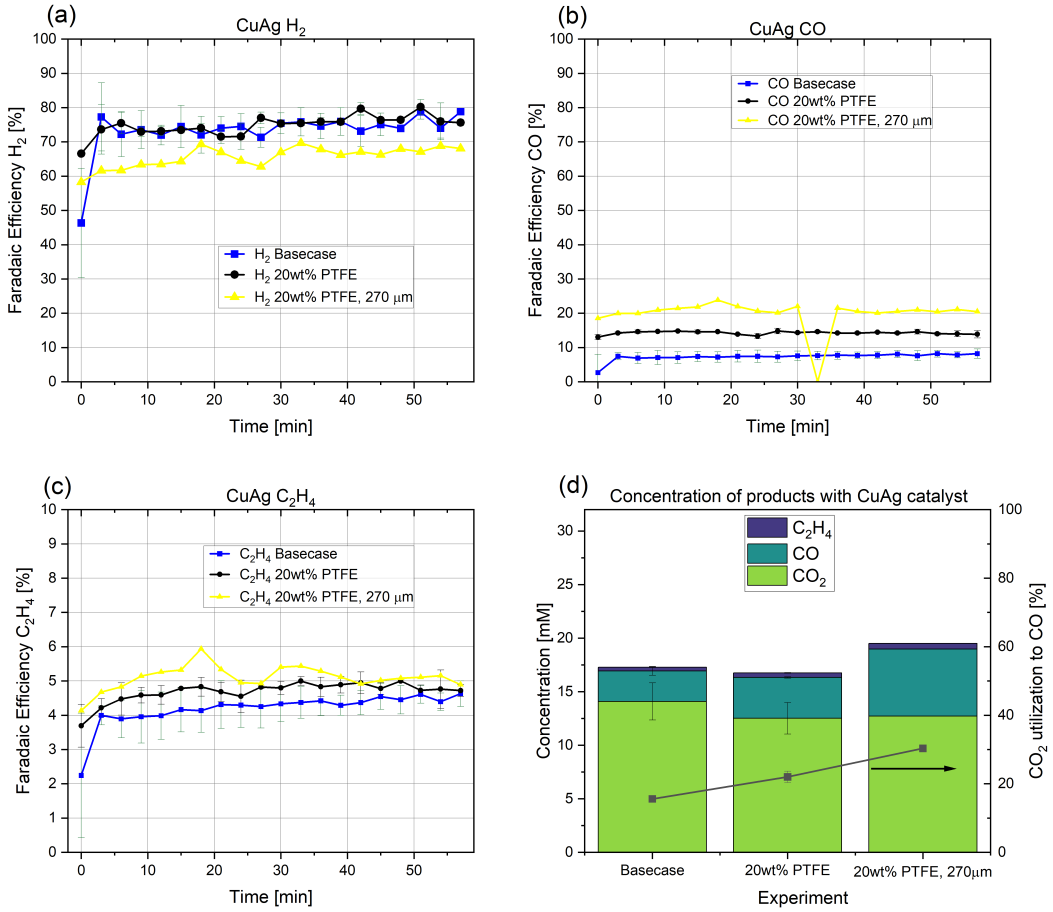

Figure C.5: Results from CuAg bimetallic experiments. a):H_2 FE, b): CO FE, c): C_2H_4 FE, d): Product concentration and CO_2 utilization to CO (based on method described in section 3.5.2).

C.5. C_{2+} Production and Market Outlook

Some qualities that make the production of C_{2+} compounds attractive are for example their high energy density combined with being suitable for current internal combustion engines [113], and the fact that they can directly enter into current value-chains for chemical production [114, 115]. The advantages of C_{2+} products can best be seen in their economic potential. For example ethylene and ethanol, two commonly studied CO_2RR C_{2+} products, have a combined annual market size of 236 billion USD, with an expected annual growth of just over 5% [116, 117]. Ethylene is widely used in the chemical industry, for example as a raw material for polyethylene (PE), while ethanol is much used in the food and beverage industry as well as in hand sanitizer production. By contrast, CO and methanol's combined annual market size is about 34 billion USD, also expected to grow similarly as the ethylene and ethanol markets [118, 119].

One downside of C_{2+} production is the lack of selectivity of Cu catalyst. Product separation is required, which is more difficult in the liquid phase but necessary if liquid products such as ethanol are being made. Another drawback of the electrochemical production of C_{2+} compounds on Cu is that they involve several complex electron transfer steps which are currently not well understood. For example, the reduction of CO_2 to ethylene and ethanol involve the transfer of 12 electrons. The simplified overall

reactions can be seen in reactions C.1 and C.2 below.

$$2CO_2 + 8H_2O + 12e^- \rightarrow C_2H_4 + 12OH^- \tag{C.1}$$

$$2CO_2 + 9H_2O + 12e^- \rightarrow C_2H_5OH + 12OH^- \tag{C.2}$$

In order for CO_2RR to become feasible on an industrial scale, improvements must be made in selectivity (faradaic efficiency, FE), energy efficiency (EE) and current density. Overa et al. recommended in 2022 the following criteria for industrial feasibility: over 80% C_{2+} FE, a minimum of 50% EE and 1000 mA/cm^2. Specifically for ethyelene and ethanol production, key parameters mentioned in techno-economic assessments are 70-90% FE and current density of 300 mA/cm^2 [120, 121], although it should be noted these numbers were reported in 2016. Improvements must also be made in reducing the overpotential to improve the energy efficiency of the process [122], which also affects the selectivity [113, 107].

C.6. Potential Profiles

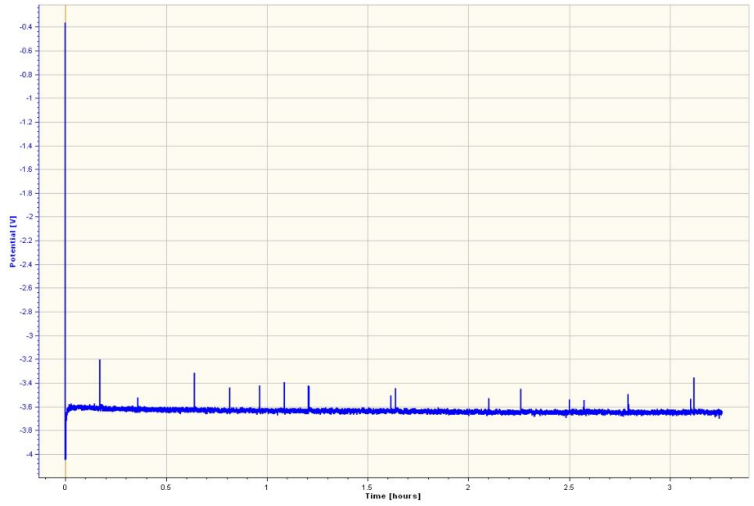

(a) 3 hour basecase run.

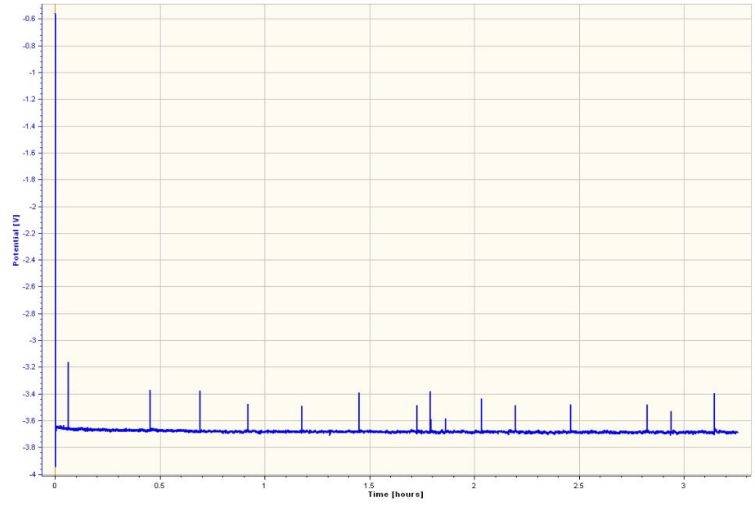

(b) 3 hour 135 μm gap run.

Figure C.6: Examples of potential profiles from experiments. a): 3 hour basecase run (electrode S22, see table C.2). b): 3 hour 135 μm gap run, electrode S24. Slightly higher overpotential can be seen, likely resulting from increased BPM overpotential from the higher i-CO_2 liberation and the increased spacing.

C.7. Other Information

Table C.1: Comparison of various cell and operational parameters between this study and comparable studies from the literature.

	Group	Berlinguette	Berlinguette	Berlinguette	Lee	This study
	Source	[23]	[37]	[37]	[45]	
Catholyte	Compound	$KHCO_3$	$KHCO_3$	$KHCO_3$	$KHCO_3$	$KHCO_3$
	Flow [ml/min]	90	100	100	50	50
	Molarity [mol/L]	3	3	3	3	3
	Volume [ml]	125	NA	NA	40 or 120	70
Anolyte	Compound	KOH	KOH	KOH	KOH	KOH
	Flow [ml/min]	40	40	40	50	70
	Molarity [mol/L]	1	1	1	1	1
	Volume [ml]	1000	NA	NA	40	140
Carrier gas	Compound	N2	Ar or N2 ***	Ar or N2 ***	Ar	Ar
	Flow [mln/min]	160	160	160	100	100
Cathode	Type	GDE	Foam	GDE	GDE	GDE
	MPL/PTFE	No/No	NA	Yes/Yes	Yes/Yes	Yes/Yes
	GDL Sonication	Yes	Yes	Yes	NA	Yes
	GDL type	H23	NA	CeTech with MPL	22BB	39BB
	Area [cm2]	4	4	4	6.25 (active)	6.25 (5 active)
Catalyst	Catalyst	Ag	Ag	Ag	Ag/Cu	Ag
	PVD	500nm	No	No	No	No
	Loading [mg/cm2]	1.3	NA	3.7	1	1.0 - 1.8
	T during coating	30	NA	NA	NA	70
	Ionomer	Naf 4wt%	NA	Naf 4wt%	20wt% Naf / Sust	4wt% Naf
Anode	Type	Ni foam	Ni foam	Ni foam	Ni foam	Ni foam
	Fresh	Yes	NA	NA	NA	Yes *
	Thickness	NA	NA	NA	NA	2.0 mm
	Area [cm^2]	4	4	4	6.25 (active)	2.9 x 3.3
Flow plate (cathode)	Pattern	Serpentine	Interdigitated	NA	6.25 cm2 flow channels mentioned	Interdigitated
	Channels width/depth/ribs [mm]	1.5/1.5/1	NA	NA	NA	1.0/1.0/1.0
	material	Titanium **	ABS plastic coated with Ag paint for conductivity	ABS plastic coated with Ag paint for conductivity	Titanium	Titanium
Flow plate (anode)	Pattern	Serpentine	NA	NA	6.25 cm^2 flow channels mentioned	Open
	Channels width/depth/ribs [mm]	1.5/1.5/1	NA	NA	NA	NA
	Material	Stainless steel **	NA	NA	Stainless steel	Stainless steel
	Assembly torque [Nm]	3	NA	NA	NA	3
Membrane	Type	BPM	BPM	BPM	BPM	BPM
	Fresh	Yes	NA	NA	NA	No (changed regularly)
Measurement / Reporting values	Normalized to 100%	Yes	Yes	Yes	NA	No
	Saturate electrolytes with produts before running GC (time)	15mins	15mins	15mins	NA	No
	Average (time)	No	No	No	No	Yes (60 mins)
	Single value	Yes	Yes	Yes	Yes	Yes
Other	EDTA	0.02M	0.02M	0.02M	NA	No
	Flow-cell	Custom made in-house	NA	NA	NA	Electro-Cell
	Magnetic electrolyte stirring	NA	NA	NA	NA	Yes

*After Initial Tests Experimental phase.

**In Suppl. info mention cathode flow-plate is Titanium and anode SS, but reverse in paper [23].

*** In Suppl. info mention Ar is carrier gas but in the paper mention N_2 [37].

Table C.2: Overview of the experiments discussed in the Results and Discussion chapter in the order of being presented. Included information for reference is the catalyst loading, peak and average CO FE, run time and average cell potential, which remained quite stable for the experiments. Also mentioned is the time base for reporting the CO FE average values, which might be slightly different from the run duration for the sake of even comparison.

Run nr.	Experiment	Electrode ID	Ag loading [mg/cm^2]	FE CO peak [%]	FE CO avg. [%]	Run time [min]	Time base for FE CO avg. [min]	Cell Potential [V]
Run6	Ag loading 1 mg/cm^2, 1	D	1.25	32	27	60	60	3.65
Run7	Ag loading 1 mg/cm^2, 2	E	1.12	39	34	60	60	3.57
Run8	Ag loading 2 mg/cm^2, 1	A	1.98	31	21	60	60	3.4
Run9	Ag loading 2 mg/cm^2, 2	B	1.86	41	30	60	60	3.42
Run10	Ag loading 3 mg/cm^2, 1	G	2.85	32	28	60	60	3.38
Run11	Ag loading 3 mg/cm^2, 2	H	2.83	38	34	60	60	3.46
Run17	Nafion loading 3wt%, 1	N	1.01	33	25	60	60	3.5
Run18	Nafion loading 3wt%, 2	M	0.96	38	29	60	60	3.5
Run15	Nafion loading 30wt%, 1	L	1.31	35	30	60	60	3.45
Run16	Nafion loading 30wt%, 2	R	1.09	31	28	60	60	3.55
Run19	PTFE loading 30wt%, 1	P1	0.96	36	26	60	60	3.58
Run20	PTFE loading 30wt%, 2	P2	0.99	39	27	60	60	3.54
Run41	GDL H23 basecase, 1	S4	1.41	50	29	45	42	3.59
Run52	GDL H23 basecase, 2	S10	1.33	34	23	45	42	3.44
Run53	GDL 39BB basecase, 1	S12	1.28	51	40	45	42	3.54
Run56	GDL 39BB basecase, 2	S13	1.22	45	36	45	42	3.7
Run48	GDL H23 non-sonicated, 1	A7	1.31	36	21	42	42	3.42
Run49	GDL H23 non-sonicated, 2	A8	1.36	36	22	42	42	3.42
Run54	GDL 39BB non-sonicated, 1	A5	1.22	48	38	42	42	3.55
Run55	GDL 39BB non-sonicated, 2	A6	1.23	48	41	42	42	3.68
Run45	H23 0.7mm Serpentine, 1	S7	1.39	6	4	30	24	3.35
Run47	H23 0.7mm Serpentine, 2	S8	1.49	10	6	30	24	3.29
Run91	H23 1.0mm Serpentine	S39	1.36	37	29	30	24	3.47
Run59	H23 1.5mm Serpentine, 1	S20	1.71	22	19	30	24	3.5
Run60	H23 1.5mm Serpentine, 2	S21	1.76	26	15	30	24	3.55
Run46	39BB 0.7mm Serpentine, 1	S6	1.18	31	27	24	24	3.38
Run61	39BB 0.7mm Serpentine, 2	S16	1.12	25	22	24	24	3.3
Run92	39BB 1.0mm Serpentine	S37	1.10	35	32	24	24	3.46
Run57	39BB 1.5mm Serpentine, 1	S14	1.49	44	40	24	24	3.55
Run58	39BB 1.5mm Serpentine, 2	S15	1.47	45	41	24	24	3.55
Run86	H23 1.5mm Interdigitated	S38	1.50	41	27	30	24	3.5
Run85	39BB 1.5mm Interdigitated	S34	1.15	36	30	30	24	3.4
Run66	H23 500nm PVD Ag film, 1	B3	1.50	54	37	51	42	3.7
Run67	H23 500nm PVD Ag film, 2	B4	1.46	45	28	51	42	3.44
Run42	39BB 500nm PVD Ag film, 1	B1	1.46	40	33	51	42	3.55
Run43	39BB 500nm PVD Ag film, 2	B2	1.30	38	34	51	42	3.62
Run50	CL-BPM gap 135 μm, 1	S9	1.17	61	51	42	42	3.55
Run51	CL-BPM gap 135 μm, 2	S11	1.33	55	51	42	42	3.58
Run62	CL-BPM gap 270 μm, 1	S17	1.06	74	62	42	42	3.72
Run63	CL-BPM gap 270 μm, 2	S18	1.31	82	70	42	42	3.72
Run68	CL-BPM gap 270 μm, 3	S19	1.30	76	66	42	42	3.63
Run70	3 hr basecase, 1	S22	1.44	45	31	180	174	3.61
Run71	3 hr basecase, 2	S23	1.54	44	25	180	174	3.59
Run72	3 hr CL-BPM gap 135 μm, 1	S24	1.12	71	55	180	174	3.69
Run74	3 hr CL-BPM gap 135 μm, 2	S26	1.39	65	51	180	174	3.68
Run76	3 hr CL-BPM gap 270 μm, 1	A8IB	1.47	75	55	180	174	3.5
Run77	3 hr CL-BPM gap 270 μm, 2	A7IB	1.44	74	51	180	174	3.49
Run78	3 hr CL-BPM gap 405 μm, 1	A5IB	1.50	71	45	174	174	3.62
Run79	3 hr CL-BPM gap 405 μm, 2	A6IB	1.55	79	49	174	174	3.4
Run73	Stability basecase, 1	S25	1.22	65	29	870	870	3.41
Run80	Stability basecase, 2	S28	1.30	59	23	870	870	3.32
Run89	Stability CL-BPM gap 135 μm, 1	A10IB	1.47	68	41	870	870	3.45
Run90	Stability CL-BPM gap 135 μm, 2	A12IB	1.31	72	46	870	870	3.45
Run82	Pulsed Start/OCP 15/1 mins	S30	1.44	78	NA	75	NA	NA
Run83	Pulsed CV Start/Stop 10/5 mins	S32	1.26	71	NA	57	NA	NA
Run84	Pulsed CV Start/Stop 15/5 mins	S33	1.25	80	NA	168	NA	NA
Run44	Catholyte flowrate, stability	S5	1.33	35	33	54	54	3.7
Run87	HCO_3^-/CO_3^{2-} pH 8.5	S35	1.26	39	33	60	42	3.55
Run88	HCO_3^-/CO_3^{2-} pH 9.5	S36	1.18	16	14	60	42	3.45
Run94	HCO_3^- pH 8.37 single-pass	A26IB	1.25	59	51	54	42	3.46
Run95	HCO_3^-/CO_3^{2-} pH 8.5 single-pass	A27IB	1.12	55	47	51	42	3.51
Run96	HCO_3^-/CO_3^{2-} pH 9.0 single-pass	A28IB	0.99	50	41	54	42	3.64
Run97	HCO_3^-/CO_3^{2-} pH 9.5 single-pass	A29IB	1.10	31	26	54	42	3.53
Run98	HCO_3^-/CO_3^{2-} pH 10.0 single-pass	A30IB	1.06	18	17	54	42	3.67

Table C.3: An overview of the experiments discussed in the CuAg bimetallic section of the Results and Discussion chapter. Mentioned is the CuSus/AgNaf catalyst/ionomer loadings (the ionomers were 15wt%), the average FE of CO and C2H4, reported for the also mentioned run time, and finally the average cell potential.

Run nr.	Experiment	Electrode ID	CuSus / AgNaf loading [cm^2]	FE CO avg. [%]	FE avg. C_2H_4 [%]	Run time [min]	Cell Potential [V]
Run25	CuAg Basecase, 1	L1	1.47 / 1.54	10	4	57	3.43
Run26	CuAg Basecase, 2	L2	1.47 / 1.70	13	5	57	3.41
Run64	CuAg 20wt% PTFE, 1	L5	1.26 / 1.78	14	5	57	3.5
Run65	CuAg 20wt% PTFE, 2	L6	1.26 / 1.68	14	4	57	3.43
Run69	CuAg 20wt% PTFE + 270 μm gap	L7	1.60 / 2.67	20	5	57	3.62

Table C.4: An overview of the metals detected in the ICP-OES measurements. Only a few samples were measured as metals were detected in very low quantities.

Run	Experiment	Electrode ID	Ag [ppm]	Cu [ppm]	Ba [ppm]	Ca [ppm]	Fe [ppm]	Na [ppm]	Cl [ppm]
Run43	39BB 500nm PVD Ag film, 2	B2	0.26	0.08	NA	NA	NA	NA	NA
Run44	Electrolyte Flowrates	S5	0.14	0.18	NA	NA	NA	NA	NA
Run89	Stability CL-BPM gap 135 μm, 1	A10IB	NA	NA	0,07	0.03	0.05	108.7	4.95
Run74	3 hr CL-BPM gap 135 μm, 2	S26	NA	NA	0,08	0.08	0.04	156.32	12.36
Run71	3 hr basecase, 2	S23	NA	NA	0,09	0.23	0.05	161.79	24.26
Run78	3 hr CL-BPM gap 405 μm, 1	A5IB	NA	NA	0,08	0.14	0.1	146.32	16.32
NA	Blank	NA	NA	NA	0,07	0.02	0.03	110.06	26.36

Table C.5: Overview of the liquid products HPLC measurements, presented in the order of being discussed in the Results and Discussion chapter. The only liquid product detected was formate, in the range of 1-4%. As such, it was not deemed necessary to measure every sample for liquid products nor include formate in graphs when reporting results.

Run nr.	Experiment	Electrode ID	FE Formate [%]	Run time [min]
Run7	Ag loading 1 mg/cm^2, 2	E	3.1	60
Run9	Ag loading 2 mg/cm^2, 2	B	0.9	60
Run10	Ag loading 3 mg/cm^2, 1	G	0.8	60
Run11	Ag loading 3 mg/cm^2, 2	H	1.4	60
Run19	PTFE loading 30wt%, 1	P1	1.5	60
Run20	PTFE loading 30wt%, 2	P2	1.6	60
Run91	H23 1.0mm Serpentine	S39	0.7	30
Run59	H23 1.5mm Serpentine, 1	S20	0.2	30
Run92	39BB 1.0mm Serpentine	S37	1.0	24
Run57	39BB 1.5mm Serpentine, 1	S14	2.0	24
Run58	39BB 1.5mm Serpentine, 2	S15	1.8	24
Run86	H23 1.5mm Interdigitated	S38	0.5	30
Run85	39BB 1.5mm Interdigitated	S34	0.7	30
Run42	39BB 500nm PVD Ag film, 1	B1	1.3	51
Run50	CL-BPM gap 135 m, 1	S9	2.8	42
Run51	CL-BPM gap 135 m, 2	S11	3.6	42
Run62	CL-BPM gap 270 m, 1	S17	1.9	42
Run63	CL-BPM gap 270 m, 2	S18	2.5	42
Run68	CL-BPM gap 270 m, 3	S19	2.1	42
Run70	3 hr basecase, 1	S22	1.4	180
Run71	3 hr basecase, 2	S23	0.8	180
Run72	3 hr CL-BPM gap 135 m, 1	S24	2.7	180
Run74	3 hr CL-BPM gap 135 m, 2	S26	2.8	180
Run76	3 hr CL-BPM gap 270 m, 1	A8IB	2.1	180
Run77	3 hr CL-BPM gap 270 m, 2	A7IB	1.7	180
Run78	3 hr CL-BPM gap 405 m, 1	A5IB	1.1	180
Run79	3 hr CL-BPM gap 405 m, 2	A6IB	1.3	180
Run73	Stability basecase, 1	S25	0.1	870
Run80	Stability basecase, 2	S28	0.0	870
Run89	Stability CL-BPM gap 135 m, 1	A12IB	0.1	870
Run90	Stability CL-BPM gap 135 m, 2	A10IB	0.1	870
Run82	Pulsed Start/OCP 15/1 mins	S30	1.8	75
Run84	Pulsed CV Start/Stop 15/5 mins	S33	1.5	168
Run87	HCO_3^-/CO_3^{2-} pH 8.5	S35	1.0	60
Run88	HCO_3^-/CO_3^{2-} pH 9.5	S36	0.6	60
Run25	CuAg Basecase, 1	L1	4.1	57
Run26	CuAg Basecase, 2	L2	3.1	57
Run64	CuAg 20wt% PTFE, 1	L5	2.0	57
Run65	CuAg 20wt% PTFE, 2	L6	2.8	57